UV LUMINOSITY FUNCTIONS AT $Z \sim 4$, 5, AND 6 FROM THE HUDF AND OTHER DEEP HST ACS FIELDS: EVOLUTION AND STAR FORMATION HISTORY

Rychard J. Bouwens[2], Garth D. Illingworth[2], Marijn Franx[3], Holland Ford[4]

1 Based on observations made with the NASA/ESA Hubble Space Telescope, which is operated by the Association of Universities for Research in Astronomy, Inc., under NASA contract NAS 5-26555. These observations are associated with programs #9425, 9575, 9797, 9803, 9978, 10189, 10339, 10340, and 10632.
2 Astronomy Department, University of California, Santa Cruz, CA 95064
3 Leiden Observatory, Postbus 9513, 2300 RA Leiden, Netherlands and
4 Department of Physics and Astronomy, Johns Hopkins University, 3400 North Charles Street, Baltimore, MD 21218
Draft version February 1, 2008

ABSTRACT

We use the ACS $BViz$ data from the HUDF and all other deep HST ACS fields (including the GOODS fields) to find large samples of star-forming galaxies at $z \sim 4$ and $z \sim 5$ and to extend our previous $z \sim 6$ sample. These samples contain 4671, 1416, and 627 B, V, and i dropouts, respectively, and reach to extremely low luminosities ($0.01 - 0.04 L_{z=3}^{*}$ or $M_{UV} \sim -16$ to -17), allowing us to determine the rest-frame UV luminosity function (LF) and faint-end slope α at $z \sim 4 - 6$ to high accuracy. We find faint-end slopes α of -1.73 ± 0.05 at $z \sim 4$, -1.66 ± 0.09 at $z \sim 5$, and -1.74 ± 0.16 at $z \sim 6$ – suggesting that the faint-end slope is very steep and shows little evolution with cosmic time. We find that M_{UV}^{*} brightens considerably in the 0.7 Gyr from $z \sim 6$ to $z \sim 4$ (by ~ 0.7 mag from $M_{UV}^{*} = -20.24 \pm 0.19$ to $M_{UV}^{*} = -20.98 \pm 0.10$). The observed increase in the characteristic luminosity over this range is almost identical to that expected for the halo mass function – suggesting that the observed evolution is likely due to the hierarchical coalescence and merging of galaxies. The evolution in ϕ^{*} is not significant. The UV luminosity density at $z \sim 6$ is modestly lower ($0.45 \pm 0.09 \times$) than that at $z \sim 4$ (integrated to -17.5 AB mag) though a larger change is seen in the dust-corrected star-formation rate density. We thoroughly examine published LF results and assess the reasons for their wide dispersion. We argue that the results reported here are the most robust available. The extremely steep faint-end slopes α found here suggest that lower luminosity galaxies play a significant role in reionizing the universe. Finally, recent search results for galaxies at $z \sim 7 - 8$ are used to extend our estimates of the evolution of M^{*} from $z \sim 7 - 8$ to $z \sim 4$.

Subject headings: galaxies: evolution — galaxies: high-redshift

1. INTRODUCTION

The luminosity function represents a key observable in astronomy. It tells us how many galaxies at some epoch emit light of a given luminosity. Comparisons of the luminosity function with other quantities like the halo mass function provide critical insight into galaxy formation by establishing the efficiency of star formation at different mass scales (van den Bosch et al. 2004; Vale & Ostriker 2004). At ultraviolet (UV) wavelengths, this luminosity function has been of keen interest because of its close relationship with the star formation rate. With the exception of galaxies with the largest star formation rates and therefore likely significant dust extinction (e.g., Wang & Heckman 1996; Adelberger & Steidel 2000; Martin et al. 2005b), UV light has been shown to be a very good tracer of this star formation rate. Studies of the evolution of this LF can help us understand the physical processes that govern star formation. Among these processes are likely gas accretion and hierarchical buildup at early times, SNe and AGN feedback to regulate this star formation, and gravitational instability physics.

Over the past few years, there has been substantial progress in understanding the evolution of the rest-frame UV LF across cosmic time, building significantly upon the early work done on these LFs at $z \sim 3 - 4$ from Lyman-Break Galaxy (LBG) selections (Madau et al. 1996; Steidel et al. 1999) and work in the nearby universe ($z \lesssim 0.1$: e.g., Sullivan et al. 2000). At lower red-

shift, progress has come through deep far-UV data from the Galaxy Evolution Explorer (GALEX: Martin et al. 2005a) which have allowed us to select large samples of LBGs at $z \lesssim 1.5$ (Arnouts et al. 2005; Schiminovich et al. 2005) and thus derive the LF at the same rest-frame wavelength ($\sim 1600 \AA$) as higher redshift samples. At the same time, there has been an increasing amount of very deep, wide-area optical data available from ground and space to select large dropout samples at $z \sim 4 - 6$ (e.g., Giavalisco et al. 2004b; Bunker et al. 2004; Dickinson et al. 2004; Yan & Windhorst 2004; Ouchi et al. 2004; Bouwens et al. 2006, hereinafter, B06; Yoshida et al. 2006). This has enabled us to determine the UV-continuum LF across the entire range $z \sim 0 - 6$ and attempt to understand its evolution across cosmic time (Shimasaku et al. 2005; B06; Yoshida et al. 2006; Tresse et al. 2006).

Although there has been an increasing consensus on the evolution of the LF at $z < 2$ (Arnouts et al. 2005; Gabasch et al. 2004; Dahlen et al. 2006; Tresse et al. 2006), it is fair to say that the evolution at $z \gtrsim 3$ is still contentious, with some groups claiming that the evolution occurs primarily at the bright-end (Shimasaku et al. 2005; B06; Yoshida et al. 2006), others claiming it occurs at the faint-end (Iwata et al. 2003; Sawicki & Thompson 2006a; Iwata et al. 2007), and still other teams suggesting the evolution occurs in a luminosity-independent manner (Beckwith et al. 2006). Perhaps, the most physically rea-

sonable of these scenarios and the one with the broadest observational support (Dickinson et al. 2004; Shimasaku et al. 2005; B06; Bouwens & Illingworth 2006; Yoshida et al. 2006) is the scenario where evolution happens primarily at the bright-end of the LF. In this picture, fainter galaxies are established first and then the brighter galaxies develop later through hierarchical buildup. Observationally, this buildup is seen as an increase in the characteristic luminosity as a function of cosmic time (Dickinson et al. 2004; B06; Yoshida et al. 2006). Less evolution is apparent in the normalization ϕ^* and faint-end slope α (B06; Yoshida et al. 2006).

Despite much observational work at the bright end of the LF at high redshift, the observations have not provided us with as strong of constraints on what happens at the faint-end of the luminosity function. Most large-scale surveys for galaxies at $z \sim 3-6$ have only extended to ~ 27 AB mag (e.g., Yoshida et al. 2006; Giavalisco et al. 2004b; Ouchi et al. 2004; Sawicki & Thompson 2005), which is equivalent to $\sim 0.3 L^*_{z=3}$ at $z \sim 4-5$. This is unfortunate since galaxies beyond these limits may be quite important in the overall picture of galaxy evolution, particularly if the faint-end slope α is steep. For faint-end slopes α of -1.6, lower luminosity galaxies ($\lesssim 0.3 L^*_{z=3}$) contribute nearly 50% of the total luminosity density, and this fraction will even be higher if the faint-end slope is steeper yet. Since these galaxies will almost certainly play a more significant role in the luminosity densities and star formation rates at very early times, clearly it is helpful to establish how the LF is evolving at lower luminosities. This topic has been of particular interest recently due to speculation that lower luminosity galaxies may reionize the universe (Bremer & Lehnert 2003; Yan & Windhorst 2004a,b; B06; Stark et al. 2007a; Labbé et al. 2006).

With the availability of deep optical data over the Hubble Ultra Deep Field (HUDF: Beckwith et al. 2006), we have the opportunity to extend current luminosity functions (LFs) to very low luminosities. The HUDF data are deep enough to allow us to select dropout samples to ~ 29.5 AB mag, which corresponds to an absolute magnitude of ~ -16.5 AB mag at $z \sim 4$, or $\sim 0.01\ L^*$, which is ≈ 5 mag below L^*. This is almost 2 mag fainter than has been possible with any other data set and provides us with unique leverage to determine the faint-end slope. Previously, we have used an i-dropout selection over the HUDF to determine the LF at $z \sim 6$ to very low luminosities (-17.5 AB mag), finding a steep faint-end slope $\alpha = -1.73 \pm 0.21$ and a characteristic luminosity $M^* \sim -20.25$ that was ~ 0.6 mag fainter than at $z \sim 3$ (B06; see also work by Yan & Windhorst 2004; Bunker et al. 2004; Malhotra et al. 2005). Beckwith et al. (2006) also considered a selection of dropouts over the HUDF and used them in conjunction with a selection of dropouts over the wide-area Great Observatories Origins Deep Survey (GOODS) fields (Giavalisco et al. 2004a) to examine the evolution of the LF at high-redshift. Beckwith et al. (2006) found that the LFs at $z \sim 4-6$ could be characterized by a constant $M^* \sim -20.4$, steep faint-end slope $\alpha \sim -1.6$, and evolving normalization ϕ^*. Bunker et al. (2004) and Yan & Windhorst (2004) also examined the evolution of the LF from $z \sim 6$ to $z \sim 3$, intepreting the evolution in terms of a changing normalization ϕ^* and faint-end slope α, respectively.

It is surprising to see that even with such high-quality selections as are possible with the HUDF, there is still a wide dispersion of results regarding the evolution of the UV LF at high redshift. This emphasizes how important both uncertainties and systematics can be for the determination of the LF at these redshifts. These include data-dependent uncertainties like large-scale structure and small number statistics to more model-dependent uncertainties (or systematics) like the model redshift distribution, selection volume, and k-corrections. In light of these challenges, it makes sense for us *(i)* to rederive the LFs at $z \sim 4-6$ in a uniform way using the most comprehensive set of HST data available while *(ii)* considering the widest variety of approaches and assumptions.

To this end, we will make use of a comprehensive set of multicolour ($BViz$) HST data to derive the rest-frame UV LFs at $z \sim 4$, $z \sim 5$, and $z \sim 6$. These data include the exceptionally deep HUDF data, the two wide-area GOODS fields, and four extremely deep ACS pointings which reach to within ~ 1 mag to 0.5 mag of the HUDF. These latter data include two deep ACS parallels (~ 20 arcmin^2) to the UDF NICMOS field (HUDF-Ps: Bouwens et al. 2004a; Thompson et al. 2005) and the two HUDF05 fields (~ 23 arcmin^2: Oesch et al. 2007). Though these data have not been widely used in previous LF determinations at $z \sim 4-5$, they provide significant statistics faintward of the GOODS probe, provide essential controls for large scale structure, and serve as an important bridge in linking ultra-deep HUDF selections to similar selections made over the much shallower GOODS fields. By deriving the LFs at $z \sim 4$ and $z \sim 5$, we will fill in the redshift gap left by our previous study (B06) between $z \sim 6$ and $z \sim 3$. We will also take advantage of the additional HST data now available (i.e., the two HUDF05 fields) to refine our previous determination of the LF at $z \sim 6$ (B06). In doing so, we will obtain an entirely self-consistent determination of the UV LF at $z \sim 4$, $z \sim 5$, and $z \sim 6$. This will allow us to make a more direct assessment of the evolution of the LF from $z \sim 6$ to $z \sim 3-4$ than we were able to make in our previous comparison with the LF at $z \sim 3$ from Steidel et al. (1999). It also puts us in a position to evaluate the wide variety of different conclusions drawn by different teams in analyzing the evolution of the LF at very high redshift (Bunker et al. 2004; Yan & Windhorst 2004; Iwata et al. 2003; Beckwith et al. 2006; Yoshida et al. 2006; Iwata et al. 2007). While deriving these LFs, we will consider a wide variety of different approaches and assumptions to ensure that the results we obtain are as robust and broadly applicable as possible.

We begin this paper by describing our procedures for selecting our B, V, and i-dropout samples (§2). We then derive detailed completeness, flux, and contamination corrections to model our shallower HUDF05, HUDF-Ps, and GOODS selections in a similar fashion to the way we model the HUDF data. We then move onto a determination of the rest-frame UV LFs at $z \sim 4$, $z \sim 5$, and $z \sim 6$ (§3). In §4, we assess the robustness of the current LF determinations – comparing the present results with those in the literature and trying to understand the wide dispersion of previous LF results. Finally, we discuss the implications of our results (§5) and then include a summary (§6). Where necessary, we assume $\Omega_0 = 0.3$, $\Omega_\Lambda = 0.7$, $H_0 = 70\,\mathrm{km/s/Mpc}$. Although these param-

eters are slightly different from those determined from the WMAP three-year results (Spergel et al. 2006), they allow for convenient comparison with other recent results expressed in a similar manner. Throughout, we shall use $L^*_{z=3}$ to denote the characteristic luminosity at $z \sim 3$ (Steidel et al. 1999). All magnitudes are expressed in the AB system (Oke & Gunn 1983).

2. SAMPLE SELECTION

2.1. Observational Data

A detailed summary of the ACS HUDF, HUDF-Ps, and GOODS data we use for our dropout selections is provided in our previous work (B06). Nevertheless, a brief description of the data is included here. The ACS HUDF data we use are the v1.0 reductions of Beckwith et al. (2006) and extend to 5σ point-source limits of $\sim 29 - 30$ in the $B_{435}V_{606}i_{775}z_{850}$ bands. The HUDF-Ps reductions we use are from B06 and take advantage of the deep ($\gtrsim 72$ orbit) $BViz$ ACS data fields taken in parallel with the HUDF NICMOS program (Thompson et al. 2005). Together the parallel data from this program sum to create two very deep ACS fields that we can use for dropout searches. While of somewhat variable depths, the central portions of these fields (12-20 arcmin^2) reach some $0.6 - 0.9$ mag deeper than the data in the original ACS GOODS program (Giavalisco et al. 2004a). Finally, for the ACS GOODS reductions, we will use an updated version of those generated for our previous $z \sim 6$ study (B06). These reductions not only take advantage of all the original data taken with ACS GOODS program, but also include all the ACS data associated with the SNe search (A. Riess et al. 2007, in preparation), GEMS (Rix et al. 2004), HUDF NICMOS (Thompson et al. 2005), and HUDF05 (Oesch et al. 2007) programs. These latter data (particularly the SNe search data) increase the depths of the i_{775} and z_{850} band images by $\gtrsim 0.2$ and $\gtrsim 0.5$ mags over that available in the GOODS v1.0 reductions (Giavalisco et al. 2004a).

Finally, we also take advantage of two exceptionally deep ACS fields taken over the NICMOS parallels to the HUDF (called the HUDF05 fields: Oesch et al. 2007). Each field contains 10 orbits of ACS V_{606}-band data, 23 orbits of ACS i_{775}-band data, and 71 orbits of ACS z_{850}-band data. As such, these fields are second only to the HUDF in their total z_{850}-band exposure time. Though these data were taken to search for galaxies at $z > 6.5$ (e.g., Bouwens & Illingworth 2006), they provide us with additional data for the UV LF determinations at $z \sim 5 - 6$. These data were not available to us in our previous study on the LF at $z \sim 6$ (B06). The ACS data over these fields were reduced using the ACS GTO pipeline "apsis" (Blakeslee et al. 2003). "Apsis" handles image alignment, cosmic ray rejection, and the drizzling process. To maximize the quality of our reductions, we median stacked the basic post-calibration data after masking out the sources and then subtracted these medians from the individual exposures before drizzling them together to make the final images. The reduced fields reach to ~ 29 AB mag at 5σ in the V_{606}, i_{775}, and z_{850} bands using $\sim 0.2''$-diameter apertures. This is only ~ 0.4 mag shallower than the HUDF in the z_{850} band. A detailed summary of the properties of each of our fields is contained in Table 1.

TABLE 1
Observational Data.

Passband	Detection Limits[a] (5σ)	PSF FWHM (arcsec)	Areal Coverage (arcmin^2)
	HUDF		
B_{435}	29.8	0.09	11.2
V_{606}	30.2	0.09	11.2
i_{775}	30.1	0.09	11.2
z_{850}	29.3	0.10	11.2
J_{110}	27.3	0.33	5.8
H_{160}	27.1	0.37	5.8
	HUDF05		
V_{606}	29.2	0.09	20.2[b]
i_{775}	29.0	0.09	20.2[b]
z_{850}	28.9	0.10	20.2[b]
	HUDF-Ps		
B_{435}	29.1	0.09	12.2[b]
V_{606}	29.4	0.09	12.2[b]
i_{775}	29.0	0.09	12.2[b]
z_{850}	28.6	0.10	12.2[b]
	GOODS fields		
B_{435}	28.4	0.09	324
V_{606}	28.6	0.09	324
i_{775}	27.9	0.09	324
z_{850}	27.6	0.10	324
J	~ 25	$\sim 0.45''$	131
K_s	~ 24.5	$\sim 0.45''$	131

[a]$0.2''$-diameter aperture for the ACS data, $0.6''$-diameter aperture for NICMOS data, and $0.8''$-diameter for ISAAC data. In contrast to the detection limits quoted in our previous work, here our detection limits have been corrected for the nominal light outside these apertures (assuming a point source). The detection limits without this correction are typically ~ 0.3 mag fainter.

[b]Only the highest S/N regions from the HUDF-Ps and HDF05 fields were used in the searches to obtain a consistently deep probe of the LF over these regions.

2.2. Catalog Construction and Photometry

Our procedure for doing object detection and photometry on the HUDF, HUDF-Ps, HUDF05, and GOODS fields is very similar to that used previously (Bouwens et al. 2003b; B06). Briefly, we perform object detection for B, V, and i-dropout selections by constructing χ^2 images (Szalay et al. 1999) from the V_{606}, i_{775}, and z_{850}-band data, i_{775} and z_{850}-band data, and z_{850}-band data, respectively. χ^2 images are constructed by adding together the relevant images in quadrature, weighting each by $1/\sigma^2$, where σ is the RMS noise on the image. SExtractor (Bertin & Arnouts 1996) was then run in double-image mode using the square root of the χ^2 image as the detection image and the other images to do photometry. Colors were measured using Kron-style (1980) photometry (MAG_AUTO) in small scalable apertures (Kron factor 1.2, with a minimum aperture of 1.7 semi-major (semi-minor) axis lengths). These colors were then corrected up to total magnitudes using the excess light contained within large scalable apertures (Kron factor 2.5, with a minimum aperture of 3.5 semi-major (semi-minor) axis lengths). We measured these corrections off the square root of the χ^2 image to improve the S/N. Figure 5 of Coe et al. (2006) provides a graphic description of a similar procedure. The median diameter of these apertures was $\sim 0.6''$ for the faintest sources in our samples. An additional correction was made to account for light

outside of our apertures and on the wings of the ACS Wide Field Camera (WFC) PSF (Sirianni et al. 2005). Typical corrections were $\sim 0.1 - 0.2$ mag.

To assess the quality of our total magnitude measurements, we compared our measurements (which are based on global backgrounds) with those obtained using local backgrounds and found that our total magnitude measurements were ~ 0.04 mag brighter in the mean. Comparisons with similar flux measurements made available from the GOODS and HUDF teams (Giavalisco et al. 2004a; Beckwith et al. 2006) also showed good agreement ($\sim \pm 0.2$ mag scatter), though our total magnitude measurements were typically ~ 0.08 mag brighter. We believe this offset is the result of the ~ 0.1 mag correction we make for light on the PSF wings (Sirianni et al. 2005).

While constructing our dropout catalogs, one minor challenge was in the deblending of individual sources. The issue was that SExtractor frequently split many of the more asymmetric, multi-component dropout galaxies in our samples into more than one distinct source. This would have the effect of transforming many luminous sources in our selection into multiple lower luminosity sources and thus bias our LF determinations. To cope with this issue, we experimented with a number of different procedures for blending sources together based upon their colours. In the end, we settled on a procedure whereby dropouts were blended with nearby sources if (1) they lay within 4 Kron radii and (2) their colours did not differ at more than 2σ significance. Since SExtractor does not allow for the use of colour information in the blending of individual sources, it was necessary for us to implement this algorithm outside the SExtractor package. We found that our procedure nearly always produced results which were in close agreement with the choices we would make after careful inspection.

2.3. *Selection Criteria*

We adopted selection criteria for our B, V, and i dropout samples which are very similar to those used in previous works. Our selection criteria are

$$(B_{435} - V_{606} > 1.1) \wedge (B_{435} - V_{606} > (V_{606} - z_{850}) + 1.1)$$
$$\wedge (V_{606} - z_{850} < 1.6)$$

for our B-dropout sample and

$$[(V_{606} - i_{775} > 0.9(i_{775} - z_{850})) \vee (V_{606} - i_{775} > 2))] \wedge$$
$$(V_{606} - i_{775} > 1.2) \wedge (i_{775} - z_{850} < 1.3)$$

for our V-dropout sample and

$$(i_{775} - z_{850} > 1.3) \wedge ((V_{606} - i_{775} > 2.8) \vee (S/N(V_{606}) < 2))$$

for our i-dropout sample, where $\wedge$ and $\vee$ represent the logical **AND** and **OR** symbols, respectively, and **S/N** represents the signal to noise. Our V-dropout and i-dropout selection criteria are identical to that described in Giavalisco et al. (2004b) and B06, respectively. Meanwhile, our B-dropout criteria, while slightly different from that used by Giavalisco et al. (2004b), are now routinely used by different teams (e.g., Beckwith et al. 2006).

We also required sources to be clearly extended (SExtractor stellarity indices less than 0.8) to eliminate intermediate-mass stars and AGNs. Since the SExtractor stellarity parameter rapidly becomes unreliable near

the magnitude limit of each of our samples (see, e.g., the discussion in Appendix D.4.3 of B06), we do not remove point sources faintward of the limits $i_{775,AB} > 26.5$ (GOODS), $i_{775,AB} > 27.3$ (HUDF-Ps/HUDF05), and $i_{775,AB} > 28$ (HUDF) for our B-dropout sample and $z_{850,AB} > 26.5$ (GOODS), $z_{850,AB} > 27.3$ (HUDF-Ps/HUDF05), and $z_{850,AB} > 28$ (HUDF) for our V and i-dropout samples. Instead contamination from stars is treated on a statistical basis. Since only a small fraction of galaxies faintward of these limits appear to be stars ($\lesssim 6\%$ of the dropout candidates brightward of 27.0 are unresolved in our GOODS selections and $\lesssim 1\%$ of the dropout candidates brightward of 28.0 are unresolved in our HUDF selections), these corrections are small and should not be a significant source of error. Sources which were not 4.5σ detections in the selection band ($0.3''$-diameter apertures) were also removed to clean our catalogs of a few spurious sources associated with an imperfectly flattened background. Finally, each dropout in our catalogs was carefully inspected to remove artifacts (e.g., diffraction spikes or low-surface brightness features around bright foreground galaxies) that occasionally satisfy our selection criteria.

In total, we found 711 B-dropouts, 232 V-dropouts, and 132 i-dropouts over the HUDF and 3828 B-dropouts, 888 V-dropouts, and 365 i-dropouts over the two GOODS fields. This is similar to (albeit slightly larger than) the numbers reported by Beckwith et al. (2006) over these fields. We also found 283 B-dropouts over the HUDF-Ps (12 arcmin^2) and 332 V-dropouts and 160 i-dropouts over the HUDF-Ps and HUDF05 fields (32 arcmin^2). Altogether, our catalogs contain 4671, 1416, and 627 unique B, V, and i-dropouts (151, 36, and 30 of the above B, V, and i-dropouts occur in more than one of these catalogs). Table 2 provides a convenient summary of the properties of our B, V, and i dropout samples. Figure 1 compares the surface density of dropouts found in our compilation with those obtained in the literature (Giavalisco et al. 2004b; Beckwith et al. 2006). With a few notable exceptions (see, e.g., Figure 12), we are in good agreement with the literature.

2.4. *Flux/Completeness Corrections*

The above samples provide us with an unprecedented data set for determining the LFs at high-redshift over an extremely wide range in luminosity. However, before we use these samples to determine the LFs at $z \sim 4 - 6$, we need to understand in detail how object selection and photometry affects what we observe. These issues can have a significant effect on the properties of our different selections, as one can see in Figure 1 by comparing the surface density of dropouts observed in the HUDF, HUDF05, HUDF-Ps, and GOODS fields, where clear differences are observed at faint magnitudes due to obvious differences in the completeness of these samples at such magnitudes.

To accomplish these aims, we will use a very similar strategy to what we employed in previous examinations of the rest-frame UV LF at $z \sim 6$ (B06). Our strategy will be to derive transformations which correct the dropout surface densities from what we would derive for noise-free (infinite S/N) data to that recoverable at the depths of our various fields. These transformations will be made using a set of two-dimensional matrices,

TABLE 2
SUMMARY OF B, V, AND i-DROPOUT SAMPLES.[a]

Sample	Area (arcmin^2)	B-dropouts #	Limit[a]	$L/L_{z=3}^*$ [b]	V-dropouts #	Limit[a]	$L/L_{z=3}^*$ [b]	i-dropouts #	Limit[a]	$L/L_{z=3}^*$ [b]
CDFS GOODS	172[*]	2105	$i \le 28.0$	≥ 0.07	447	$z \le 28.0$	≥ 0.1			
CDFS GOODS-i	196[**]							223	$z \le 28.0$	≥ 0.15
HDFN GOODS	152	1723	$i \le 28.0$	≥ 0.07	441	$z \le 28.0$	≥ 0.1	142	$z \le 28.0$	≥ 0.15
HUDF-Ps	12	283	$i \le 29.0$	≥ 0.04	88	$z \le 28.5$	≥ 0.08			
HUDF-Ps-i	17[**]							64	$z \le 28.5$	≥ 0.1
HUDF05	20	—	—	—	244	$z \le 29.0$	≥ 0.05	96	$z \le 29.0$	≥ 0.06
HUDF	11	711	$i \le 30.0$	≥ 0.01	147	$z \le 29.5$	≥ 0.03	132	$z \le 29.5$	≥ 0.04
					232	$i \le 30.0$	≥ 0.02			

[*]Due to our inclusion of the ACS parallels to the UDF NICMOS field in our reductions of the CDF South GOODS field (§2.3), the total area available there for B and V-dropout searches exceeded that available in the HDF-North GOODS field.
[**]Because our i-dropout selections do not require deep B-band data, we can take advantage of some additional area around the CDF-S GOODS and HUDF-Ps fields to expand our selection beyond what is available to our B and V-dropout selections.
[a]The magnitude limit is the $\sim 5\sigma$ detection limit for objects in a 0.2″-diameter aperture.
[b]Magnitude limit in units of $L_{z=3}^*$ (Steidel et al. 1999).

called transfer functions. These functions are computed for each dropout selection and field under consideration here (HUDF, HUDF05, HUDF-Ps, and GOODS). We describe the derivation of these transfer functions in detail in Appendix A.1. A summary of the properties of these functions is also provided in this section.

2.5. Contamination Corrections

Dropout samples also contain a small number of contaminants. We developed corrections for three types of contamination: (i) intrinsically-red, low-redshift interlopers, (ii) objects entering our samples due to photometric scatter, and (iii) spurious sources. We estimated the fraction of intrinsically red objects in our samples as a function of magnitude using the deep K_s-band data over the Chandra Deep Field (CDF) South GOODS field (B. Vandame et al. 2007, in preparation). Contaminants were identified in our B, V, and i-dropout selections with a $(i_{775} - K_s)_{AB} > 2$, $(z_{850} - K_s)_{AB} > 2$, and $(z_{850} - K_s)_{AB} > 1.6$ criterion, respectively. The contamination rate from photometric scatter was estimated by performing selections on degradations of the HUDF. Appendix D.4.2 of B06 provides a description of how we previously calculated this at $z \sim 6$. The contribution of these two contaminants to our samples was relatively small, on order $\sim 2\%$, $\sim 3\%$, and $\sim 3\%$, respectively, though this contamination rate is clearly magnitude dependent and decreases towards fainter magnitudes. The contamination rate from spurious sources was determined by repeating our selection on the negative images (e.g., Dickinson et al. 2004; B06) and found to be completely negligible ($\lesssim 1\%$).

2.6. Number Counts

Before closing this section and moving onto a determination of the UV LF at $z \sim 4 - 6$, it is useful to derive the surface density of B, V, and i-dropouts by combining the results from each of our samples and implementing each of the above corrections. Although we will make no direct use of these aggregate surface densities in our derivation of the rest-frame UV LF, direct tabulation of these surface densities can be helpful for observers who are interested in knowing the approximate source density of high-redshift galaxies on the sky or for theorists

who are interested in making more direct comparisons to the observations. We combine the surface densities from our various fields using a maximum likelihood procedure. The surface densities are corrected for field-to-field variations using the factors given in Table B3. Both incompleteness and flux biases are treated using the transfer functions which take our selections from HUDF depths to shallower depths. Our final results are presented in Table 3.

3. DETERMINATION OF THE UV LF AT $Z \sim 4 - 6$

The large B, V, and i dropout samples we have compiled permit us to determine the rest-frame UV LFs at $z \sim 4$, $z \sim 5$, and $z \sim 6$ to very faint UV luminosities (AB mags ~ -16, ~ -17, and ~ -17.5, respectively), with significant statistics over a wide range in magnitude. This provides us with both the leverage and statistics to obtain an unprecedented measure of the overall shape of the LF for galaxies at $z \sim 4$, $z \sim 5$, and $z \sim 6$.

To maximize the robustness of our LF results, we will consider a wide variety of different approaches to determining the LF at $z \sim 4$, $z \sim 5$, and $z \sim 6$. We begin by invoking two standard techniques for determining the LF in the presence of large-scale structure (both modified for use with apparent magnitudes). The first technique is the Sandage, Tammann, & Yahil (1979: STY79) approach and the second is the stepwise maximum likelihood (SWML) method (Efstathiou et al. 1988). With these approaches, we will determine the LF both in stepwise form and using a Schechter parametrization. We then expand our discussion to consider a wide variety of different approaches for determining the LF at $z \sim 4$, $z \sim 5$, and $z \sim 6$ to ensure that the Schechter parameters are not overly sensitive to our approach and various assumptions we make about the form of the SEDs of galaxies at $z \gtrsim 4$. These tests are developed in Appendices B and C. We will then update our STY79 LF determinations to correct for the effect of evolution across our samples (Appendix B.8: Table 7). In §3.4, we examine the robustness of the conclusions that we derive regarding the faint-end slope and then finally we compute the luminosity densities and star formation rate densities at $z \sim 4 - 6$ using our LF results.
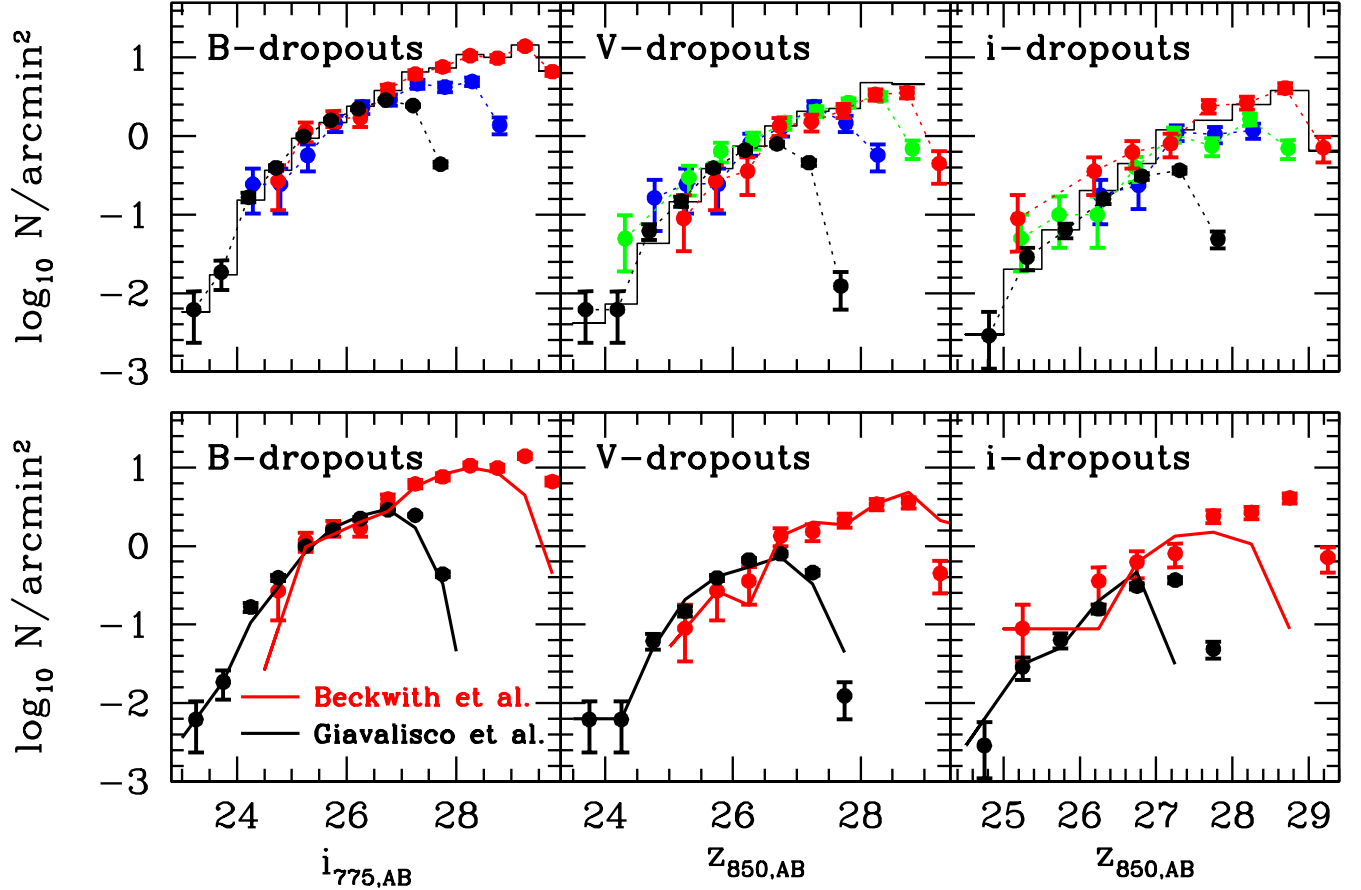
FIG. 1.— *(top left)* The surface density of *B*-dropouts (per 0.5 mag interval) found in the ACS GOODS (*black circles*), HUDF-Ps (*blue circles*), and HUDF data (*red circles*) before correction for incompleteness, contamination, flux biases, and field-to-field variations. The data points have been slightly offset relative to each other in the horizontal direction for clarity. The black histogram show the surface density of *B*-dropouts obtained after combining the results from the HUDF + HUDF-Ps + GOODS fields and correcting for the above effects (§2.6: see also Table 3). Our *B*-dropout selections suffer from significant incompleteness in the ACS GOODS data faintward of $i_{775,AB} \sim 27$ AB mag, while the *B*-dropout selections over the HUDF-Ps become rather incomplete at $i_{775,AB} \sim 28$ AB mag. *(top center and right)* Similar to the top left panel, except for *V*-dropouts *(top center)* and *i*-dropouts *(top right)*. The *green circles* shows the surface density of *V*-dropouts over the HUDF05 fields before any corrections are made. *(bottom panels)* Similar to top panels, but comparing current determinations of the dropout surface densities (*solid circles*) with previous determinations in the literature from the ACS GOODS data (Giavalisco et al. 2004a: *black solid lines*) and HUDF data (Beckwith et al. 2006: *red solid lines*). In general, our determinations agree quite well with those in the literature, particularly at bright magnitudes. Notable exceptions include the surface densities of the fainter *i*-dropouts in the HUDF and GOODS fields. We find a much larger number of faint *i*-dropouts over the GOODS fields than are found in the original GOODS v1.0 reductions of Giavalisco et al. (2004a) because we take advantage of the considerable SNe search data taken over these fields which increase the depths by ~ 0.4 mag (§2.1; B06). For a discussion of the differences in the HUDF *i*-dropout counts, we refer the reader to §4.3 and Figure 12.

3.1. *STY79 Method*

We will begin by estimating the rest-frame *UV* LF from our *B*, *V*, *i*-dropout samples using a Schechter parameterization

$$\phi^*(\ln(10)/2.5)10^{-0.4(M-M^*)(\alpha+1)}e^{-10^{-0.4(M-M^*)}} \quad (1)$$

and the maximum likelihood procedure of STY79. The parameter ϕ^* is the normalization, M^* is the characteristic luminosity, and α is the faint-end slope in the Schechter parametrization. The STY79 procedure has long been the technique of choice for computing the LF over multiple fields because it is insensitive to the presence of large-scale structure. The central idea behind this technique is to consider the likelihood of reproducing the relative distribution of dropouts in magnitude space given a LF. Because only the distribution of sources is considered in this measure and not the absolute surface densities, this approach is only sensitive to the shape of the LF and not its overall normalization. This makes this

approach immune to the effects of large-scale structure and our LF fit results very robust.

It is worthwhile to note however that for our particular application of this approach, our results will not be completely insensitive to large-scale structure. This is because lacking exact redshifts for individual sources in our samples we will need to consider the apparent magnitudes of individual galaxies in computing the likelihoods and not the absolute magnitudes. This will make our results slightly sensitive to large-scale structure along the line of sight due to the effect of redshift on the apparent magnitudes. However, as we demonstrate in Appendix C, the expected effect of this structure is extremely small, introducing 1σ variations of ~ 0.05 mag in the value of M^* and ~ 0.02 in the value of the faint-end slope α.

To use this approach to evaluate the likelihood of model LFs, we need to compute the surface density of dropouts as a function of magnitude $N(m)$ from the model LFs, so we can compare these numbers against

TABLE 3
Corrected surface densities of B, V, and i-dropouts from all fields.[a]

Magnitude	Surface Density (arcmin^{-2})
B-dropouts ($z \sim 4$)	
$23.00 < i_{775} < 23.50$	0.006 ± 0.005
$23.50 < i_{775} < 24.00$	0.019 ± 0.008
$24.00 < i_{775} < 24.50$	0.173 ± 0.022
$24.50 < i_{775} < 25.00$	0.412 ± 0.035
$25.00 < i_{775} < 25.50$	1.053 ± 0.057
$25.50 < i_{775} < 26.00$	1.685 ± 0.071
$26.00 < i_{775} < 26.50$	2.703 ± 0.097
$26.50 < i_{775} < 27.00$	4.308 ± 0.134
$27.00 < i_{775} < 27.50$	7.408 ± 0.656
$27.50 < i_{775} < 28.00$	8.263 ± 0.701
$28.00 < i_{775} < 28.50$	12.228 ± 1.120
$28.50 < i_{775} < 29.00$	11.401 ± 1.082
$29.00 < i_{775} < 29.50$	16.167 ± 1.288
$29.50 < i_{775} < 30.00$	7.668 ± 0.887
V-dropouts ($z \sim 5$)	
$23.50 < z_{850} < 24.00$	0.005 ± 0.003
$24.00 < z_{850} < 24.50$	0.008 ± 0.004
$24.50 < z_{850} < 25.00$	0.048 ± 0.010
$25.00 < z_{850} < 25.50$	0.163 ± 0.021
$25.50 < z_{850} < 26.00$	0.432 ± 0.035
$26.00 < z_{850} < 26.50$	0.842 ± 0.053
$26.50 < z_{850} < 27.00$	1.513 ± 0.084
$27.00 < z_{850} < 27.50$	2.314 ± 0.244
$27.50 < z_{850} < 28.00$	2.540 ± 0.257
$28.00 < z_{850} < 28.50$	5.403 ± 0.529
$28.50 < z_{850} < 29.00$	5.181 ± 0.815
i-dropouts ($z \sim 6$)	
$24.50 < z_{850} < 25.00$	0.003 ± 0.003
$25.00 < z_{850} < 25.50$	0.023 ± 0.008
$25.50 < z_{850} < 26.00$	0.072 ± 0.019
$26.00 < z_{850} < 26.50$	0.230 ± 0.039
$26.50 < z_{850} < 27.00$	0.501 ± 0.075
$27.00 < z_{850} < 27.50$	1.350 ± 0.208
$27.50 < z_{850} < 28.00$	1.791 ± 0.261
$28.00 < z_{850} < 28.50$	2.818 ± 0.404
$28.50 < z_{850} < 29.00$	4.277 ± 0.625
$29.00 < z_{850} < 29.50$	0.738 ± 0.260

[a]The surface densities of dropouts quoted here have been corrected to the same completeness levels as our HUDF selections. They will therefore be essentially complete to $i_{775,AB} \sim 29$, $z_{850,AB} \sim 28.5$, and $z_{850,AB} \sim 28.5$ for our B, V, and i-dropout selections, respectively.

the observations. We use a two stage approach for these computations, so we can take advantage of the transfer functions we derived in Appendix A.1. These functions provide us with a very natural way of incorporating the effects of incompleteness and photometric scatter into our comparisons with the observations, so we will want to make use of them. In order to do this, we first need to calculate the surface density of dropouts appropriate for our deepest selection (the HUDF). Then, we will correct this surface density to that appropriate for our shallower field using the transfer functions.

The nominal surface densities in our HUDF selections $N(m)$ are computed from the model LFs $\phi(M)$ as

$$\int_z \phi(M(m,z))P(m,z)\frac{dV}{dz}dz = N(m) \qquad (2)$$

where $\frac{dV}{dz}$ is the cosmological volume element, $P(m,z)$ is the probability of selecting star-forming galaxies at a magnitude m and redshift z in the HUDF, M is the absolute magnitude at $1600\,\mathring{A}$, and m is the apparent magnitude in the i_{775}, z_{850}, or z_{850} band depending upon whether we are dealing with a B, V, or i-dropout selec-

tion. Note that the i_{775} and z_{850} bands closely correspond to rest-frame $1600\,\mathring{A}$ at the mean redshift of our B and V-dropout samples ($z \sim 3.8$ and $z \sim 5.0$, respectively), whereas for our $z \sim 6$ i-dropout selection, the z_{850} band corresponds to rest-frame $1350\,\mathring{A}$.

With the ability to compute the surface density of dropouts in our different fields for various model LFs, we proceed to determine the LF which maximizes the likelihood of reproducing the observed counts with model LFs at $z \sim 4$, $z \sim 5$, and $z \sim 6$. The formulas we use for computing these likelihoods are given in Appendix A.2, along with the equations we use to evaluate the integral in Eq. 2 and implement the transfer functions from Appendix A.1. We compute the selection efficiencies $P(m,z)$ through extensive Monte-Carlo simulations, where we take real B-dropouts from the HUDF, artificially redshift them across the redshift windows of our samples, add them to our data, and then reselect them using the same procedure we use on the real data. A lengthy description of these simulations are provided in Appendix A.3, but the following are some essential points: (1) The HUDF B-dropout galaxy profiles used in our effective volume simulations for each of our dropout samples are projected to higher redshifts assuming a $(1+z)^{-1.1}$ size scaling (independent of luminosity) to match the size evolution observed at $z \sim 2 - 6$ (B06). (2) The distribution of UV-continuum slopes in our $z \sim 4$ B-dropout effective volume simulations is taken to have a mean of -1.5 and 1σ scatter of 0.6 for UV-luminous L^* star-forming galaxies. For our higher redshift samples and at lower UV luminosities, the mean UV-continuum slope is taken to be ~ -2. In all cases, these slopes were chosen to match that found in the observations (Meurer et al. 1999; Stanway et al. 2006; B06; R.J. Bouwens et al. 2007, in preparation). (3) To treat absorption from neutral hydrogen clouds, we have implemented an updated version of the Madau (1995) prescription so that it fits more recent $z \gtrsim 5$ Lyman forest observations (e.g., Songaila 2004) and includes line-of-sight variations (e.g., as performed in Bershady et al. 1999). In calculating the equivalent absolute magnitude M for an apparent magnitude m at $z \sim 6$, we use an effective volume kernel $V_{m,k}$ to correct for the redshift-dependent absorption from the Lyman forest on the observed z_{850}-band fluxes (Appendix A.2). For our $z \sim 4$ LF, we restrict our analysis to galaxies brighter than $i_{775,AB} = 29.0$ since we found that our fit results were moderately sensitive to the colour distribution we used to calculate the selection volumes (Figure A2: Appendix B.4).

The best-fit Schechter parameters are $M^*_{1600,AB} = -21.06 \pm 0.10$, and $\alpha = -1.76 \pm 0.05$ at $z \sim 4$ for our B-dropout sample, $M^*_{1600,AB} = -20.69 \pm 0.13$ and $\alpha = -1.69 \pm 0.09$ at $z \sim 5$ for our V-dropout sample, and $M^*_{1350,AB} = -20.29 \pm 0.19$ and $\alpha = -1.77 \pm 0.16$ at $z \sim 6$ for our i-dropout sample. Since $z \sim 6$ galaxies appear to be very blue ($\beta \sim -2$: Stanway et al. 2005; B06), we expect $M_{1600,AB}$ at $z \sim 6$ to be almost identical ($\lesssim 0.1$ mag) to the value of $M_{1350,AB}$. To determine the equivalent normalization ϕ^* for our derived values of α and M^*, we compute the expected number of dropouts over all of our fields and compare that with the observed number of dropouts in those fields. Following this procedure, we find $\phi^* = 0.0011 \pm 0.0002$ Mpc^{-3} for our
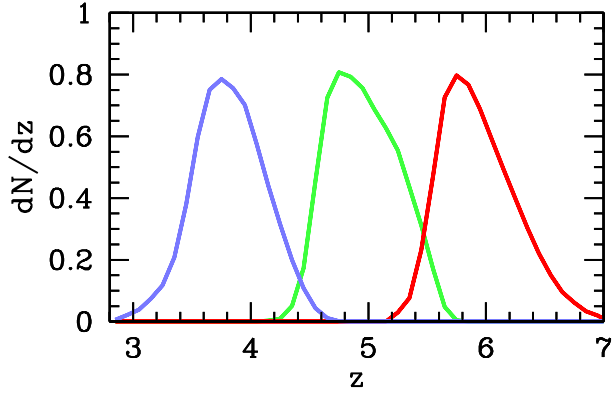
FIG. 2.— Redshift distributions computed for our HUDF B, V, and i-dropout samples (*blue, green, and red lines, respectively*) using our best-fit Schechter parameters (Table 5) from the STY79 approach and the selection efficiencies given in Figure A2. The mean redshift for our HUDF B, V, and i-dropout selections is 3.8, 5.0, and 5.9, respectively.

B-dropout sample, $\phi^* = 0.0009^{+0.0003}_{-0.0002}$ Mpc^{-3} for our V-dropout sample, and $\phi^* = 0.0012^{+0.0006}_{-0.0004}$ Mpc^{-3} for our i-dropout sample. We present these LF values in Table 5. The clearest evolution here is in the characteristic luminosity M^* which brightens significantly across this redshift range: from ~ -20.3 at $z \sim 6$ to ~ -21.1 at $z \sim 4$. In contrast, both the faint-end slope α and normalization ϕ^* of the LF remain relatively constant, with $\alpha \sim -1.74$ and $\phi^* \sim 0.001$ Mpc^{-3}. For context, we have computed the redshift distributions for our HUDF B, V, and i-dropout selections using these best-fit LFs and presented them in Figure 2.

We plot the likelihood contours for different combinations of α and M^* in Figure 4. These contours were used in our error estimates on α and M^*. For our estimates of the uncertainties on the normalization ϕ^*, we first calculated the field-to-field variations expected over an ACS GOODS field (~ 150 arcmin^2). Assuming that our B, V, and i dropout selections span a redshift window of $dz = 0.7$, $dz = 0.7$, and $dz = 0.6$, respectively, have a bias of 3.9, 3.4, and 4.1, respectively (Lee et al. 2006; Overzier et al. 2006), and using a pencil beam geometry for our calculations, we derive field-to-field variations of $\sim 22\%$ RMS, $\sim 18\%$ RMS, and $\sim 22\%$ RMS, respectively. These values are similar to those estimated to other studies (Somerville et al. 2004; B06; Beckwith et al. 2006; cf. Stark et al. 2007c). With these estimates, we were then able to derive likelihood contours in ϕ^* by marginalizing over α and M^*, using the relationship between ϕ^* and the other Schechter parameters and supposing that ϕ^* has a 1σ uncertainty equal to the RMS values given above divided by $\sqrt{2}$ (to account for the fact that each GOODS field provides us an independent measure of the volume density of galaxies).

3.2. *SWML*

As a second approach, we parametrize our derived LF in a stepwise fashion, with 0.5 mag intervals. This approach is commonly known as the Stepwise Maximum Likelihood (SWML) method (Efstathiou et al. 1988) and allows us to look at the evolution of the LF in a more model-independent way than would be possible if we considered Schechter parametrizations alone. As with our STY79 determinations, we maximize the likelihood of
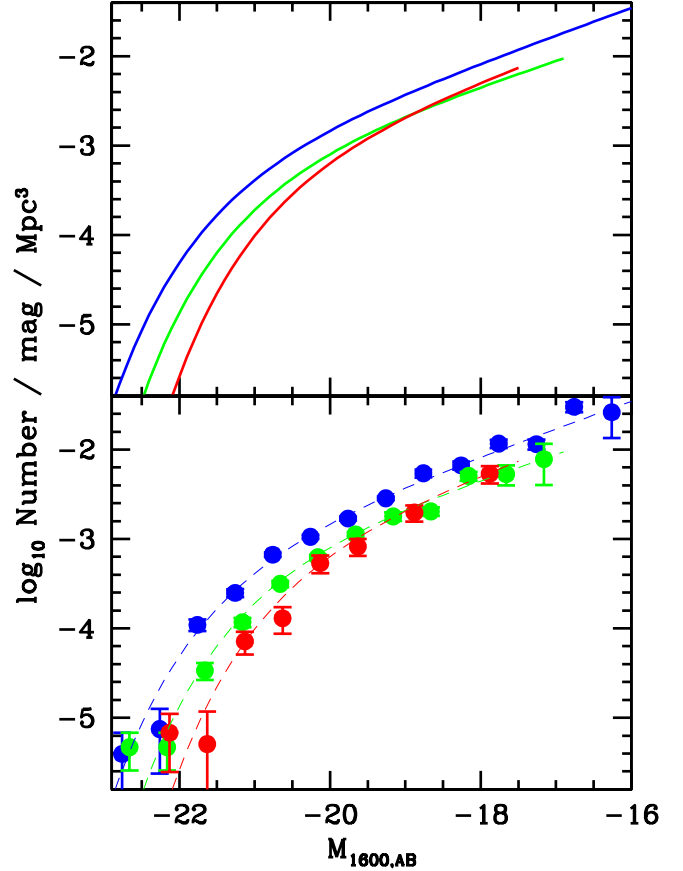

FIG. 3.— (*top panel*) Rest-frame UV (~ 1600 Å) luminosity functions at $z \sim 4$ (blue), $z \sim 5$ (green), and $z \sim 6$ (red), shown in terms of their best-fit Schechter functions (solid lines) which were derived from fits to the number counts using the STY79 method (§3.1). Though nominally our $z \sim 6$ LF requires a k-correction to transform it from ~ 1350 Å to ~ 1600 Å, the blue rest-frame UV slopes of $z \sim 6$ galaxies (e.g., Stanway et al. 2005; Yan et al. 2005; B06) means the correction is negligible. (*bottom panel*) Independent determinations of the LFs at $z \sim 4$, $z \sim 5$, and $z \sim 6$ using the SWML method (§3.2) are shown with blue, green, and red solid dark circles, respectively (1σ errors). The rest-frame UV LF shows a rapid build-up in the number of luminous galaxies from $z \sim 6$ to $z \sim 4$. On the other hand, the number of lower luminosity systems ($M_{1600,AB} > -19.5$ mag) shows much less evolution over this interval.

reproducing the observed surface densities of dropouts in our different fields given a LF. Similar to that technique, this approach is robust to the presence of large-scale structure. In order to match the magnitude interval used in our stepwise LF, we bin the number counts N_m, effective volume kernels $V_{m,k}$, and transfer functions $T_{m,l}$ on 0.5 mag intervals (see Appendix A.2). We compute the surface densities from the model LFs in the same way as for the STY79 approach, using Eq. A4 from Appendix A.2. The likelihoods are computed using Eq. A5. Errors on each of the parameters ϕ_k are derived using the second derivatives of the likelihood $\mathcal{L}$. We normalize our stepwise LFs $\phi(M)$ by requiring them to match the total number of dropouts over all of our search fields. Our stepwise determinations are tabulated in Table 4 and also included in the bottom panel of Figure 3. All LFs are Schechter-like in overall shape, as one can see by comparing the stepwise determinations with the independently derived Schechter fits (*dashed lines*).
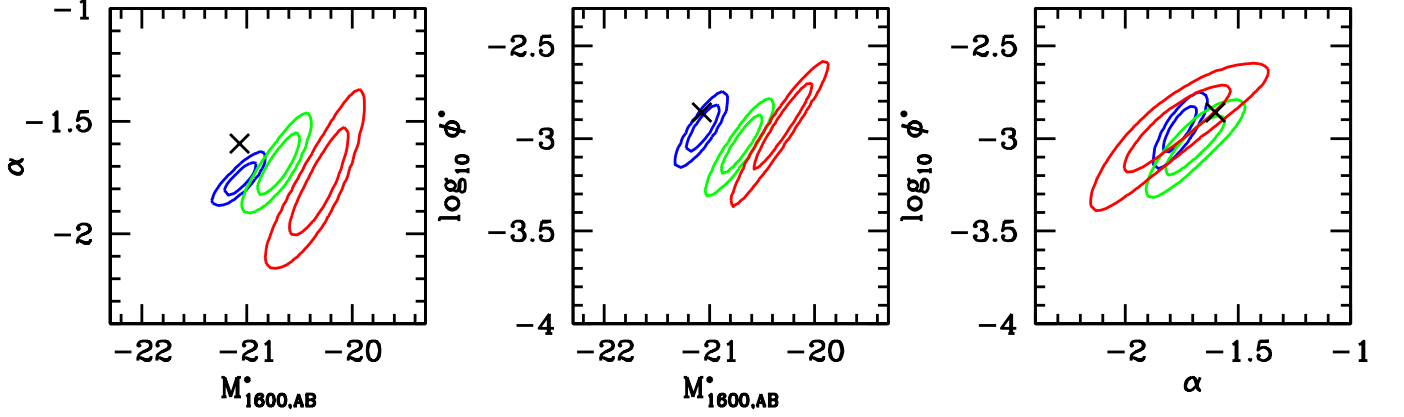
FIG. 4.— Best-fit Schechter parameters and likelihood contours for the $z \sim 4$ (*blue contours*), $z \sim 5$ (*green contours*), and $z \sim 6$ (*red contours*) UV ($\sim 1600\,\mathring{A}$) luminosity functions using the STY79 method (see §3.1). Shown are the 68% and 95% likelihood contours for different Schechter parameter combinations. Though our $z \sim 6$ LF nominally requires a k-correction to transform it from $\sim 1350\,\mathring{A}$ to $\sim 1600\,\mathring{A}$, the correction is negligible. Our best-fit parameters (and likelihood contours) for the $z \sim 6$ LF are similar to those in B06.

TABLE 4
STEPWISE DETERMINATION OF THE REST-FRAME UV LF AT $z \sim 4$, $z \sim 5$, AND $z \sim 6$ USING THE SWML METHOD (§3.2).

$M_{1600,AB}$[a]	ϕ_k (Mpc^{-3} mag^{-1})
B-dropouts ($z \sim 4$)	
-22.26	0.00001 ± 0.00001
-21.76	0.00011 ± 0.00002
-21.26	0.00025 ± 0.00003
-20.76	0.00067 ± 0.00004
-20.26	0.00106 ± 0.00006
-19.76	0.00169 ± 0.00008
-19.26	0.00285 ± 0.00012
-18.76	0.00542 ± 0.00055
-18.26	0.00665 ± 0.00067
-17.76	0.01165 ± 0.00123
-17.26	0.01151 ± 0.00148
-16.76	0.02999 ± 0.00375
-16.26	0.02610 ± 0.01259
V-dropouts ($z \sim 5$)	
-21.66	0.00003 ± 0.00001
-21.16	0.00012 ± 0.00001
-20.66	0.00031 ± 0.00003
-20.16	0.00062 ± 0.00004
-19.66	0.00113 ± 0.00007
-19.16	0.00179 ± 0.00020
-18.66	0.00203 ± 0.00022
-18.16	0.00506 ± 0.00057
-17.66	0.00530 ± 0.00134
-17.16	0.00782 ± 0.00380
i-dropouts ($z \sim 6$)	
-22.13	0.00001 ± 0.00001
-21.63	0.00001 ± 0.00001
-21.13	0.00007 ± 0.00002
-20.63	0.00013 ± 0.00004
-20.13	0.00054 ± 0.00012
-19.63	0.00083 ± 0.00018
-18.88	0.00197 ± 0.00041
-17.88	0.00535 ± 0.00117

[a]The LF is tabulated at $1350\,\mathring{A}$ at $z \sim 6$.

TABLE 5
STY79 DETERMINATIONS OF THE SCHECHTER PARAMETERS FOR THE REST-FRAME UV LFs AT $z \sim 4$, $z \sim 5$, AND $z \sim 6$.

Dropout Sample	$<z>$	M_{UV}^*[a]	ϕ^* (10^{-3} Mpc^{-3})	α
B[b]	3.8	-21.06 ± 0.10	1.1 ± 0.2	-1.76 ± 0.05
V[b]	5.0	-20.69 ± 0.13	$0.9^{+0.3}_{-0.2}$	-1.69 ± 0.09
i[b]	5.9	-20.29 ± 0.19	$1.2^{+0.6}_{-0.4}$	-1.77 ± 0.16

[a]Values of M_{UV}^* are at $1600\,\mathring{A}$ for our B and V-dropout samples and at $\sim 1350\,\mathring{A}$ for our i-dropout sample. Since $z \sim 6$ galaxies are blue ($\beta \sim -2$: Stanway et al. 2005; B06), we expect the value of M^* at $z \sim 6$ to be very similar ($\lesssim 0.1$ mag) at $1600\,\mathring{A}$ to the value of M^* at $1350\,\mathring{A}$.

[b]Parameters determined using the STY79 technique (§3.1) not including evolution across the redshift window of the samples (see Table 7 for the parameters determined including evolution).

3.3. *Robustness of Schechter Parameter Determinations*

It seems legitimate to ask how robust the Schechter parameters are that we derived in §3.1 using the STY79 method. There are a number of different approaches to treating large-scale structure uncertainties, for example, and we could have easily adopted a different approach (i.e., matching up the counts from each of our surveys and then deriving the LFs through a direct approach as we did in B06). By the same token, we also could have chosen to derive the LFs using a different set of SED templates, different assumptions regarding the Lyα equivalent widths, different opacity models for absorption from neutral hydrogen clouds, or even different dropout criteria. To ensure that our LF determinations were not unreasonably affected by these choices, we repeated the present determinations of the LF at $z \sim 4$, $z \sim 5$, and $z \sim 6$ adopting a wide variety of different approaches. A detailed description of each of these determinations is provided in Appendix B. The corresponding Schechter parameters are summarized in Table 6. In general, these other determinations are in reasonable agreement with our fiducial STY79 determinations, though it is clear that there are a few variables that can have a small ($\pm20\%$) effect on the derived parameters.

The following are our most significant findings: (1) We found less evolution in the value of M^* from $z \sim 6$ to $z \sim 4$ when making the measurement at a bluer rest-frame wavelength (i.e., $\sim 1350\,\mathring{A}$) than we did when making this measurement at $\sim 1600\,\mathring{A}$. This is likely the result of the fact that L^* galaxies at $z \sim 4$ (Ouchi et al. 2004) are much redder than they are at $z \sim 5-6$ (Lehnert & Bremer 2003; Stanway et al. 2005; B06). (2) The

inclusion of Lyα emission lines in the SEDs of the model star-forming galaxies (assuming that 33% of the sources have rest-frame equivalent widths of 50$\mathring{A}$: see Appendix B.5) has a modest effect on the selection volumes computed for our three dropout samples and results in a modest decrease in ϕ^* at $z \sim 4$ (by 10%), but increase in ϕ^* at $z \sim 5$ and $z \sim 6$ (by ~ 10%). (3) At $z \sim 4$, we found that our LF fit results could be somewhat sensitive to the distribution of UV colours used – depending upon the faint-end limit we adopted in our analysis. As a result, we restricted ourselves to galaxies brighter than 29 AB mag in our $z \sim 4$ LF fits above to improve the overall robustness of the fit results. (4) We found that the Schechter parameters for our high-redshift LFs only show a slight ($\lesssim 10$%) dependence upon the model we adopted for the opacity coming from neutral hydrogen clouds. (5) If we allow for evolution in M* across the redshift window of each sample (by 0.35 mag per unit redshift as we find in our fiducial STY79 determinations), we recovered a slightly fainter value of M* (by $\sim$0.06 mag), a higher value of ϕ^* (by $\sim$10%), and a shallower faint-end slope α (by $\sim$0.02) for our LF. (6) In each and every analysis we considered, we found a significant (~ 0.5 mag to ~ 0.9 mag) brightening of M^* from $z \sim 6$ to $z \sim 4$, suggesting that this evolutionary finding is really robust. We also consistently recovered a very steep ($\alpha \lesssim -1.7$) faint-end slope. We would consider both of these conclusions to be quite solid.

Of all the issues considered in this section, the only issue which would clearly bias our LF determinations and for which we can accurately make a correction is the issue of evolution across the redshift selection windows of our dropout samples. Since this issue only has a minimal effect on the LF fit results (i.e., $\Delta M \sim 0.06$ mag, $\Delta\phi^*/\phi^* \sim 0.1$, $\Delta\alpha \sim 0.03$) and an even smaller effect on integrated quantities like the luminosity density, we will not be repeating much of the analysis done thus far to include it. Instead, we will simply adopt the results of the STY79 approach including this evolution in M^* with redshift (Table 6: see Appendix B.8) hereafter as our preferred determinations of the Schechter parameters at $z \sim 4$, $z \sim 5$, and $z \sim 6$ (see Table 7).

3.4. *Faint-end Slope*

It is worthwhile to spend a little time reemphasizing how robust the current determination of a steep faint-end slope really is and how readily this result can be derived from the data. In fact, we could have determined the faint-end slope α at $z \sim 4$ simply from our HUDF B-dropout selection alone. At a rudimentary level, this can be seen from the number counts, which in our HUDF B-dropout sample increases from surface densities of 3 sources arcmin^{-2} at $i_{775,AB} \sim 25.5$ to 30 sources arcmin^{-2} at $i_{775,AB} \sim 29$, for a faint-end slope of $\sim 0.3\,\mathrm{dex/mag} \sim 0.7$ (*red line* in Figure 5). Since the selection volume is largely independent of magnitude over this range, one can essentially "read off" the faint-end slope from the number counts and find that it is steep ~ -1.7. Use of our LF methodology on our HUDF selections permits a more rigorous determination and yields $\alpha = -1.76 \pm 0.07$ at $z \sim 4$. We should emphasize that these results are robust and are not likely to be sensitive to concerns about large-scale structure (the counts are
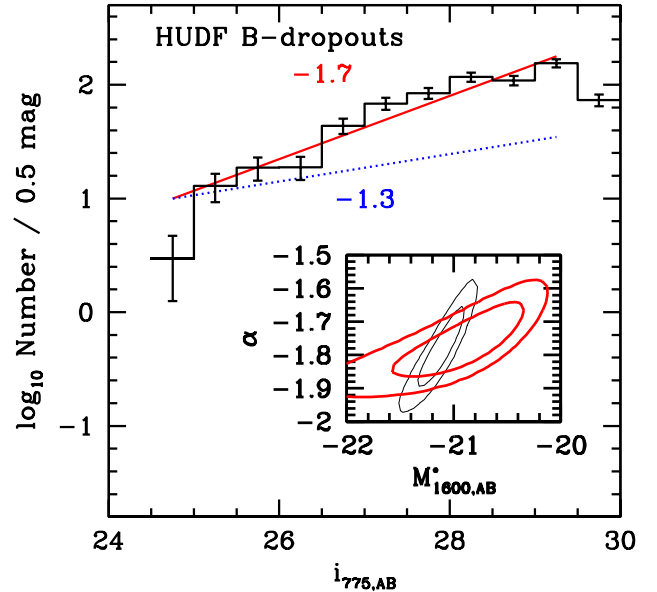

FIG. 5.— Surface density (number counts) of B-dropouts in the HUDF as a function of their i_{775}-band magnitude. The surface density of dropouts increases quite rapidly towards faint magnitudes. Since the selection volume is independent of magnitude (to first approximation), it is possible to obtain a rough estimate of the faint-end slope α of the LF from the number counts. Since the number counts have a faint-end slope of ~ 0.7 (*shown as a solid red line*), this corresponds to a faint-end slope α for the *LF* of ~ -1.7. Note that if the faint-end slope of the LF were ~ -1.3 (as obtained in the recent determinations of Sawicki & Thompson 2006a and Gabasch et al. 2004), the faint-end slope of the number counts would need to be ~ 0.3 (*shown as a dotted blue line*), which it clearly is not. (*inset*) 68% and 95% likelihood contours on the values of M^* and α from our HUDF B-dropout selection (*thick red lines*) and GOODS B-dropout selection (*thin black lines*) considered separately. The HUDF data demonstrate quite clearly that the faint-end slope α of the UV LF at $z \sim 4$ is very steep (-1.76 ± 0.07). Note that independent support for such a steep faint-end slope is provided from our GOODS B-dropout selection (*likelihood contours shown with the thin black lines*), where the preferred value is -1.78 ± 0.08. Our HUDF-Ps B-dropout selection also supports a steep faint-end slope $\lesssim -1.5$ (95% confidence).

drawn from a single field), small number statistics (the HUDF contains $\gtrsim 700$ B-dropout sources), or contamination (all known contaminants have *shallower* faint-end slopes). Even the model selection volumes are not a concern for our conclusion that the faint-end slope is steep since we can derive this conclusion from simple fits to the number counts (i.e., the *red line* in Figure 5) as argued above and the inclusion of realistic selection volumes (which *decrease* towards fainter magnitudes) would only cause the inferred faint-end slope to be steeper. Similarly steep slopes are obtained from independent fits to the B-dropouts in our other fields (HUDF-Ps and both GOODS fields) and our other dropout selections, suggesting that a steep (~ -1.7) faint-end slope is really a generic feature of high-redshift luminosity functions (see also Beckwith et al. 2006; Yoshida et al. 2006; Oesch et al. 2007).

3.5. *Luminosity / SFR Densities*

Having derived the rest-frame UV LF at $z \sim 4$, $z \sim 5$, and $z \sim 6$, we can move on to establish the luminosity densities at these epochs. The luminosity densities are of great interest because of their close link to the SFR densities. But, unlike the SFR densities inferred from

TABLE 6
DETERMINATIONS OF THE SCHECHTER PARAMETERS FOR THE REST-FRAME UV LFs AT $z \sim 4$, $z \sim 5$, AND $z \sim 6$.

Method	M_{UV}^* [a]	B-dropouts ($z \sim 4$) ϕ^* (10^{-3} Mpc^{-3})	α	M_{UV}^* [a]	V-dropouts ($z \sim 5$) ϕ^* (10^{-3} Mpc^{-3})	α
STY79	-21.06 ± 0.10	1.1 ± 0.2	-1.76 ± 0.05	-20.69 ± 0.13	$0.9^{+0.3}_{-0.2}$	-1.69 ± 0.09
χ^2 (w/ LSS correction)[b]	-21.07 ± 0.10	1.1 ± 0.2	-1.76 ± 0.04	-20.69 ± 0.13	0.9 ± 0.3	-1.72 ± 0.09
χ^2 (w/o LSS correction)[c]	-21.04 ± 0.10	1.1 ± 0.2	-1.74 ± 0.04	-20.62 ± 0.13	1.0 ± 0.3	-1.66 ± 0.09
STY79 (~ 1350 Å)[d]	-20.84 ± 0.10	1.4 ± 0.3	-1.81 ± 0.05	-20.73 ± 0.26	0.8 ± 0.4	-1.68 ± 0.19
STY79 (mean $\beta = -1.4$)[e]	-21.20 ± 0.14	0.9 ± 0.2	$-1.86 \pm 0.06^*$	-20.66 ± 0.12	1.0 ± 0.3	-1.66 ± 0.09
STY79 (mean $\beta = -2.1$)[e]	-21.16 ± 0.14	0.9 ± 0.2	-1.79 ± 0.05	-20.65 ± 0.12	1.1 ± 0.3	-1.70 ± 0.09
STY79 (Lyα contribution)[f]	-21.05 ± 0.10	1.0 ± 0.2	-1.76 ± 0.05	-20.70 ± 0.13	1.0 ± 0.3	-1.68 ± 0.09
STY79 (alt criteria)[g]	-20.97 ± 0.13	1.0 ± 0.2	-1.81 ± 0.06	-20.57 ± 0.11	1.3 ± 0.3	-1.63 ± 0.08
STY79 (Madau opacities)[h]	-21.06 ± 0.10	1.1 ± 0.2	-1.75 ± 0.05	-20.66 ± 0.12	1.0 ± 0.3	-1.71 ± 0.09
STY79 (Evolving M*)[i,**]	-20.98 ± 0.10	1.3 ± 0.2	-1.73 ± 0.05	-20.64 ± 0.13	1.0 ± 0.3	-1.66 ± 0.09
		i-dropouts ($z \sim 6$)				
STY79	-20.29 ± 0.19	$1.2^{+0.6}_{-0.4}$	-1.77 ± 0.16			
χ^2 (w/ LSS correction)[b]	-20.53 ± 0.25	$0.7^{+0.4}_{-0.2}$	-2.06 ± 0.20			
χ^2 (w/o LSS correction)[c]	-20.36 ± 0.25	$0.9^{+0.5}_{-0.3}$	-1.88 ± 0.20			
STY79 (mean $\beta = -1.4$)[e]	-20.22 ± 0.18	$1.2^{+0.5}_{-0.3}$	-1.73 ± 0.16			
STY79 (mean $\beta = -2.1$)[e]	-20.26 ± 0.19	$1.2^{+0.6}_{-0.3}$	-1.73 ± 0.16			
STY79 (Lyα contribution)[f]	-20.31 ± 0.19	$1.3^{+0.6}_{-0.4}$	-1.76 ± 0.16			
STY79 (alt criteria)[g]	-20.39 ± 0.23	$1.0^{+0.5}_{-0.4}$	-1.78 ± 0.17			
STY79 (Madau opacities)[h]	-20.32 ± 0.19	$1.3^{+0.6}_{-0.4}$	-1.76 ± 0.16			
STY79 (Evolving M*)[i,**]	-20.24 ± 0.19	$1.4^{+0.6}_{-0.4}$	-1.74 ± 0.16			

[a] Values of M_{UV}^* are at 1600 Å for our B and V-dropout samples and at ~ 1350 Å for our i-dropout sample. Since $z \sim 6$ galaxies are blue ($\beta \sim -2$: Stanway et al. 2005; B06), we expect the value of M^* at $z \sim 6$ to be very similar ($\lesssim 0.1$ mag) at 1600 Å to the value of M^* at 1350 Å.
[b,c,d,e,f,g,h,i] LF determinations considered in Appendices B.1, B.2, B.3, B.4, B.5, B.6, B.7, and B.8, respectively.
[*] Only galaxies brighter than 28 AB mag are used in the fit results (see Appendix B.4)
[**] Adopted determinations of the Schechter parameters: see Table 7

TABLE 7
ADOPTED DETERMINATIONS OF THE SCHECHTER PARAMETERS FOR THE REST-FRAME UV LFs AT $z \sim 4$, $z \sim 5$, $z \sim 6$, AND $z \sim 7.4$.

Dropout Sample	$<z>$	M_{UV}^* [a]	ϕ^* (10^{-3} Mpc^{-3})	α
B [b]	3.8	-20.98 ± 0.10	1.3 ± 0.2	-1.73 ± 0.05
V [b]	5.0	-20.64 ± 0.13	1.0 ± 0.3	-1.66 ± 0.09
i [b]	5.9	-20.24 ± 0.19	$1.4^{+0.6}_{-0.4}$	-1.74 ± 0.16
z [c]	7.4	-19.3 ± 0.4 (C) -19.7 ± 0.3 (L)	(1.4)	(-1.74)

[a] Values of M_{UV}^* are at 1600 Å for our B and V-dropout samples, at ~ 1350 Å for our i-dropout sample, and at ~ 1900 Å for our z-dropout sample. Since $z \sim 6$ galaxies are blue ($\beta \sim -2$: Stanway et al. 2005; B06), we expect the value of M^* at $z \sim 6$ to be very similar ($\lesssim 0.1$ mag) at 1600 Å to the value of M^* at 1350 Å. Similarly, we expect M^* at $z \sim 7-8$ to be fairly similar at ~ 1600Å to the value at ~ 1900Å.
[b] Parameters determined using the STY79 technique (§3.1) including evolution across the redshift window of the samples (Appendix B.8). They therefore differ from those in Table 5 which do not.
[c] M_{UV}^* are derived from both the conservative and less-conservative z_{850}-dropout search results of Bouwens & Illingworth (2006) (denoted here as "(C)" and "(L)" respectively) assuming simple evolution in M^* and keeping the values of ϕ^* and α fixed at the values we derived for these parameters at $z \sim 6$ (see §5.4). Since both ϕ^* and α show no significant evolution over the interval $z \sim 6$ to $z \sim 4$, we assume that this holds at even earlier times and that $\phi^* = 0.0014$ Mpc^{-3} and $\alpha = -1.74$. These determinations are only mildly sensitive to the assumed values of ϕ^* and α. Steeper values of α (i.e., $\alpha \sim -2$) yield M^*'s that are ~ 0.1 mag brighter and shallower values of α (i.e., $\alpha \sim -1.4$) yield M^*'s that are 0.1 mag fainter. Changing ϕ^* by a factor of 2 only changes M^* by 0.3 mag.

luminosity density measurements, the luminosity densities are much more directly relatable to the observations themselves, requiring fewer assumptions. As such, they can be more useful when it comes to comparisons between different determinations in the literature, particularly when these determinations are made at the same redshift.

It is common in determinations of the luminosity density to integrate the LF to the observed faint-end limit. Here we consider two faint-end limits: $0.04\ L_{z=3}^*$ (to match the limits reached by our LF at $z \sim 6$) and $0.3\ L_{z=3}^*$ (to match the limits reached at $z \sim 7-10$: Bouwens et al. 2004c; Bouwens et al. 2005; Bouwens & Illingworth 2006). For convenience, we have compiled the calculated luminosity densities for our $z \sim 4$ and $z \sim 5$ UV LFs in Table 8. We have also included these luminosity densities for our most recent search results for galaxies at $z \sim 7-8$ (Bouwens & Illingworth 2006). The UV luminosity density at $z \sim 6$ is modestly lower ($0.45 \pm 0.09\times$) than that at $z \sim 4$ (integrated to -17.5 AB mag).

The inferred evolution in the UV luminosity density from $z \sim 6$ to $z \sim 4$ does not change greatly if we include the expected flux from very low luminosity galaxies, since the LFs have very similar slopes. Integrating our best-fit LFs to a much fainter fiducial limit, i.e., -10 AB mag (significant suppression of galaxy formation would seem to occur faintward of this limit if not at even brighter magnitudes: e.g., Read et al. 2006; Wyithe & Loeb 2006; Dijkstra et al. 2004), we find a luminosity density at $z \sim 6$ which is just 0.5 ± 0.2 times the luminosity density at $z \sim 4$. This is very similar to the evolution

TABLE 8
Observed Luminosity Densities.[a]

Dropout Sample	$< z >$	$\log_{10}\mathcal{L}$ (ergs s^{-1} Hz^{-1} Mpc^{-3}) $L > 0.3L^*_{z=3}$	$L > 0.04L^*_{z=3}$
B	3.8	26.09±0.05	26.42±0.05
V	5.0	25.74±0.06	26.11±0.06
i	5.9	25.59±0.08	26.07±0.08
z	7.4	24.75±0.48	25.58

[a]Based upon LF parameters in Table 7. At $z \sim 7.4$, the luminosity densities are based upon the search results for the Bouwens & Illingworth (2006) conservative selection (§5.4).

found (0.45±0.09) when integrating our LFs to -17.5 AB mag.

We have compared our results to several previous determinations in the Figure 6. To our bright magnitude limit (*top panel*), the present results appear to be in good agreement with several previous findings at $z \sim 4$ (Giavalisco et al. 2004b; Ouchi et al. 2004). At $z \sim 5$, our results are somewhat lower than those of Giavalisco et al. (2004b) and Yoshida et al. (2006). To our faint magnitude limit (*bottom panel*), the only previous determinations which are available at $z \sim 4$, $z \sim 5$, and $z \sim 6$ are those of Beckwith et al. (2006). At each redshift interval, our determinations of the luminosity density are similar, albeit slightly higher. For a more complete discussion of how the present LFs and thus luminosity densities compare with previous determinations, we refer the reader to §4.3.

It is also of interest to convert the luminosity densities into the equivalent *dust-uncorrected* SFR densities using the Madau et al. (1998) conversion factors:

$$L_{UV} = \text{const x } \frac{\text{SFR}}{M_\odot \text{yr}^{-1}} \text{ergs s}^{-1}\text{ Hz}^{-1} \qquad (3)$$

where const $= 8.0 \times 10^{27}$ at 1500 $\mathring{A}$ and where a 0.1-125 $M_\odot$ Salpeter IMF and a constant star formation rate of $\gtrsim 100$ Myr are assumed. In view of the young ages ($\sim$ 10-50 Myr) of many star-forming galaxies at $z \sim 5-6$ (e.g., Yan et al. 2005; Eyles et al. 2005; Verma et al. 2007), there has been some discussion about whether the latter assumption would cause us to systematically underestimate the SFR density of the universe at very early times (Verma et al. 2007).

To calculate the total SFR density at early times, we must of course make a correction for the dust obscuration. Correcting for dust obscuration is a difficult endeavor and can require a wide variety of multiwavelength observations to obtain an accurate view of the total energy output by young stars. We will not attempt to improve upon previous work here and will simply rely upon several estimates of the dust extinction obtained in previous work. At $z \lesssim 3$, we will use the dust corrections of Schiminovich et al. (2005) and at $z \sim 6$ we will use a dust correction of ~ 0.18 dex (factor of ~ 1.5), which we derived from the β's observed for $z \sim 6$ i-dropouts (Stanway et al. 2005; Yan et al. 2005; B06) and the IRX-β relationship (Meurer et al. 1999). The IRX-β relationship provides a fairly good description of the dust extinction at $z \sim 0$ (e.g., Meurer et al. 1999) and $z \sim 2$ (Reddy & Steidel 2004; Reddy et al. 2006).
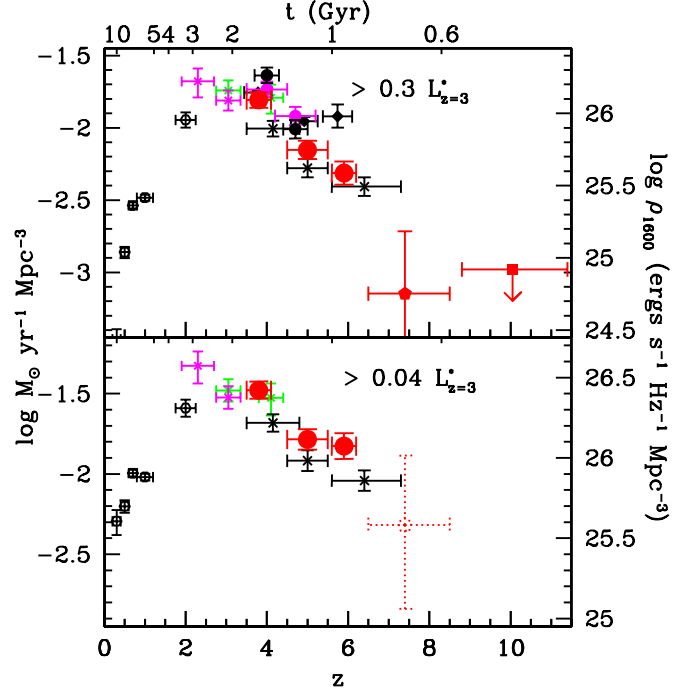

FIG. 6.— The rest-frame UV continuum luminosity density integrated to $0.3L^*_{z=3}$ (top panel) and $0.04L^*_{z=3}$ (bottom panel) as a function of redshift. The equivalent star formation rate density is also shown assuming no extinction correction. The rest-frame UV continuum luminosity density is converted to a star formation rate density assuming a constant $> 10^8$ yr star formation model and a Salpeter (1955) IMF (Madau et al. 1998). The present determinations are shown as large red circles, with 1σ errors. Also shown are the luminosity density determinations by Schiminovich et al. (2005: *black hexagons*), Steidel et al. (1999: *green crosses*), Giavalisco et al. (2004b: *black diamonds*), Ouchi et al. (2004: *magenta circles*), Yoshida et al. (2006: *black circles*), Beckwith et al. (2006: *black crosses*), Reddy et al. (2007: *magenta crosses*), Bouwens & Illingworth (2006: *red pentagons*), and Bouwens et al. (2005: *red square* shown with its 1σ upper limit). The dotted hexagon in the lower panel shows the inferred luminosity density at $z \sim 7.4$ assuming our fit results for the Bouwens & Illingworth (2006) conservative selection (§5.4: Table 7).

At redshifts of $z \sim 4 - 5$, we will interpolate between the dust extinctions estimated at $z \sim 2 - 3$ and those at $z \sim 6$. The results of these calculations are shown in Figure 7 for the luminosity densities integrated down to $0.04L^*_{z=3}$ (the faint-end limit for our $z \sim 6$ searches) and $0.3L^*_{z=3}$ (the faint-end limit for our $z \sim 7 - 10$ searches). These star formation rate densities are also tabulated in Table 9. At $z \sim 6$, the star formation rate density is just ~ 0.3 times the SFR density at $z \sim 4$ (integrated to -17.5 AB mag). Clearly the star formation rate density seems to increase much more rapidly from $z \sim 6$ to $z \sim 4$ than the UV luminosity density does. This is a direct result of the apparent evolution in the dust obscuration over this redshift interval.

4. ROBUSTNESS OF LF RESULTS

In the previous section, we used our very deep and wide-area B, V, and i dropout selections to determine the UV-continuum LF at $z \sim 4$, $z \sim 5$, and $z \sim 6$ to $\sim 3 - 5$ mag below L^*. This is fainter than all previous probes not including the HUDF data. Since these determinations reach such luminosities with significant statistics and over multiple fields, they have the promise to provide us with a powerful measure of how galaxies are

TABLE 9
INFERRED STAR FORMATION RATE DENSITIES.[a]

Dropout Sample	$< z >$	$\log_{10}$ SFR density ($M_\odot$ Mpc^{-3} yr^{-1})	
		$L > 0.3 L^*_{z=3}$	$L > 0.04 L^*_{z=3}$
		Uncorrected	
B	3.8	-1.81 ± 0.05	-1.48 ± 0.05
V	5.0	-2.15 ± 0.06	-1.78 ± 0.06
i	5.9	-2.31 ± 0.08	-1.83 ± 0.08
z	7.4	-3.15 ± 0.48	-2.32
		Dust-Corrected	
B	3.8	-1.38 ± 0.05	-1.05 ± 0.05
V	5.0	-1.85 ± 0.06	-1.48 ± 0.06
i	5.9	-2.14 ± 0.08	-1.65 ± 0.08
z	7.4	-2.97 ± 0.48	-2.14

[a]Based upon LF parameters in Table 7 (see §3.5). At $z \sim 7.4$, the luminosity densities are based upon the search results for the Bouwens & Illingworth (2006) conservative selection.
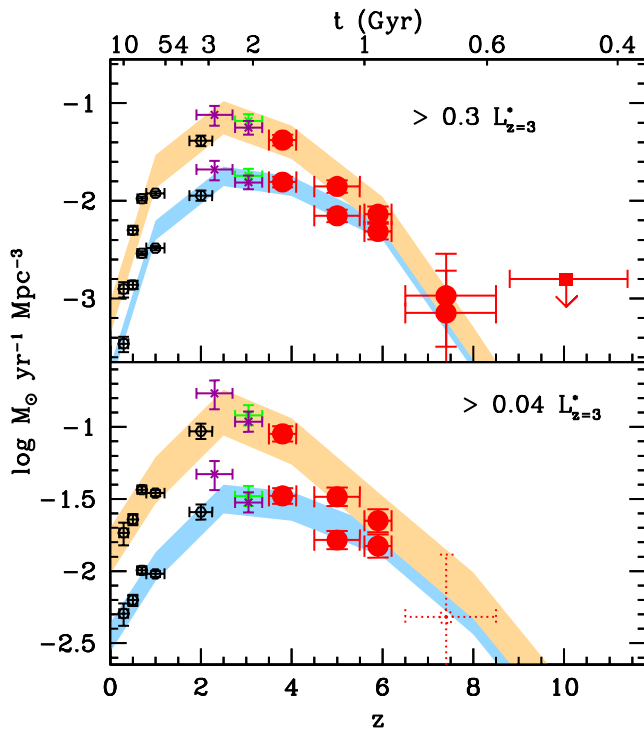
FIG. 7.— Star formation rate density of the universe integrated down to 0.3 $L^*_{z=3}$ (*top panel*) and 0.04$L^*_{z=3}$ (*bottom panel*). This SFR density is shown both with and without a correction for dust extinction (*upper and lower set of points, respectively*). This is also indicated with the shaded red and blue regions, where the width of the region shows the approximate uncertainties estimated by Schiminovich et al. (2005). Symbols for the data points are the same for Figure 6. At $z \lesssim 3$, the dust corrections we assume are 1.4 mag and are intermediate between the high and low estimates of Schiminovich et al. (2005: 1.8 mag and 1.0 mag, respectively). At $z \sim 6$, the dust corrections are 0.4 mag as determined from the steep UV-continuum slopes (B06). At $z \sim 4 - 5$, the dust corrections are interpolations between the $z \sim 3$ and $z \sim 6$ values.

evolving at early times. However, given the considerable spread in LF results to date and significant differences in interpretation, it is important first to discuss the robustness of the current LF results. We devote some effort to this issue because the wide dispersion in observational results is really limiting their value.

4.1. *Completeness of Current Census*

In this work, our goal was to derive rest-frame UV LFs that was representative of the star-forming galaxy population at $z \sim 3.5 - 6.5$. However, since our LFs were based upon simple colour selections, it seems legitimate to ask how complete these selections are, and whether our selection might miss a fraction of the high-redshift galaxy population. Such concerns have become particularly salient recently given claims from spectroscopic work that LBG selections may miss a significant fraction of the high-redshift galaxy population that are UV bright at $z \gtrsim 3$ (e.g., Le Fèvre et al. 2005; Paltani et al. 2006). We refer our readers to Franx et al. (2003), Reddy et al. (2005), and van Dokkum et al. (2006) for an excellent discussion of these issues at slightly lower redshifts ($z \sim 2 - 3$).

Figure 8 shows a colour-colour diagram illustrating our $z \sim 4$ B-dropout and $z \sim 5$ V-dropout selections. The expected colours of galaxies with different UV continuum slopes plotted as a function of redshift to show how our selection depends upon the UV colour. To illustrate how the observed distribution of dropout colours compares with these selections, a small sample of bright dropouts are overplotted on these diagrams. We elected to only include the bright dropouts on this diagram because it is only at bright magnitudes that we can efficiently select dropouts over a wide-range of UV-continuum slopes. Since all high-redshift galaxies will become quite red in their Lyman-break colours ($B-V$ for $z \gtrsim 4$ galaxies and $V-i$ for $z \gtrsim 5$ galaxies), it seems clear that the only way galaxies will miss our selection is if they are too red in their UV-continuum slopes. As is evident in the figure, the majority of the dropouts in our B and V-dropout selections are significantly bluer than our selection limits in $(V_{606} - z_{850})_{AB}$ and $(i_{775} - z_{850})_{AB}$, respectively. Unless is a distinct population of star-forming galaxies which are much redder than these limits (i.e., the UV colour distribution is bimodal), we can conclude that our selection must be largely complete at bright magnitudes. Another way of seeing this is to compare the distribution of observed UV-continuum slopes β (calculated from the $i_{775} - z_{850}$ colours) for bright ($i_{775,AB} < 24.6$) B-dropouts from our sample with the selection limit (*insert* on Figure 8), and it is again apparent that the bulk of our sample is significantly blueward of the selection limit.

Independent evidence for the $z \sim 4$ galaxy population having very blue UV-continuum slopes is reported by Brammer & van Dokkum (2007). By applying a Balmer-break selection to the Faint Infrared Extragalactic Survey (FIRES) data (Labbé et al. 2003; Förster Schreiber et al. 2006), Brammer & van Dokkum (2007) attempt to isolate a sample of $z \sim 4$ galaxies with sizeable breaks. Since almost all ($\gtrsim 90\%$) of the galaxies in their $z \sim 4$ sample have measured UV-continuum slopes bluer than 0.5 (and none having UV-continuum slopes redder than 1.0), this again argues that the $z \sim 4$ galaxy population is very blue in general. The key point to note in the Brammer & van Dokkum (2007) analysis is that in contrast to our LBG selection their Balmer-break selection should not be significantly biased against galaxies with very red UV-continuum slopes. Therefore, unless there is a distinct population of UV-bright galaxies with minimal Balmer breaks *and* very red UV-continuum slopes
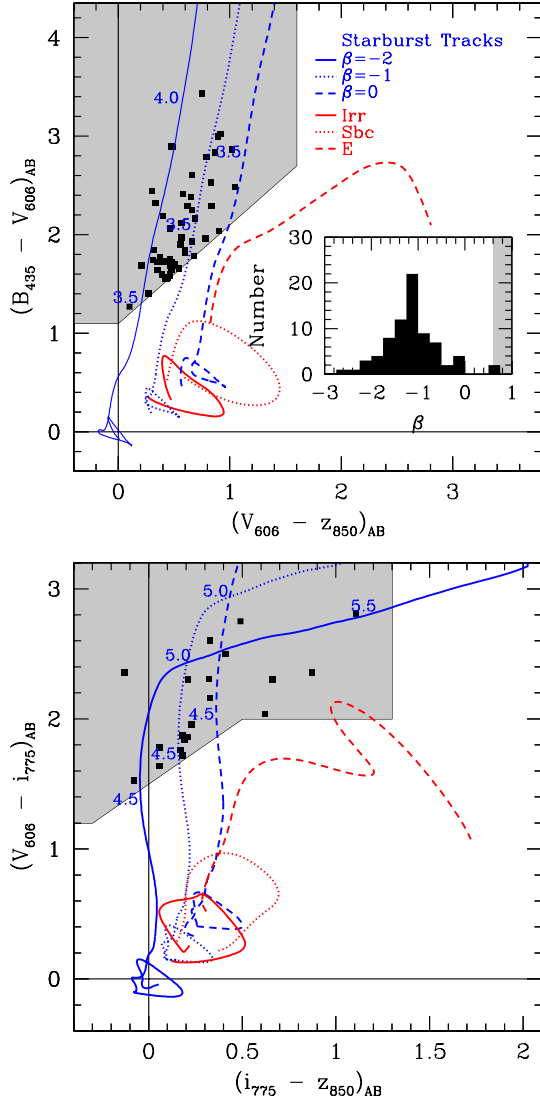
FIG. 8.— (*top*) Colour-colour diagram used to select B-dropout galaxies over our deep ACS fields. The blue tracks shown the expected colours of starbursts with different UV-continuum slopes as a function of redshift, while the red lines show the colours of low-redshift interlopers. Attenuation from the Lyman forest was calculated using an opacity model which better fits recent observations (e.g., Songaila 2004: see Appendix A.3) than the Madau (1995) prescription does. The black squares shows the position of all bright ($i_{775,AB} < 24.6$) sources in our B-dropout sample. Only sources which are detected in the B band are shown to simplify the interpretation of this figure. This diagram shows that our B-dropout selection should be effective in selecting star-forming galaxies with UV-continuum slopes β of $\sim$0.5 and bluer. Since most B-dropouts in our sample are much bluer than this selection limit, this suggests that our census of star-forming galaxies at $z \sim 3 - 4$ is largely complete ($\gtrsim 90\%$) at bright magnitudes (unless there is a distinct population of galaxies with much redder UV continuum slopes). The insert presents the selection more explicitly in terms of β, comparing the distribution of UV-continuum slopes for this bright sample of B-dropouts with the region in β space where galaxies are not selectable ($\beta \gtrsim 0.5$: *grey region*). Again, it is quite clear that the observed distribution of β's is much bluer on average than the selection limit. (*Bottom*) Similar colour-colour diagram for our V-dropout selection. Black squares represent all the bright ($z_{850,AB} < 25$) V-dropouts in CDF-South GOODS field and HUDF ($z_{850,AB} < 27$) with optical-infrared colours consistent with these sources being at high redshift ($z \gtrsim 4$). Our V-dropout criterion should select star-forming galaxies to very red UV-continuum slopes ($\beta \lesssim 2 - 3$). We do not show the distribution of UV-continuum slopes for our bright V-dropout samples because they cannot be derived from the optical data. To measure such slopes, we require two fluxes unaffected by Lyman forest absorption and we only have one (z_{850}-band flux) for V-dropouts.

(which seems unlikely given that galaxies with redder UV colours have more dust, which in turn suggests a more evolved stellar population), it would appear that our census of UV-bright galaxies at $z \sim 4 - 6$ is largely complete. Apparently, the very red $\beta \sim 1 - 2$ population seen at $z \sim 2 - 3$ (e.g., van Dokkum et al. 2006) has not developed significantly by $z \sim 4$.

4.2. Cosmic Variance

One generic concern for the determination of any luminosity function is the presence of large-scale structure. This structure results in variations in the volume density of galaxies as a function of position. For our dropout studies, these variations are mitigated by the large co-moving distances surveyed in redshift space ($\sim 300 - 500$ Mpc for a $\Delta z \sim 0.7$) for typical selections (see, e.g., Figure A2). Since these distances cover $\sim 40 - 100$ correlation lengths, typical field-to-field variations of $\sim 16 - 35\%$ are found in the surface density of dropouts (Somerville et al. 2004; Bunker et al. 2004; B06; Beckwith et al. 2006).

Fortunately, these variations should only have a very minor effect on our results, and this effect will largely be on the normalization of our LFs. It should not have a sizeable effect on the shape of our LF determinations, because of our use of the STY79 and SWML techniques – which are only mildly sensitive to these variations in the modified form used here (see Appendix C). The uncertainty in the normalization of our LFs was derived by taking the expected variations expected over each GOODS field (22% RMS, 18% RMS, and 22% RMS for our B, V, and i-dropout selections, respectively: see §3.1) and dividing by $\sqrt{2}$ to account for the fact that we have two independent fields. This implies a $\sim 14\%$ RMS uncertainty in the overall normalization. We incorporated this into our final results by convolving our likelihood distributions for ϕ^* with this smoothing kernel (§3.1).

4.3. Comparison with Previous Determinations at $z \sim 4$, $z \sim 5$, and $z \sim 6$

It is helpful to compare LFs with several previous determinations to put the current results in context and provide a sense for their reliability. We will structure this section somewhat in order of depth, beginning with a discussion of all pre-HUDF determinations of the UV LF at $z \sim 4$ and at $z \sim 5$ before moving onto more recent work involving the HUDF (Beckwith et al. 2006). We postpone a discussion of the UV LF at $z \sim 6$ until the end of this section because we had included a fairly comprehensive discussion of previous $z \sim 6$ determinations in B06.

4.3.1. Comparison at $z \sim 4$

At $z \sim 4$, there had already been a number of notable determinations of the UV LF (Steidel et al. 1999; Ouchi et al. 2004; Gabasch et al. 2004; Sawicki & Thompson 2006a; Giavalisco 2005; Yoshida et al. 2006; Paltani et al. 2006; Tresse et al. 2006). These include a determination of the $z \sim 4$ LF from Steidel et al. (1999) based upon an early imaging survey for G dropouts, a determination based upon a B-dropout search over deep wide-area imaging (1200 arcmin^2) available over the Subaru XMM-Newton Deep Field and Subaru Deep Field (SDF: Ouchi

TABLE 10
DETERMINATIONS OF THE BEST-FIT SCHECHTER PARAMETERS FOR THE REST-FRAME UV LFs AT $z \sim 4$.

Reference	M_{UV}^*	ϕ^* (10^{-3} Mpc^{-3})	α
This work	-20.98 ± 0.10	1.3 ± 0.2	-1.73 ± 0.05
Yoshida et al. (2006)	$-21.14^{+0.14}_{-0.15}$	$1.5^{+0.4}_{-0.4}$	-1.82 ± 0.09
Beckwith et al. (2006)	-20.7	1.3	-1.6 (fixed)
Sawicki & Thompson (2006)	$-21.0^{+0.4}_{-0.5}$	0.9 ± 0.5	$-1.26^{+0.40}_{-0.36}$
Giavalisco (2005)	-21.20 ± 0.04	1.20 ± 0.03	-1.64 ± 0.10
Ouchi et al. (2004)	-21.0 ± 0.1	1.2 ± 0.2	-2.2 ± 0.2
Steidel et al. (1999)	-21.2	1.1	-1.6 (assumed)
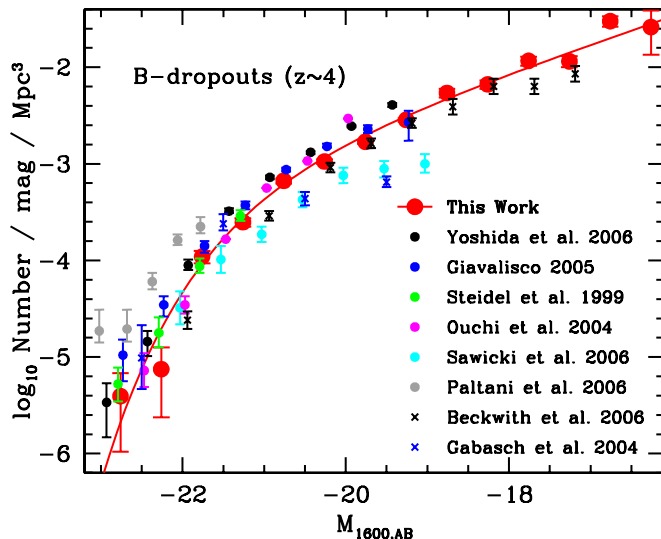
FIG. 9.— Comparison of our rest-frame UV-continuum LFs (Figure 3: *red line* and *red circles*) at $z \sim 4$ with those of other groups. Included in the comparison are the LFs of Steidel et al. (1999: *green circles*), Ouchi et al. (2004: *magenta circles*), Gabasch et al. (2004: *blue crosses*), Giavalisco (2005: *blue circles*), Sawicki & Thompson (2006a: *cyan circles*), Beckwith et al. (2006: *black crosses*), Yoshida et al. (2006: *black circles*), and Paltani et al. (2006: *grey circles*). In general, our $z \sim 4$ LF are in good agreement with previous determinations at bright magnitudes, but diverge somewhat from these determinations at fainter magnitudes.

et al. 2004), a determination based on a G-dropout search over ~ 180 arcmin^2 of imaging over the three Keck Deep Fields (Sawicki & Thompson 2006a), an earlier determination based upon the two wide-area (316 arcmin^2) ACS GOODS fields (Giavalisco 2005; Giavalisco et al. 2004b), a determination based upon a B-dropout search over a deeper version of the SDF (Yoshida et al. 2006), and several determinations based upon the VVDS spectroscopic sample (Paltani et al. 2006; Tresse et al. 2006). A comparison of these determinations is in Figure 9 and Table 10.

We will split our discussions between the bright and faint ends of the $z \sim 4$ LF. At bright magnitudes, our LF is in good agreement with most previous determinations. Though there is a fair amount of scatter between the individual LFs, the observed differences seem consistent with originating from small systematics in the photometry (± 0.1 mag). Our LF agree less well with the LFs derived from the VVDS spectroscopic sample (Le Fèvre et al. 2005; Paltani et al. 2006), underproducing their volume densities by factors of ~ 3. It is unclear why the VVDS results would be so different from those derived from standard LBG selections though it has been sug-

gested that this excess may arise from galaxies whose SEDs are quite a bit different from the typical LBG. In §4.1, we investigated whether this excess could result from galaxies with particularly red UV-continuum slopes, but found no evidence for a significant population of such galaxies at $z \sim 4$ using the GOODS broadband imaging data, in agreement with the results of Brammer & van Dokkum (2007). Despite this null result, it is possible that spectroscopic surveys have identified a population of bright galaxies at $z \sim 3 - 4$ whose colours are somewhat different from those typically used to model LBG selections (though there is some skepticism on this front: see, e.g., Reddy et al. 2007).

While such a population would need to be large to match the Paltani et al. (2006) numbers, it is interesting to ask what the effect of such a population would be on our derived UV LFs. To investigate this, we have replaced the bright points in our $z \sim 4$ LF with the Paltani et al. (2006) values (from their $z \sim 3 - 4$ LF) and then refit this LF to a Schechter function. We find $M^* = -21.88$, $\phi^* = 0.0005$ Mpc^{-3}, and $\alpha = -1.82$. Not surprisingly, the characteristic luminosity M^* is brighter than measured from our LBG selection, and the faint-end slope α a little steeper, but these changes only result in a slight ($\sim 14\%$) increase in the overall luminosity density at $z \sim 4$ to our faint-end limit (-16 AB mag). This being said, the reduced χ^2 ($= 3.2$) for the fit is poor, so we should perhaps not take these best-fit Schechter parameters too seriously.

At fainter magnitudes, differences with respect to other LFs become much more significant. At the one extreme, there is the Ouchi et al. (2004), Giavalisco (2005), and Yoshida et al. (2006) determinations which exceed our determination by factors of ~ 1.5, and at the other extreme, this is the determinations of Gabasch et al. (2004) and Sawicki & Thompson (2006a), which are a factor of $\sim 2 - 3$ lower. For the two most discrepant LFs, the difference in volume densities is nearly a factor of ~ 4. What could be the source of such a significant disagreement? Though it is difficult to be sure, there are a number of factors which could contribute to this large dispersion (e.g., the assumed Lyα equivalent width distribution, the assumed SED template set, the assumed β distribution, large-scale structure errors: see Appendix B). Perhaps, the most problematic, however, are the incompleteness, contamination, and flux biases present near the detection limit of these probes. Since these effects can be quite challenging to model and may result in modest to significant errors (factors of ~ 1.5 to 2 in the volume density), it is quite possible that some systematics have been introduced in performing the corrections.
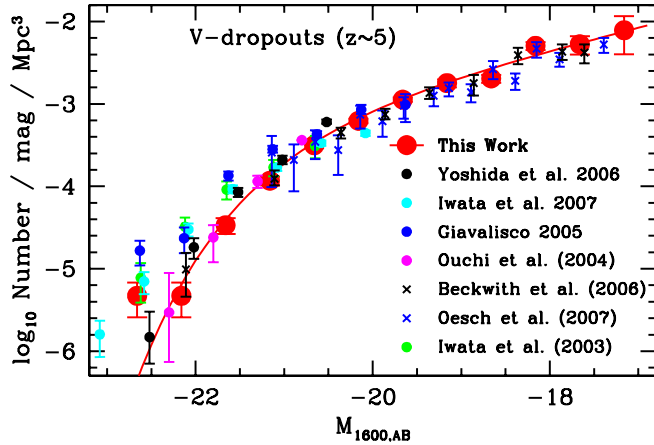
Fig. 10.— Comparison of our rest-frame *UV*-continuum LFs (Figure 3: *red line* and *red circles*) at $z \sim 5$ with those of other groups. Included in the comparison are the LFs of Iwata et al. (2003: *green circles*), Ouchi et al. (2004: *magenta circles*), Giavalisco (2005: *blue circles*), Yoshida et al. (2006: *black circles*), Iwata et al. (2007: *cyan circles*), Beckwith et al. (2006: *black crosses*), and Oesch et al. (2007: *blue crosses*). We are unable to match the Iwata et al. (2003) and Iwata et al. (2007) LFs at the bright end.

By contrast, we would expect our own determinations to be essentially immune to such large errors (to at least an AB mag of $\lesssim 28 - 28.5$) given that our deepest data set the HUDF extends some ~ 2.5 mag deeper than the data used in most previous determinations (the deep determinations of Beckwith et al. 2006 are discussed below). Even in our shallowest data sets, systematics should be much less of a concern in this magnitude range since we are able to make use of the significantly deeper HUDF, HUDF-Ps, and HUDF05 data to quantify the completeness, flux biases, and contamination through degradation experiments (see Appendix A.1). In conclusion, because of this greater robustness of our selection at faint magnitudes, we would expect our LF to be the most accurate in these regimes.

4.3.2. *Comparison at $z \sim 5$*

Now we will compare our results with several determinations of the LF at $z \sim 5$ using moderately deep data (Iwata et al. 2003; Ouchi et al. 2004; Giavalisco 2005; Yoshida et al. 2006; Iwata et al. 2007). Iwata et al. (2003) made their determination from deep Subaru data (~ 575 arcmin^2) they had around the larger HDF-North, Giavalisco (2005) from the wide-area (~ 316 arcmin^2) ACS GOODS data, Ouchi et al. (2004) from the deep wide-area (~ 1200 arcmin^2) Subaru data they had over the Subaru XMM-Newton Deep Field and SDF, Yoshida et al. (2006) from an even deeper imaging over the SDF, and Iwata et al. (2007) from the ~ 1290 arcmin^2 Subaru data around the HDF-North and J053+1234 region. A comparison of these LF determinations is provided in Figure 10 and Table 11.

Our $z \sim 5$ results are in excellent agreement with many previous studies (Yoshida et al. 2006; Ouchi et al. 2004), particularly at fainter magnitudes $z_{850,AB} > 25$. However, we are not able to reproduce the large number density of bright galaxies found by Iwata et al. (2003), Giavalisco (2005), and Iwata et al. (2007). We are unsure of why this might be – since field-to-field variations should not produce such large differences, but it has been spec-

ulated that a significant fraction of the candidates in the probes deriving the higher volume densities (e.g., Iwata et al. 2003; Iwata et al. 2007) may be contaminants (e.g., Ouchi et al. 2004). While Iwata et al. (2007) have argued, however, that such contamination rates are unlikely for their bright samples given the success of their own spectroscopic follow-up campaign ($\gtrsim 6$ out of 8 sources that they followed up at $24 < z_{AB} < 24.5$ were at $z \gtrsim 4$), we were only partially able to verify this success over the HDF-North GOODS field, where our searches overlap. Of the three bright ($z_{AB} \leq 24.5$) sources cited by Iwata et al. (2007) with spectroscopic redshifts, one (GOODS J123647.96+620941.7) appears to be an AGN. This suggests that a modest fraction of the sources in the Iwata et al. (2007) bright selection may be point-like contaminants like AGN (we note that Iwata [2007, private communcation] report that they removed this particular AGN from their bright sample). We will continue to regard our determination of the volume densities of the LF at $z \sim 5$ as the most robust due to the superb resolution and photometric quality of the GOODS data set (which allowed us to very effectively cull out high-redshift galaxies from our photometric samples and to reject both stars and AGNs).

Having discussed previous LFs at $z \sim 4 - 5$ based on shallower data, we compare our LF determinations with that obtained by Beckwith et al. (2006) at $z \sim 4$ and $z \sim 5$ using the HUDF data and Oesch et al. (2007) at $z \sim 5$ using the HUDF+HUDF05 data. We begin with the results of Oesch et al. (2007). Oesch et al. (2007) based their LFs on large *V*-dropout selections over the HUDF+HUDF05 fields and then combined their results with the Yoshida et al. (2006) results to derive best-fit Schechter parameters. Compared to our $z \sim 5$ LF results (which also take advantage of data from the GOODS, HUDF-Ps, and HUDF05-2 fields), the Oesch et al. (2007) LF appears to be in good overall agreement, albeit a little ($\sim 20-30\%$) lower at the faint-end. These differences appear to be attributable to (1) the larger ($\sim 20\%$) contamination corrections made by Oesch et al. (2007) and (2) Oesch et al. (2007) not correcting their fluxes for the light lost on the wings of the PSF (typically a $\sim 0.1-0.25$ mag correction for the small kron apertures appropriate for faint galaxies: Sirianni et al. 2007).

Beckwith et al. (2006) based their LFs on large *B* and *V*-dropout samples derived from the ACS HUDF and GOODS fields and used nearly identical selection criteria to those considered here. They also considered a LF fit which included several previous determinations (Steidel et al. 1999; Ouchi et al. 2004; Sawicki & Thompson 2006a) to demonstrate the robustness of their results. Their results are plotted in Figures 9 and 10 with the black crosses. Both LFs seem to be fairly similar to our own in their overall shape, but appear to be shifted to slightly lower volume densities. At the faint end of the LF, this shift is the most prominent. After careful consideration of the Beckwith et al. (2006) results, it appears that this occurs because Beckwith et al. (2006) do not include the modest incompleteness (see Figure A2) that occurs at fainter magnitudes near the upper redshift end of the selection (i.e., $z \gtrsim 4$ and $z \gtrsim 5.2$) due to photometric scatter. In addition, at $z \sim 5$, the faint end of the Beckwith et al. (2006) LF is derived from the HUDF, which as we show in Appendix B.1 (Table B1) is un-

TABLE 11
DETERMINATIONS OF THE BEST-FIT SCHECHTER PARAMETERS FOR THE REST-FRAME UV LFs AT $z \sim 5$.

Reference	M^*_{UV}	ϕ^* (10^{-3} Mpc^{-3})	α
This work	-20.64 ± 0.13	1.0 ± 0.3	-1.66 ± 0.09
Oesch et al. (2007)	-20.78 ± 0.21	0.9 ± 0.3	-1.54 ± 0.10
Iwata et al. (2007)	-21.28 ± 0.38	0.4 ± 0.3	$-1.48^{+0.38}_{-0.32}$
Yoshida et al. (2006)	$-20.72^{+0.16}_{-0.14}$	$1.2^{+0.4}_{-0.3}$	-1.82 (fixed)
Beckwith et al. (2006)	-20.55	0.9	-1.6 (fixed)
Giavalisco (2005)	-21.06 ± 0.05	0.83 ± 0.03	-1.51 ± 0.18
Iwata et al. (2003)	-21.4	0.4	-1.5
Ouchi et al. (2004)	-20.7 ± 0.2	1.4 ± 0.8	-1.6 (fixed)
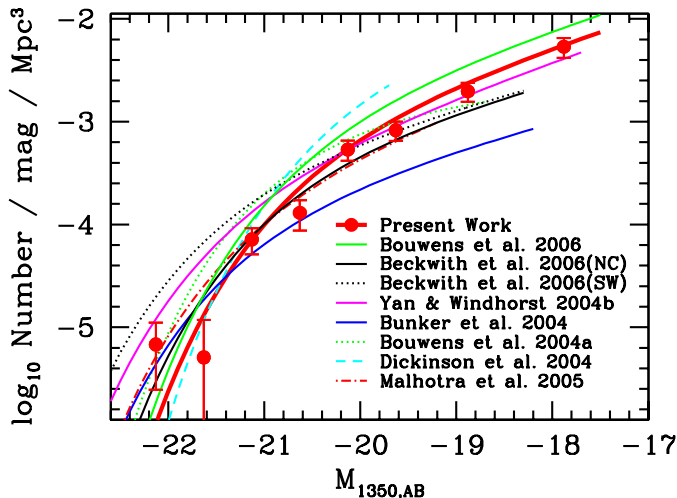
FIG. 11.— Comparison between the present determination of the LF at $z \sim 6$ and other determinations in the literature. Included in these comparisons are the LFs by Dickinson et al. (2004: *dashed light blue line*), Bouwens et al. (2004a: *dotted green line*), Yan & Windhorst (2004: *solid magenta line*), Bunker et al. (2004: *solid blue line*), and Malhotra et al. (2005: *red dot-dashed line*). For Beckwith et al. (2006), we present both the LF derived from a fit to the number counts (*solid line*) and that obtained by applying a simple offset to the counts (*dotted black line*). The present determination of the $z \sim 6$ LF is a slight refinement on our previous determination (B06) and includes ~ 100 additional i-dropouts identified over the two very deep HUDF05 fields (reaching to within 0.4 mags of the HUDF in the z_{850} band).

derdense in V_{606}-dropouts (see also Oesch et al. 2007). Since Beckwith et al. (2006) do not use an approach that is insensitive to field-to-field variations (e.g., STY79 or SWML), we would expect this underdensity in $z \sim 5$ V-dropouts in the HUDF to propagate directly into the Beckwith et al. (2006) LF and therefore the faint-end of their $z \sim 5$ LF to be low. Together these two effects appear to account for the differences seen.

4.3.3. Comparison at $z \sim 6$

Finally, we discuss the UV LF at $z \sim 6$. Already, there have been quite a significant number of LF determinations at $z \sim 6$ (e.g., Dickinson et al. 2004; Bouwens et al. 2004a; Yan & Windhorst 2004; Bunker et al. 2004; Malhotra et al. 2005; B06; Beckwith et al. 2006). See Figure 11 for these comparisons. Most of these determinations have been made using some combination of i-dropouts selected from the HUDF, HUDF-Ps, and GOODS data. Since almost all of these determinations have already received significant discussion in our $z \sim 6$ study (B06), we will only comment on the two most

recent determinations (B06 and Beckwith et al. 2006). One of these determinations is our own and based upon a slightly smaller data set (the B06 determination did not include the ~ 100 i-dropouts available over the second and third deepest i-dropout search fields: HUDF05-1 and HUDF05-2). In general, the present determination is in good agreement with the previous one (B06), though somewhat ($\sim 30\%$) lower in normalization. This latter change is not unexpected given the errors on our previous determination and occurred as a result of a lower surface density of dropouts in the two HUDF05 fields (see Table B2 and B3) and the different SED templates and opacity model we assume. We explore the effect of these assumptions on our LF results in Appendix B.

Beckwith et al. (2006) also made a determination of the UV LF at $z \sim 6$ using the same methodology they used at $z \sim 4$ and $z \sim 5$. We consider the Beckwith et al. (2006) $z \sim 6$ determination obtained from the fit to their number counts (i.e., $M^* = -20.5$, $\phi^* = 0.0007$ Mpc^{-3}, $\alpha = -1.6$).[1] A comparison with both our previous (B06) and updated determination is provided in Figure 11. While the Beckwith et al. (2006) LF is in excellent agreement with the present determinations at bright magnitudes, at fainter magnitudes the Beckwith et al. (2006) LF is markedly lower ($\approx 2\times$) than our results. Why might this be? A comparison of the total number of galaxies in the Beckwith et al. (2006) HUDF catalog shows only 54% as many sources as our catalog to the same faint limit and only 25% as many sources over the interval $28.0 < z_{850,AB} < 28.7$ (Figure 12). While one might imagine that the differences might be due to differing levels of incompleteness, Beckwith et al. (2006) estimate that only $\sim 35\%$ of the galaxies are missing at $28 < z_{850,AB} < 28.7$ (see Figure 13 from Beckwith et al. 2006), which is much smaller than the $\sim 75\%$ we estimate empirically through a comparison with our counts.

What then is the probable cause for this discrepancy? We suspect that it is due to the systematic differences between the z_{850}-band photometry Beckwith et al. (2006) use to select their sample (which appear to come from the photometric catalog initially provided with the HUDF release since an application of the Beckwith et al. 2006 criteria to that catalog yields precisely the same set of

---

[1] Beckwith et al. (2006) also presented a stepwise determination of the $z \sim 6$ LF obtained directly from the number counts assuming a distance modulus and selection volume. We do not make a comparison against that determination since the Beckwith et al. (2006) assumption of a simple distance modulus leads to substantial biases in the reported LF. Note the significant differences between the solid and dotted black lines in Figure 11.

TABLE 12
DETERMINATIONS OF THE BEST-FIT SCHECHTER PARAMETERS FOR THE REST-FRAME UV LFs AT $z \sim 6$.

Reference	M_{UV}^*	ϕ^* (10^{-3} Mpc^{-3})	α
This work	-20.24 ± 0.19	$1.4^{+0.6}_{-0.4}$	-1.74 ± 0.16
Bouwens et al. 2006	-20.25 ± 0.20	$2.0^{+0.9}_{-0.8}$	-1.73 ± 0.21
Beckwith et al. 2006	-20.5	0.7	-1.6 (fixed)
Malhotra et al. 2005	-20.83	0.4	-1.8 (assumed)
Yan & Windhorst 2004b	-21.03	0.5	-1.8
Bunker et al. 2004	-20.87[a]	0.2	-1.6
Dickinson et al. 2004	-19.87[a]	5.3	-1.6 (fixed)
Bouwens et al. 2004a	-20.26	1.7	-1.15

[a]Since the quoted LF was expressed in terms of the $z \sim 3$ LF (Steidel et al. 1999) which is at rest-frame 1700Å, it was necessary to apply a k-correction (~ 0.2 mag) to obtain the equivalent luminosity at 1350 Å to make a comparison with the other LFs given here.

i-dropouts as are found in their paper) and that used in our analysis, which as shown in the insert to Figure 12 are systematically brighter by ~ 0.4 mag near the HUDF magnitude limit (*red crosses*). Though such significant differences may be cause for concern, it is interesting to note that the z_{850}-band magnitudes provided by Beckwith et al. (2006) for i-dropouts in the HUDF (Table 8 from that work) are also typically ~ 0.3 mag brighter than that initially provided with the HUDF release (*black crosses*). So it would appear that Beckwith et al. (2006) quote different z_{850}-band magnitudes for i-dropouts in the HUDF than they initially provided with the HUDF release and which they used to select their i-dropout sample!

4.4. State of the LF at $z \sim 6$, 5, and 4

Not surprisingly there has already been a great deal of discussion regarding how the UV LF evolves at high redshift ($z \sim 3-6$) based upon previous determinations, with some studies arguing for an evolution in the faint-end slope (Yan & Windhorst 2004), some studies advocating for an evolution in ϕ^* (Beckwith et al. 2006), other studies suggesting an evolution in the characteristic luminosity (B06; Yoshida et al. 2006), and yet other studies arguing for an evolution at the faint-end of the LF (Iwata et al. 2003; Sawicki & Thompson 2006a; Iwata et al. 2007).

In this paper, we found strong evidence for *(i)* an increase in the characteristic luminosity M^* as a function of cosmic time, from ~ -20.2 at $z \sim 6$ to ~ -21.1 at $z \sim 3$ and *(ii)* a steep faint-end slope $\alpha \sim -1.7$ at $z \sim 4 - 6$. While this agrees with the evolution found by some groups (B06; Yoshida et al. 2006; M. Giavalisco et al. 2007, in preparation), it is in significant contradiction with others (Iwata et al. 2007; Sawicki & Thompson 2006a; Beckwith et al. 2006). We find it quite disturbing that there are a wide variety of different conclusions being drawn by different teams.[2] However, we think that our large data set, unprecedented in both its size and leverage (both in redshift and luminosity), should allow us to come to more robust conclusions than have previously been obtained. We are encouraged by the fact that

[2] The diversity of conclusions drawn in high-redshift LF studies certainly illustrates how difficult it is to accurately control for systematics. Of course, one additional complicating factor is clearly the extremely steep faint-end slopes possessed by high-redshift LFs. This makes it very difficult to locate the "knee" in the LF and therefore distinguish evolution in ϕ^* from evolution in M^*.
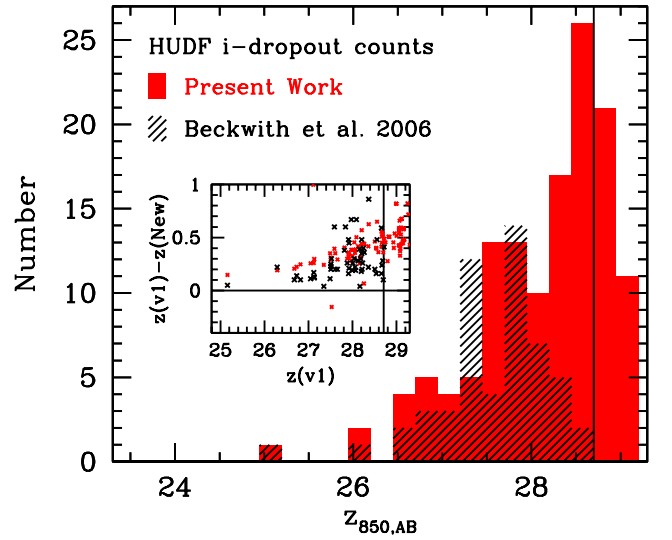

FIG. 12.— Number of i-dropouts in the HUDF as a function of z_{850}-band magnitude in the present compilation (*red histogram*) and that obtained by Beckwith et al. (2006: *hatched histogram*). The selection limit for the Beckwith et al. (2006) probe is shown with the solid vertical line. While the two studies are in good agreement at bright magnitudes ($z_{850,AB} < 28$), there are significant differences at fainter levels. In particular, the Beckwith et al. (2006) catalog only contains 25% as many sources as our catalog over the interval $28 < z_{850,AB} < 28.7$ and 54% as many to their magnitude limit $z_{850,AB} < 28.7$. While one might imagine that the differences might be due to different levels of incompleteness, Beckwith et al. (2006) estimate that only $\sim 35\%$ of the galaxies are missing at $28 < z_{850,AB} < 28.7$ (see Figure 13 from Beckwith et al. 2006), which is much smaller than the $\sim 75\%$ we estimate empirically through a comparison with our counts. The insert shows the differences between the z_{850}-band photometry of the i-dropouts in our catalogs (denoted here as "New") and that initially provided with the HUDF release (denoted as "v1") versus z_{850}-band magnitude (*red crosses*). We note that our z_{850}-band magnitudes are typically ~ 0.4 mag brighter than that provided with the HUDF release. This could be the cause of the discrepancy, if Beckwith et al. (2006) used the photometry from the initial HUDF release to select their sources (as it appears they did since an application of the i-dropout criteria to the photometry from the initial release yields precisely the Beckwith et al. 2006 i-dropout sample). Since the published photometry of Beckwith et al. (2006) [Table 8 from that work] is in good agreement with our work and also typically ~ 0.3 mag brighter than the initial release (the differences between the Beckwith et al. 2006 photometry and that initially provided with the initial release are shown in the insert as the black crosses), it would appear that Beckwith et al. (2006) selected their i-dropout sample using photometry (from the initial release) which is significantly fainter (~ 0.3 mag) than what they publish (which should represent their best estimates of the total magnitudes) and what we derive. This suggests their HUDF i-dropout selection may be subject to at least a few small concerns.

one of the most recent studies using the deep wide-area (636 arcmin^2) Subaru Deep Field (Yoshida et al. 2006) obtain similar values for M^* and α to what we find at $z \sim 4$ and $z \sim 5$ and derive almost essentially the same evolution in M^* over this interval (~ 0.35 mag). Similar results are obtained by Ouchi et al. (2004) using somewhat shallower data over the Subaru Deep Field and by M. Giavalisco et al. (2007, in preparation) using an independent analysis of the HUDF + GOODS data.

One of the most noteworthy of several previous studies to differ from the present conclusions is that conducted by Beckwith et al. (2006). The Beckwith et al. (2006) analysis is noteworthy because while Beckwith et al. (2006) use a very similar data set to own (our data set also includes four deep intermediate depth ACS fields, i.e., the two HUDF05 and two HUDF-Ps fields), Beckwith et al. (2006) arrive at significantly different conclusions from our own. Beckwith et al. (2006) argue that the evolution in the UV LFs at $z \sim 4 - 6$ can be most easily explained through an evolution in ϕ^* and cannot be explained through an evolution in M^*. What could be the cause of these different conclusions? After a careful analysis of the Beckwith et al. (2006) results, we have three significant comments. First of all, Beckwith et al. (2006) determine their LFs using the surface density of galaxies binned according to their flux in passbands affected by absorption from the Lyα forest (i.e., V_{606} for their $z \sim 4$ LF, i_{775} for their $z \sim 5$ LF, and z_{850} for their $z \sim 6$ LF). This is worrisome since the Lyα forest absorption is quite sensitive to the redshift of the sources, and therefore any systematic errors in the model redshift distributions (or forest absorption model) will propagate into the luminosities used for deriving their LFs. While we understand that Beckwith et al. (2006) used this procedure to determine the LF at $z \sim 4$, $z \sim 5$, and $z \sim 6$ in a self-consistent way, in doing so they have introduced unnecessary uncertainties into these determinations at $z \sim 4$ and $z \sim 5$. These LFs can be derived from UV-continuum fluxes not subject to these uncertainties.[3]

Secondly, the value of M^* that Beckwith et al. (2006) derive at $z \sim 4$ (alternatively quoted as -20.3, -20.5, and -20.7 depending on the fitting procedure) is significantly fainter than the values (i.e., $M^* \lesssim -21.0$) that have been derived in previous studies (Steidel et al. 1999; Sawicki & Thompson 2006a; Paltani et al. 2006: see Table 10). While these differences will partially result from Beckwith et al. (2006)'s determining the LF at $\sim 1400\text{\AA}$ (L^* galaxies at $z \sim 4$ are somewhat redder in their UV-continuum slopes β than -2.0 and thus yield somewhat fainter values of M^* at $1400\text{\AA}$ than they do at $1600\text{ \AA}$: Appendix B.3), probably the biggest reason for these differences is one of procedure. Beckwith et al. (2006) derive their LFs using the surface density of dropouts binned in terms of the flux in bands affected by Lyman-forest absorption ($\sim 0.2 - 1.0$ mag) while other analyses use UV-continuum fluxes where this absorption has no effect. As discussed in the paragraph above, analyses which are much less sensitive to modeling this absorp-

tion would seem to be more reliable than those which are more sensitive. If the value of M^* in the Beckwith et al. (2006) analysis is systematically too faint (and ϕ^* too high) for these reasons, this would shift the evolution from M^* (which is what we believe the data suggest) to ϕ^* (which is what Beckwith et al. 2006 report).

Third, at $z \sim 6$, we disagree with the value of ϕ^* and M^* obtained by Beckwith et al. (2006). Our basic disagreement hinges on the assessment we made of the Beckwith et al. (2006) HUDF i-dropout selection at faint magnitudes ($28 < z_{850,AB} < 28.7$: see §4.3.3 and Figure 12) and our suspicion that this selection may be somewhat incomplete due to a flux bias (Figure 12). If indeed this incompleteness was not properly accounted for in the Beckwith et al. (2006) analysis, it would effectively lower their value of ϕ^* and brighten M^*. Again, this would shift the evolution in the LF from M^* to ϕ^*.

5. DISCUSSION

The unprecedented depth and size of current B, V, and i-dropout samples, along with the great experience represented in the previously determined LFs from the literature, have enabled us to establish what we think are the most robust $z \sim 4$, $z \sim 5$, and $z \sim 6$ LFs to date. These LFs extend significantly fainter than has been possible in all previous efforts that have not included the ultra-deep HUDF data – providing us with unique leverage for constraining the evolution at the faint-end of the LF. These deep LFs put us in a strong position to discuss a number of issues which are of current interest in studies of galaxy evolution.

5.1. *Evolution of the rest-frame UV LF*

Having established the evolution of the LF from $z \sim 6$ to $z \sim 4$, it is interesting to compare this evolution with that found at lower redshifts (Steidel et al. 1999; Arnouts et al. 2005; Wyder et al. 2005). We look at this evolution in terms of the three Schechter parameters ϕ^*, M^*, and α (Figures 13-14). This may give us some clue as to the physical mechanisms that are likely to be at work in global evolution of the galaxy population. The clearest trend seems to be present in the evolution of M^*, which brightens rapidly at early times, reaches a peak around $z \sim 4$, and then fades to $z \sim 0$. The simplest explanation for the observed brightening in M^*_{1600} from $z \sim 6$ to $z \sim 4$ is that it occurs through hierarchical coalescence and merging of smaller halos into larger systems. Not only do we expect such a buildup to occur at early times in almost any generic model for galaxy formation, but as we will see in §5.2, such a mechanism predicts growth which is very similar *quantitatively* to that observed in our data.

At later times ($z \lesssim 3$), this steady brightening in M^* halts and then turns around, so that after this epoch the most luminous star-forming galaxies become progressively fainter with time. This may be partially due to the gradual depletion of the cold gas reservoirs in galaxies with cosmic time (independent of mass) and partially due to the preferential depletion of gas in the highest mass galaxies (e.g., Erb et al. 2006; Reddy et al. 2006; Noeske et al. 2007). This latter process would cause vigorous star-formation activity to move from the most massive galaxies to galaxies of lower and lower mass. This process has hence been called "downsizing" (Cowie et al.

---

[3] Of course, in our determinations of the LF at $z \sim 6$ from i-dropout samples, we cannot easily avoid coping with the effects of Lyα absorption on the z_{850}-band fluxes of i-dropouts in our samples, and therefore it is expected that our LF determinations at $z \sim 6$ will be affected by uncertainties in modelling this absorption.
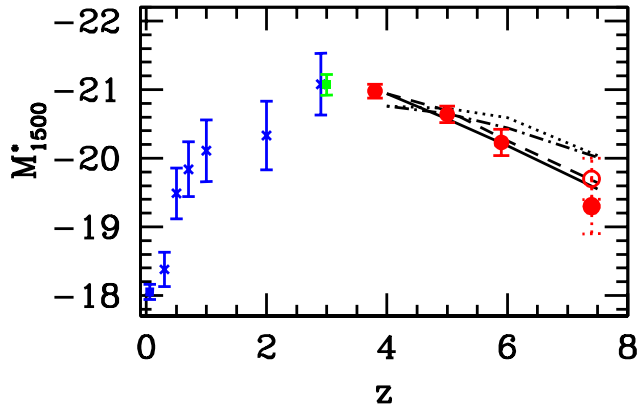
FIG. 13.— Evolution of the characteristic luminosity (M^*) of the UV LF as a function of redshift. Determinations are from the present work (red circles) at $z \sim 4 - 6$, Steidel et al. (1999) at $z \sim 3$ (green square), Arnouts et al. (2005) (blue crosses) at $0.1 \lesssim z \lesssim 3$, and Wyder et al. (2005) at $z \lesssim 0.1$ (blue square). Error bars are 1σ. See compilation in Table 7. The values of M^* shown at $z \sim 7.4$ (*solid red circle* and *open red circle*, respectively) are determined (§5.2) using the results from the conservative and less-conservative z-dropout searches over the two GOODS fields (Bouwens & Illingworth 2006) and assuming that the evolution in the rest-frame UV LF can be accommodated by changes in M^*. The evolution in M^* predicted from the Night et al. (2006) model, the momentum-driven wind model of Oppenheimer & Davé (2006), and the empirically-calibrated model of Stark et al. (2007c) are shown as the dotted, dashed, and dash-dotted lines, respectively (see §5.2-§5.3 for details). The solid line shows the evolution in M^* predicted from the halo mass function (Sheth & Tormen 1999) assuming a constant mass to light ratio. To extract a well-defined evolution in M^* with redshift from the models (which resemble power laws in shape), we needed to assume that ϕ^* was fixed, as seen in the observations (Figure 14). In addition, because the changes we derive for M^* from the models are only differential, the absolute values plotted here are a little arbitrary. The observed characteristic luminosity M^* shows significant evolution at both high-redshift and low-redshift. At high redshift ($z \gtrsim 4$), the characteristic luminosity brightens very rapidly, reaches a peak at around $z \sim 2 - 4$, and then fades to $z \sim 0$. The evolution we observe at high redshift in M^* is quite consistent with that found in the halo mass function and in the momentum-driven wind model of Oppenheimer & Davé (2006).

1996). Similar "downsizing" trends are found in many different areas of galaxy evolution, from the decrease in the cross-over mass between spheroids and disk galaxies (Bundy et al. 2005) to the greater late-stage star formation in the lowest luminosity ellipticals (e.g., Kodama et al. 2004; Cross et al. 2004; Treu et al. 2005; McIntosh et al. 2005; van der Wel et al. 2005). Such trends are also observed in the evolution of the AGN population (e.g., Pei 1995; Ueda et al. 2003), where the buildup of supermassive black-holes mirrors that in galaxy-scale star formation.

Over most of the redshift range $z \sim 0 - 6$ probed by current LF determinations, we observe no significant evolution in the normalization ϕ^* and only a modest amount of evolution in the faint-end slope α. The evolution in ϕ^* and α becomes more substantial at the lowest redshifts being probed here, as ϕ^* evolves from 10^{-3} Mpc^{-3} at $z \sim 1-6$ to 4×10^{-3} Mpc^{-3} at $z \sim 0$ (Wyder et al. 2005) and α evolves from -1.74 at $z \sim 4$ to ~ -1.2 at $z \sim 0$ (Wyder et al. 2005). Broadly, we expect some flattening of the faint-end slope α with cosmic time to match that predicted for the halo mass function. We would also expect ϕ^* to be somewhat higher at early times to account for the large population of lower luminosity galaxies pre-
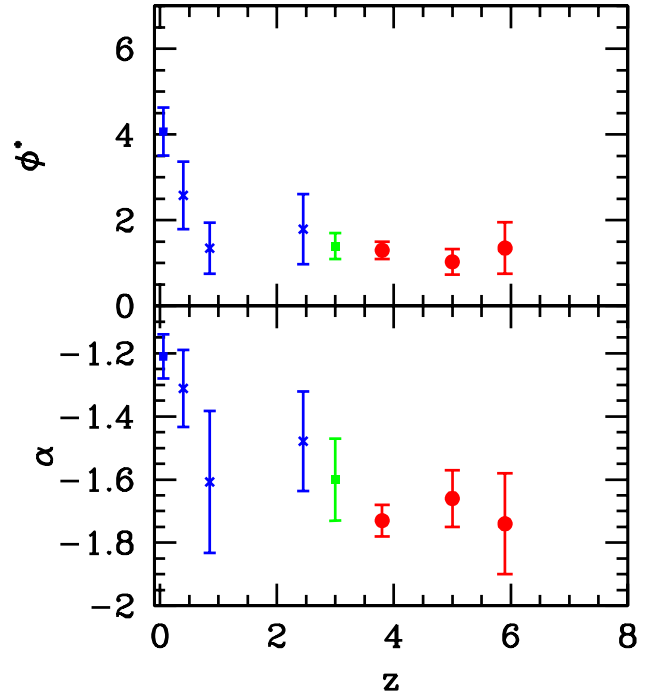

FIG. 14.— Evolution of the normalization (ϕ^*) and faint-end end slope (α) of the UV LF as a function of redshift. Determinations are as in Figure 13. Adjacent determinations from Arnouts et al. (2005) have been binned together to reduce the scatter so that possible trends with redshift could be seen more clearly. Evolution in the faint-end slope α is not very significant, though there is some hint that this slope is somewhat steeper at high redshift than it is at low redshift. Evolution in ϕ^* is not significant over the interval $z \sim 0.5$ to $z \sim 6$, but may show a possible increase at low redshift ($z \lesssim 0.5$) and high redshift ($z \sim 6$). We do not show predictions for evolution in ϕ^* from the models since they cannot be well-established independently of evolution in M^* due to the very power-law like appearance of the model LFs. The faint-end slope α is predicted to be ~ -1.8 in the theoretical models at $z \gtrsim 4$ (e.g., Night et al. 2006; Oppenheimer & Davé 2006).

dicted to be present then. At late times, we expect the value of ϕ^* to increase to compensate for the evolution in M^* and thus keep the population of lower luminosity galaxies (which appear to evolve more slowly with cosmic time: e.g., Noeske et al. 2007) more constant. While we observe this increase in ϕ^* at late times, it is unclear at present whether ϕ^* is really higher at very early times ($z \gtrsim 6$). Progress on this question should be possible from on-going searches for galaxies at $z \gtrsim 7$ (e.g., Bouwens & Illingworth 2006; Mannucci et al. 2006; Stark et al. 2007b).

5.2. *Interpreting the Observed Evolution in M^**

We have already remarked that one probable interpretation for the observed brightening in M^* is through the hierarchical coalescence and merging of galaxies into larger halos. We can look at the hypothesis in detail by comparing the observed brightening with the mass buildup seen in the halo mass function (Sheth & Tormen 1999) over this range. We will assume we can characterize the growth in the mass function by looking at the mass of halos with a fixed comoving volume density $10^{-2.5}$ Mpc^{-3} and that there is a fixed conversion from mass to UV light (halo mass to apparent star formation rate). A volume density of $10^{-2.5}$ Mpc^{-3} corresponds to that expected for halos near the knee of the luminosity function assuming a duty cycle of $\sim 25\%$ (see Stark et al.

2007c; Verma et al. 2007) and ϕ^* of 10^{-3} Mpc^{-3}, which is the approximate volume density of L^* galaxies in the observations. The duty cycle tells us the approximate fraction of halos that have lit up with star formation at any given point in time. This analysis effectively assumes that ϕ^* is fixed as a function of time, which we assume to match the observations (Figure 14). We plot the predicted brightening on Figure 13 with the solid line. We note that these predictions are only modestly sensitive to the volume densities chosen to make these comparisons. At volume densities of $\sim 10^{-2}$ Mpc^{-3}, the predicted brightening is 0.6 mag from $z \sim 6$ to $z \sim 4$ while at $\sim 10^{-3}$ Mpc^{-3}, the predicted brightening is 0.9 mag. Surprisingly, the growth in the mass function is in striking agreement with the evolution we observe in M^*, even out to $z \sim 7.4$ where we derive our values of M^* from the Bouwens & Illingworth (2006) search results (see §5.4). This remarkable agreement strongly suggests that hierarchical buildup may contribute significantly to the evolution we observe.

While this is surely an interesting finding in itself, the overall level of agreement we observe here is surprising since we make a fairly simple set of assumptions above about the relationship between the halo mass and the UV light in galaxies hosted by these halos – supposing that it is constant and non-evolving. Had we assumed this ratio evolves with cosmic time we would have made considerably different predictions for the evolution of the LF. This is interesting since there are many reasons for thinking the mass-to-light ratio might be lower at early times and therefore the evolution in M^* to be less rapid with cosmic time. For one, the efficiency of star formation is expected to be higher at early times. The universe would have a higher mean density then and therefore the gas densities and star formation rate efficiencies should be higher. In addition, the cooling times and dynamical times should be less at early times. All this suggests that the evolution in the LF should much more closely resemble that predicted by Stark et al. (2007c), who also model the evolution in the LF using the mass function but assume that the star formation time scale evolves as $H(z)^{-1} \sim (1+z)^{-3/2}$. As a result of these star formation time scales, the Stark et al. (2007c) model predicts a mass-to-light ratio which evolves as $\sim (1+z)^{-3/2}$. This model yields significantly different predictions for how M^* evolves with redshift (shown as the dash-dotted line in Figure 13). These latter predictions appear to fit our data somewhat less well than for the simple toy model we adopted above assuming no-evolution in the mass-to-light ratio. This suggests that this mass-to-light ratio may not evolve that dramatically with cosmic time. One possible explanation for this would be if supernovae feedback played a significant role in regulating the star formation within galaxies at these times – keeping it from reaching the rates theoretically achievable given the time scales and gas densities expected. Of course, while it is interesting to note the possible physical implications of our observational results, we should be cautious about drawing too strong of conclusions based upon these comparisons. Our treatment here is crude, and the observational uncertainties are still quite large.

5.3. *Comparisons with Model Results*

Given the success of our simple toy model for reproducing the observed evolution in M^*, it is interesting to ask if this success is maintained if we consider more sophisticated treatments like those developped in the literature (Finlator et al. 2006; Oppenheimer & Davé 2006; Nagamine et al. 2004; Night et al. 2006; Samui et al. 2007). The most complicated of these models include a wide variety of physics from gravitation to hydrodynamics, shocks, cooling, star formation, chemical evolution, and supernovae feedback (see, e.g., Springel & Hernquist 2003). We examined two different models produced by leading teams in this field and which we suspect are fairly representative of current work in this area. These models are the momentum-driven wind "vzw" model of Oppenheimer & Davé (2006) and the model of Night et al. (2006), which appears to be similar to the constant wind model of Oppenheimer & Davé (2006). Since LFs in these models more closely resemble power laws in overall shape than they do Schechter functions, we were not able to extract a unique value of M^* from the model LFs. We were however able to estimate an evolution in M^* by comparing the model LFs at a fixed number density and looking at the change in magnitude. In doing so, we effectively assume that the value of ϕ^* is fixed just like we find in the observations (Figure 14). To improve the S/N with which to estimate this evolution from the models, we looked at this evolution over a range of number densities (i.e., $10^{-3.2}$ Mpc^{-3} to $10^{-1.5}$ Mpc^{-3}). We plot the derived evolution from these models in Figure 13, and it is apparent that our observed evolution is in good agreement with the momentum-driven wind models of Oppenheimer & Davé (2006), but exceeds that predicted by the Night et al. (2006) model. The fact that our results agree with at least one of the two models is encouraging – since it suggests that the evolution we infer is plausible. Moreover, the fact that the two model results disagree suggests that we may be able to begin to use our observational results to begin constraining the important aspects of the theoretical models. Particularly relevant on this front are the implications for the feedback prescription, which differ quite significantly between the two models considered here. For the momentum-driven wind models, feedback is much more important at early times than it is for the Night et al. (2006) model. This feedback effectively suppresses star formation at early times and therefore results in a much more rapid brightening of M^* with cosmic time, in agreement with the observations.

5.4. *Evolution of UV Luminosity at $z > 6$*

The present determinations of the LF at $z \sim 4 - 6$ should provide us with a useful guide to the form of the LF at even earlier times and should be helpful in interpreting current searches for very high-redshift ($z > 6$) galaxies. Currently, the most accessible regime for such probes lies just beyond $z \sim 6$, at $z \sim 7 - 8$, and can be probed by a z-dropout search. At present, the most comprehensive such search was performed by our team using ~ 19 arcmin^2 of deep NICMOS data over the two GOODS fields (Bouwens & Illingworth 2006: but see also Mannucci et al. 2006). In that work, we applied a very conservative $(z_{850} - J_{110})_{AB} > 1.3$, $(z_{850} - J_{110})_{AB} > 1.3 + 0.4(J_{110} - H_{160})_{AB}$, $(J_{110} - H_{160})_{AB} < 1.2$ z_{850}-dropout criterion to that data and found only one plausible z-dropout, but expected ~ 10 sources assuming no-

evolution from $z \sim 6$. We also applied a slightly less conservative z-dropout criterion and found three other possible candidates. From this, we concluded that the volume density of bright ($\gtrsim 0.3 L^*_{z=3}$) galaxies at $z \sim 7.4$ was just $0.10^{+0.19}_{-0.07}$ and $0.24^{+0.20}_{-0.12}$ times the volume density of bright sources at $z \sim 6$ for our conservative and less conservative criteria, respectively. Both large-scale structure and Poissonian statistics are included in the estimated errors here. For both selections, the result was significant and suggested to us that there was substantial evolution from $z \sim 7-8$ to $z \sim 6$. Given the sizeable evolution we had observed in M^* between $z \sim 6$ and $z \sim 3$ (B06; see also Dickinson et al. 2004), it made sense for us to model our $z \sim 7-8$ search results in terms of an evolution of M^*, keeping ϕ^* and α fixed. We also considered a model where changes in M^* were offset by changes in ϕ^* such as to keep the total luminosity density fixed. Using these two sets of assumptions, we estimated that M^* was 1.1 ± 0.4 mag and 1.4 ± 0.4 mag fainter at $z \sim 7.4$ than it was at $z \sim 6$.

With our current work on the LFs at $z \sim 4-6$, we have been able to demonstrate more clearly than before that the most significant change in the LF occurs through a brightening of M^* from $z \sim 6$ to $z \sim 4$ (see also Yoshida et al. 2006). This strengthens the underlying motivations behind the Bouwens & Illingworth (2006) decision to model the evolution of the LF in terms of a change in M^*. The parameter ϕ^* is consistent with being constant, though it may also decrease with time, as suggested by hierarchical buildup. Unfortunately, there are still too many uncertainties in the data to be sure about the trends in ϕ^*, and so it is difficult to significantly improve upon the M^* estimates made in Bouwens & Illingworth (2006) study for our most conservative selection.

Nevertheless, we will update our estimates for M^* at $z \sim 7-8$ based upon our conservative selection to be consistent with the present determinations for ϕ^* and α at $z \sim 6$ while taking the evolution in the UV LF at $z \gtrsim 6$ to simply be in luminosity (M^*). With these assumptions (i.e., taking $\alpha = -1.74$ and $\phi^* = 0.0014$ Mpc^{-3}), we find a value of $M^*_{UV} = -19.3 \pm 0.4$ for our UV LF at $z \sim 7-8$. It also makes sense to estimate the value of M^* at $z \sim 7-8$ using the results of the less-conservative selection of Bouwens & Illingworth (2006). We did not consider this selection in our original estimates of M^* in Bouwens & Illingworth (2006) to avoid possible concerns about contamination and thus simplify the discussion. However, the contamination is not likely to be larger than 25% (see Bouwens & Illingworth 2006), and this selection offers much better statistics than for our conservative selection (4 sources vs. 1 source) as well as a larger selection window which should make our selection volume estimates more reliable. Repeating the determination of M^* using the results of our less conservative selection ($\rho(z = 7.4)/\rho(z = 6) = 0.24^{+0.20}_{-0.12}$) and assuming simple evolution in M^*, we find $M^*_{UV} = -19.7 \pm 0.3$. The normalization ϕ^* and faint-end slope α were kept fixed at 1.4×10^{-3} Mpc^{-3} and -1.74, the values preferred at $z \sim 6$, for this modelling. Though it seems probable that the faint-end slope α may be quite steep at earlier times, this does not have a big effect on the derived values for ϕ^* and M^*. For example, making a $\Delta\alpha = 0.4$ change in the assumed faint-end slope only
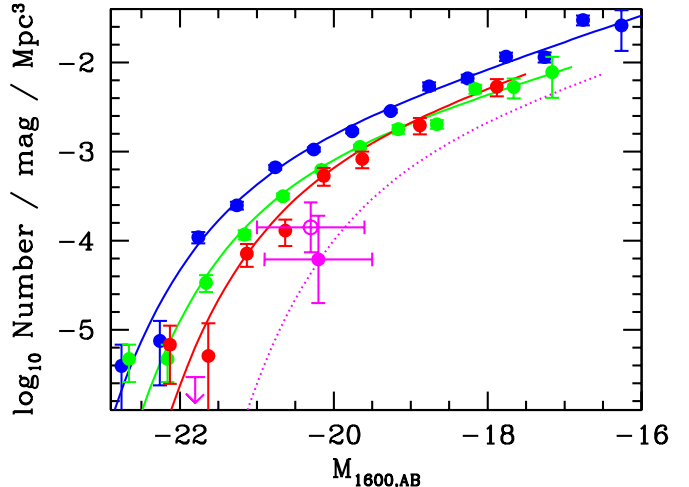

FIG. 15.— Two different determinations of the volume density of luminous star-forming galaxies at $z \sim 7.4$ compared with the UV LFs at $z \sim 4-6$ (from Figure 3). The $z \sim 7.4$ search results are shown as solid and open circles (where the error bars are 1σ) for the Bouwens & Illingworth (2006) conservative and less conservative selections, respectively. The Mannucci et al. (2006) upper limit on this volume density is shown as the magenta downward arrow at -21.8 AB mag. We have plotted one possible UV LF at $z \sim 7.4$ (dashed magenta line) which is in good agreement with the Bouwens & Illingworth (2006) determination (see §5.4).

results in a 0.1 mag change in M^*. We added this determination of M^* to Figure 13 as an open red circle, and it is in remarkable agreement with some of the theoretical predictions as well as simple extrapolations of our lower redshift results (§5.1-§5.3). We include the Bouwens & Illingworth (2006) search results in Figure 15 along with a comparison with the LFs at $z \sim 4-6$. The Mannucci et al. (2006) search results for very luminous (brighter than -21.5 AB mag) $z \sim 7$ galaxies are also included on this figure.

5.5. *Reionization*

Finally, it seems worthwhile to discuss the implications of the current LF determination on the ionizing flux output of $z \gtrsim 4$ galaxies. There has been a great deal of interest in the ionizing radiation output of high-redshift galaxies since it was discovered that hydrogen remains almost entirely ionized since a redshift of $z \sim 6$ (Becker et al. 2001; Fan et al. 2002; White et al. 2003; Fan et al. 2006) and that galaxies are the only obvious candidates to produce this radiation. The situation has even become more interesting now with the availiability of the WMAP results, indicating that the universe may have been largely ionized out to redshifts as early as $10.9^{+2.9}_{-2.3}$ (Spergel et al. 2006; Page et al. 2006; cf. Shull & Venkatesan 2007).

Yet, despite galaxies' being the only obvious source of ionizing photons at high redshift, there has been some controversy about the ability of galaxies to keep the universe reionized at high redshift. Much of the controversy has centered around the fact that the escape fraction is observed to be very low for galaxies at $z \sim 0-3$ (Leitherer et al. 1995; Hurwitz et al. 1997; Deharveng et al. 2001; Giallongo et al. 2002; Fernández-Soto et al. 2003; Malkan et al. 2003; Inoue et al. 2005; Shapley et al. 2006; cf. Steidel et al. 2001), and therefore while high-mass stars in galaxies may be efficient producers of ionizing
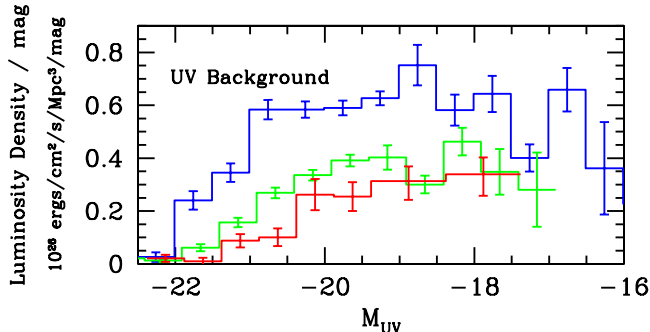
FIG. 16.— *UV* Luminosity density per unit magnitude for galaxies of various luminosities at $z \sim 4$ (*blue histogram*: from our *B*-dropout sample), $z \sim 5$ (*green histogram*: from our *V*-dropout sample) and $z \sim 6$ (*red histogram*: from our *i*-dropout sample). Error bars here are 1σ and were derived from the rest-frame *UV* LF at $z \sim 4$, $z \sim 5$, and $z \sim 6$ (Table 4). This shows that lower luminosity galaxies make up a significant part of the overall *UV* background and thus likely play an important role in reionization. Assuming that it is possible to extrapolate the LF to very low luminosities and the LFs truncate below some very faint fiducial limit of -10 AB mag, we estimate that 27%, 24%, and 34% of the total flux comes from galaxies faintward of -16 AB mag for our $z \sim 4$, $z \sim 5$, and $z \sim 6$ LFs, respectively (§5.5).

photons, only a small fraction of these photons succeed in making it out into the intergalactic medium. This has led some researchers to question whether high redshift galaxies are even capable of keeping the universe ionized (e.g., Stanway et al. 2003; Bunker et al. 2004). We must emphasize, however, that the escape fraction is still relatively poorly understood, and that the true value may still be quite appreciable (e.g., Shapley et al. 2006).

Fortunately, it appears that there may be several ways of resolving this situation – even for relatively low values of the escape fraction. One of these is to suppose that the traditional assumptions about the intergalactic medium are not quite right and that one should use a smaller value for the clumping factor (e.g., Bolton & Haehnelt 2007; Sokasian et al. 2003; Iliev et al. 2006; Sawicki & Thompson 2006b) or higher temperature for the IGM (e.g., Stiavelli et al. 2004) than has been assumed in many previous analyses of the ionization balance (i.e., Madau et al. 1999). Another possible solution is to suppose that there has been a change in the metallicities or initial mass function (IMF) of stars at early times, such that these objects have a much higher ionizing efficiency than sources at lower redshift (Stiavelli et al. 2004). One final solution has been to assume a significant contribution to the ionizing flux from very low-luminosity galaxies (e.g., Lehnert & Bremer 2003; Yan & Windhorst 2004a,b; B06).

The present determination of the luminosity functions at $z \sim 4-6$, and in particular the steep faint-end slopes $\alpha = -1.73 \pm 0.05$ ($z \sim 4$), $\alpha = -1.66 \pm 0.09$ ($z \sim 5$), and $\alpha = -1.74 \pm 0.16$ ($z \sim 6$) provide significant support for the idea that lower luminosity galaxies contribute significantly to the total ionizing flux (see also Beckwith et al. 2006). Previously, there was some support for the idea that lower luminosity galaxies may have been important from the steep faint-end slopes obtained at $z \sim 6$ (B06; Yan & Windhorst 2004b) and at lower redshift (e.g., Steidel et al. 1999; Arnouts et al. 2005; Yoshida et al. 2006). However, this conclusion was a little uncertain due to the sizeable uncertainties on the faint-end slope α at $z \sim 6$

– and some conflicting results at lower redshift (Gabasch et al. 2004; Sawicki & Thompson 2006a). Now, with the present LF determinations (see also Yoshida et al. 2006; Beckwith et al. 2006; Oesch et al. 2007), it seems quite clear that the faint-end slope α must be quite steep (i.e., ~ -1.7) at $z \gtrsim 4$ – though it is still difficult to evaluate whether this slope evolves from $z \sim 6$ to $z \sim 4$ due to considerable uncertainties on this slope at $z \sim 6$.

We can use the stepwise LF at $z \sim 4$, $z \sim 5$, and $z \sim 6$ to look at the contribution that galaxies of various luminosities make to the total ionizing flux. Assuming a luminosity-independent escape fraction, we can examine this contribution by plotting up the *UV* luminosity densities provided by galaxies at different absolute magnitudes (Figure 16). Clearly, the lower luminosity galaxies provide a sizeable fraction of the total.

What fraction of the total flux that would be provided by galaxies faintward of the current observational limits (-16 AB mag), assuming that the present LFs can be extrapolated to very faint levels? With no cut-off in the LF, this fraction is 0.31, 0.27, and 0.40 for our $z \sim 4$, $z \sim 5$, and $z \sim 6$ LFs, respectively (from Table 7). However, for the more physically-reasonable situation that the LF has a cut-off (at a fiducial limit of -10 AB mag, e.g., Read et al. 2006: see §3.5), the fraction is 0.27, 0.24, and 0.34, respectively. In all cases, this fraction is substantial and suggests that a significant fraction of the total ionizing flux may come from galaxies at very low luminosities. In fact, even if we suppose that our high-redshift LFs cut off just below the observational limit of our HUDF selection (i.e., -16 AB mag), $\gtrsim 50\%$ of the total ionizing flux would still arise from galaxies fainter than -19.0 AB mag. Since -19 AB mag is comparable to or fainter than the observational limits relevant for most previous studies of high redshift galaxies (i.e., Figures 9 and 10), this shows that most previous studies do not come close to providing a complete census of the total *UV* light or ionizing radiation at high redshift. Ultra deep probes (such are available in the HUDF) are necessary.

6. SUMMARY

Over its years in operation, the HST Advanced Camera for Surveys has provided us with an exceptional resource of ultra deep, wide-area, multiwavelength optical ($BViz$) data for studying star-forming galaxies at high redshift. Such galaxies can be effectively identified in these multiwavelength data using a dropout criterion, with B, V, and i dropout selections probing galaxies at a mean redshift of $z \sim 3.8$, $z \sim 5$, and $z \sim 5.9$. Relative to previous observations, deep ACS data reach several times fainter than ever before and do so over large areas. This allows us to investigate the properties of high-redshift star-forming galaxies at extremely low luminosities in unprecedented detail.

Here we have taken advantage of the historic sample of deep, wide-area ACS fields (HUDF, HUDF05, HUDF-Ps, and the two GOODS fields) to identify large, comprehensive selections of very faint, high-redshift galaxies. Our collective sample of B, V, and i-dropouts over these fields totalled 4671, 1416, and 627 unique sources. Putting together our deepest probe (HUDF) with our widest area probe (GOODS), our samples cover a 6-7 mag range with good statistics (factor of ~ 1000 in luminosity), extending from -23 AB mag to -16 or -17 AB

TABLE 13
SUMMARY OF KEY RESULTS.[*]

			ϕ^*		$\log_{10}$ SFR density ($M_\odot$ Mpc^{-3} yr^{-1})			
Dropout			(10^{-3}		Uncorrected[b]		Dust-Corrected	
Sample	$< z >$	M^*_{UV}[a]	Mpc^{-3})	α	$L > 0.3L^*_{z=3}$	$L > 0.04L^*_{z=3}$	$L > 0.3L^*_{z=3}$	$L > 0.04L^*_{z=3}$
B	3.8	-20.98 ± 0.10	1.3 ± 0.2	-1.73 ± 0.05	-1.81 ± 0.05	-1.48 ± 0.05	-1.38 ± 0.05	-1.05 ± 0.05
V	5.0	-20.64 ± 0.13	1.0 ± 0.3	-1.66 ± 0.09	-2.15 ± 0.06	-1.78 ± 0.06	-1.85 ± 0.06	-1.48 ± 0.06
i	5.9	-20.24 ± 0.19	$1.4^{+0.6}_{-0.4}$	-1.74 ± 0.16	-2.31 ± 0.08	-1.83 ± 0.08	-2.14 ± 0.08	-1.65 ± 0.08
z	7.4	-19.3 ± 0.4	(1.4)	(-1.74)	-3.15 ± 0.48	-2.32	-2.97 ± 0.48	-2.14

[a] Values of M^*_{UV} are at 1600 Å for our B and V-dropout samples, at ~ 1350 Å for our i-dropout sample, and at ~ 1900 Å for our z-dropout sample. Since $z \sim 6$ galaxies are blue ($\beta \sim -2$: Stanway et al. 2005; B06), we expect the value of M^* at $z \sim 6$ to be very similar ($\lesssim 0.1$ mag) at 1600 Å to the value of M^* at 1350 Å. Similarly, we expect M^* at $z \sim 7-8$ to be fairly similar at ~ 1600Å to the value at ~ 1900Å.

[b] The luminosity densities, which are used to compute the uncorrected SFR densities presented here (§3.5), are given in Table 8.

[*] These LF determinations are based upon STY79 technique, including evolution in M^* across the redshift window of each sample (see Table 7 and Appendix B.8). They therefore differ from those given in Table 5, which do not include evolution.

mag. Through detailed simulations, we have carefully modelled the completeness, photometric scatter, contamination, and selection functions for each of our samples. We then put together the information from our combined sample of B, V, and i-dropouts to derive LFs at $z \sim 4$, $z \sim 5$, and $z \sim 6$. To ensure that our LF determinations are robust, we considered a wide variety of approaches and assumptions in the determinations of these LFs and made extensive comparisons with other determinations from the literature.

Here are our principal conclusions:

Best-fit LFs: We find that the rest-frame UV LFs at $z \sim 4-6$ are well fit by a Schechter function over a $\sim 5-7$ mag (factor of ~ 100 to ~ 1000) range in luminosity, from -23 AB mag to -16 AB mag (see also Beckwith et al. 2006). The best-fit parameters for our rest-frame UV LFs are given in Table 13. The present $z \sim 6$ LF determination is in reasonable agreement with those from B06 (see Table 12), but is slightly more robust at the faint-end. The most salient finding from the individual LF determinations is that the faint-end slope α is very steep ~ -1.7 at all redshifts considered here (see §3.4).

Completeness of $z \sim 4$ B-dropout census: The bulk of the bright B-dropouts we identify over the GOODS have β's of $\lesssim -1.0$ (§4.1: see Figure 8). Since our $z \sim 4$ B-dropout selection should be effective in identifying UV-bright galaxies as red as $\beta \sim 0.5$, the fact that we do not find many such galaxies in our selection in the range $\beta \sim -0.5$ and ~ -0.5 suggests that this selection is largely complete ($\gtrsim 90\%$) at bright magnitudes. This supposition would appear to be supported by complementary selections of galaxies at $z \sim 4$ with the Balmer-break technique (Brammer & van Dokkum 2007), which also find that galaxies have very blue UV-continuum slopes ($\gtrsim 90\%$ of the galaxies in the Brammer & van Dokkum 2007 selection had β's $\lesssim 0.5$). Since Balmer-break selections do not depend upon the value of the UV-continuum slope, this again suggests that the bulk of the star-forming galaxy population at $z \sim 4$ is quite blue and will not be missed from our bright B-dropout selection.

Evolution of the LF: Comparing our best-fit Schechter parameters determined at $z \sim 6$, $z \sim 5$, and $z \sim 4$, we find little evidence for evolution in the faint-end slope α or ϕ^* from $z \sim 6$ to $z \sim 4$. On the other hand, the characteristic luminosity for galaxies M^*_{UV} brightens by ~ 0.7 mag from $z \sim 6$ to $z \sim 4$ (see also Yoshida et al. 2006).

UV Luminosity / SFR Densities: The UV luminosity densities and SFR densities we infer at $z \sim 4$, $z \sim 5$, and $z \sim 6$ are summarized in Table 13. The UV luminosity density we derive at $z \sim 6$ is modestly lower ($0.45 \pm 0.09\times$) than that at $z \sim 4$ (integrated to -17.5 AB mag). Taking into account the likely evolution in dust properties of galaxies across this interval suggested by the apparent change in mean UV-continuum slope (e.g., B06), we infer a much more significant change in the dust-corrected SFR densities over this same interval of cosmic time, i.e., the SFR density at $z \sim 6$ appears to be just ~ 0.3 times this density at $z \sim 4$ (integrated to -17.5 AB mag).

Galaxies at $z \sim 7-8$: By quantifying the evolution of the UV LF from $z \sim 6$ to $z \sim 3$, we were able to better interpret the results of recent z_{850}-dropout searches of Bouwens & Illingworth (2006) in terms of an evolution of the LF (see §5.4). Supposing that the evolution of the UV LF is simply in M^* (as observed from $z \sim 6$ to $z \sim 4$), we estimated that M^*_{UV} at $z \sim 7.4$ is equal to -19.3 ± 0.4 AB mag and -19.7 ± 0.3 AB mag using the conservative and less conservative search results of Bouwens & Illingworth (2006), respectively (see §5.4).

Comparison with Model Results: The brightening we observe in M^* from $z \sim 6$ to $z \sim 4$ (and plausibly from $z \sim 7.4$) is almost identical to what one finds in the evolution of the halo mass function over this range (see also Stark et al. 2007c) assuming a constant proportionality between mass and light (see §5.2). This suggests that hierarchical buildup largely drives the evolution in M^* over the redshift range probed by our samples. It also may indicate that there is no substantial evolution in the ratio of halo mass to UV light over this range. Since we might expect this ratio to evolve significantly due to changes in the mean gas density of the universe and therefore star formation efficiency, this suggests that feedback may be quite important in regulating the star formation of galaxies at early times. Of course, given the considerable uncertainties in the value of M^* at very high redshift ($z \gtrsim 6$), it seems worthwhile to emphasize that these conclusions are still somewhat preliminary. Our observational results are also in reasonable agreement with

that predicted by the momentum-conserving wind models of Oppenheimer & Davé (2006).

Implications for Reionization: The very steep faint-end slopes α of the UV-continuum LF (~ -1.7) suggest that lower luminosity galaxies provide a significant fraction of the total ionizing flux at $z \gtrsim 4$ (see also discussion in Lehnert & Bremer 2003; Yan & Windhorst 2004a,b; B06; Sawicki & Thompson 2006b). Assuming that the escape fraction is independent of luminosity and that the high-redshift LFs maintain a Schechter-like form to a very faint fiducial limit (-10 AB mag) and cut off beyond this limit, we estimate that 27%, 24%, and 34% of the total flux comes from galaxies faintward of -16 AB mag for our $z \sim 4$, $z \sim 5$, and $z \sim 6$ LFs, respectively (see §5.5).

The recent failure of the Advanced Camera for Surveys aboard HST is a great loss for studies of galaxies. Even with the installation of WFC3, future HST observations will require approximately three times the telescope time that ACS required to obtain comparable constraints on the faint, $z \sim 4 - 6$ population. As a result, it would appear that for the near-to-distant future the current probes of the UV LF at very high redshift will remain an important standard, until future facilities with superior surveying capabilities like JWST come online (or unless ACS is repaired).

REFERENCES

Adelberger, K. L., & Steidel, C. C. 2000, ApJ, 544, 218
Arnouts, S., et al. 2005, ApJ, 619, L43
Becker, R. H. et al. 2001, AJ, 122, 2850
Beckwith, S. V. W., et al. 2006, AJ, 132, 1729
Bershady, M. A., Charlton, J. C., & Geoffroy, J. M. 1999, ApJ, 518, 103
Bertin, E. and Arnouts, S. 1996, A&AS, 117, 39
Blakeslee, J. P., Anderson, K. R., Meurer, G. R., Benítez, N., & Magee, D. 2003a, ASP Conf. Ser. 295: Astronomical Data Analysis Software and Systems XII, 12, 257
Bolton, J. S., & Haehnelt, M. G. 2007, astro-ph/0703306
Bouwens, R., Broadhurst, T. and Silk, J. 1998a, ApJ, 506, 557
Bouwens, R., Broadhurst, T. and Silk, J. 1998b, ApJ, 506, 579.
Bouwens, R., Broadhurst, T., & Illingworth, G. 2003a, ApJ, 593, 640
Bouwens, R. J., et al. 2003b, ApJ, 595, 589
Bouwens, R. J., et al. 2004a, ApJ, 606, L25
Bouwens, R. J., Illingworth, G.D., Blakeslee, J.P., Broadhurst, T.J., & Franx, M. 2004b, ApJ, 611, L1
Bouwens, R. J., et al. 2004c, ApJ, 616, L79
Bouwens, R. J., Illingworth, G.D., Thompson, R.I., & Franx, M. 2005, ApJ, 624, L5
Bouwens, R.J., Illingworth, G.D., Blakeslee, J.P., & Franx, M. 2006, ApJ, 653, 53 (B06)
Bouwens, R. J., & Illingworth, G. D. 2006, Nature, 443, 189.
Brammer, G. B., & van Dokkum, P. G. 2007, ApJ, 654, L107
Bruzual, G., & Charlot, S. 2003, MNRAS, 344, 1000
Bundy, K., Ellis, R. S., & Conselice, C. J. 2005, ApJ, 625, 621
Bunker, A. J., Stanway, E. R., Ellis, R. S., & McMahon, R. G. 2004, MNRAS, 355, 374
Calzetti, D., Kinney, A. L., & Storchi-Bergmann, T. 1994, ApJ, 429, 582
Coe, D., Benítez, N., Sánchez, S. F., Jee, M., Bouwens, R., & Ford, H. 2006, AJ, 132, 926
Cowie, L. L., Songaila, A., Hu, E. M., & Cohen, J. G. 1996, AJ, 112, 839
Cross, N. J. G., et al. 2004, AJ, 128, 1990
Dahlen, T., Mobasher, B., Dickinson, M., Ferguson, H. C., Giavalisco, M., Kretchmer, C., & Ravindranath, S. 2006, ApJ, 654, 172
Deharveng, J.-M., Buat, V., Le Brun, V., Milliard, B., Kunth, D., Shull, J. M., & Gry, C. 2001, A&A, 375, 805
Dijkstra, M., Haiman, Z., Rees, M. J., & Weinberg, D. H. 2004, ApJ, 601, 666
Dow-Hygelund, C. C., et al. 2007, ApJ, 660, 47
Efstathiou, G., Ellis, R. S., & Peterson, B. A. 1988, MNRAS, 232, 431

Erb, D. K., Steidel, C. C., Shapley, A. E., Pettini, M., Reddy, N. A., & Adelberger, K. L. 2006, ApJ, 646, 107
Fan, X., Narayanan, V. K., Strauss, M. A., White, R. L., Becker, R. H., Pentericci, L., & Rix, H. 2002, AJ, 123, 1247
Fan, X., et al. 2005, AJ, 132, 117
Fernández-Soto, A., Lanzetta, K. M., & Chen, H.-W. 2003, MNRAS, 342, 1215
Finlator, K., Davé, R., Papovich, C., & Hernquist, L. 2006, ApJ, 639, 672
Förster Schreiber, N. M., et al. 2006, AJ, 131, 1891
Franx, M., et al. 2003, ApJ, 587, L79
Gabasch, A., et al. 2004, A&A, 421, 41
Giallongo, E., Cristiani, S., D'Odorico, S., & Fontana, A. 2002, ApJ, 568, L9
Giavalisco, M., et al. 2004a, ApJ, 600, L93
Giavalisco, M., et al. 2004b, ApJ, 600, L103
Giavalisco, M. 2005, New Astronomy Review, 49, 440
Hurwitz, M., Jelinsky, P., & Dixon, W. V. D. 1997, ApJ, 481, L31
Iliev, I. T., Mellema, G., Pen, U.-L., Merz, H., Shapiro, P. R., & Alvarez, M. A. 2006, MNRAS, 369, 1625
Inoue, A. K., Iwata, I., Deharveng, J.-M., Buat, V., & Burgarella, D. 2005, A&A, 435, 471
Iwata, I., Ohta, K., Tamura, N., Ando, M., Wada, S., Watanabe, C., Akiyama, M., & Aoki, K. 2003, PASJ, 55, 415
Iwata, I., Ohta, K., Tamura, N., Akiyama, M., Aoki, K., Ando, M., Kiuchi, G., & Sawicki, M. 2007, MNRAS, in press, astro-ph/0701841
Kodama, T., et al. 2004, MNRAS, 350, 1005
Kron, R. G. 1980, ApJS, 43, 305
Labbé, I., et al. 2003, AJ, 125, 1107
Labbé, I., Bouwens, R., Illingworth, G. D., & Franx, M. 2006, ApJ, 649, 67
Lee, K.-S., Giavalisco, M., Gnedin, O. Y., Somerville, R. S., Ferguson, H. C., Dickinson, M., & Ouchi, M. 2006, ApJ, 642, 63
Le Fèvre, O., et al. 2005, Nature, 437, 519
Lehnert, M. D. & Bremer, M. 2003, ApJ, 593, 630
Leitherer, C., Ferguson, H. C., Heckman, T. M., & Lowenthal, J. D. 1995, ApJ, 454, L19
Madau, P. 1995, ApJ, 441, 18
Madau, P., Pozzetti, L. & Dickinson, M. 1998, ApJ, 498, 106
Madau, P., Haardt, F., & Rees, M. J. 1999, ApJ, 514, 648
Malhotra, S., et al. 2005, ApJ, 626, 666
Malkan, M., Webb, W., & Konopacky, Q. 2003, ApJ, 598, 878
Mannucci, F., Buttery, H., Maiolino, R., Marconi, A. & Pozzetti, L. 2006, A&A, 461, 423
Martin, D. C., et al. 2005a, ApJ, 619, L1

Martin, D. C., et al. 2005b, ApJ, 619, L59

McIntosh, D. H., et al. 2005, ApJ, 632, 191

Meiksin, A. 2005, MNRAS, 356, 596

Meurer, G. R., Heckman, T. M., & Calzetti, D. 1999, ApJ, 521, 64

Nagamine, K., Springel, V., Hernquist, L., & Machacek, M. 2004, MNRAS, 350, 385

Night, C., Nagamine, K., Springel, V., & Hernquist, L. 2006, MNRAS, 366, 705

Noeske, K. G., et al. 2007, ApJ, 660, L47

Oesch, P. A., et al. 2007, ApJ, submitted, astro-ph/0706.2653

Oke, J. B., & Gunn, J. E. 1983, ApJ, 266, 713

Oppenheimer, B. D., & Davé, R. 2006, MNRAS, 373, 1265

Ouchi, M., et al. 2004, ApJ, 611, 660

Overzier, R. A., Bouwens, R. J., Illingworth, G. D., & Franx, M. 2006, ApJ, 648, L5

Page, L., et al. 2006, ApJ, in press, astro-ph/0603450

Paltani, S., et al. 2007, A&A, 463, 873

Pei, Y. C. 1995, ApJ, 438, 623

Read, J. I., Pontzen, A. P., & Viel, M. 2006, MNRAS, 371, 885

Reddy, N. A., & Steidel, C. C. 2004, ApJ, 603, L13

Reddy, N. A., Erb, D. K., Steidel, C. C., Shapley, A. E., Adelberger, K. L., & Pettini, M. 2005, ApJ, 633, 748

Reddy, N. A., Steidel, C. C., Fadda, D., Yan, L., Pettini, M., Shapley, A. E., Erb, D. K., & Adelberger, K. L. 2006, ApJ, 644, 792

Reddy, N.A., Steidel, C.C., Pettini, M., Adelberger, K.L., Shapley, A.E., Erb, D.K., & Dickinson, M. 2007, ApJS, in press, astro-ph/0706.4091

Samui, S., Srianand, R., & Subramanian, K. 2007, MNRAS, 377, 285

Sandage, A., Tammann, G. A., & Yahil, A. 1979, ApJ, 232, 352

Sawicki, M., & Thompson, D. 2006a, ApJ, 642, 653

Sawicki, M., & Thompson, D. 2006b, ApJ, 648, 299

Schiminovich, D., et al. 2005, ApJ, 619, L47

Shapley, A. E., Steidel, C. C., Pettini, M., & Adelberger, K. L. 2003, ApJ, 588, 65

Shapley, A. E., Steidel, C. C., Pettini, M., Adelberger, K. L., & Erb, D. K. 2006, ApJ, 651, 688

Sheth, R. K. & Tormen, G. 1999, MNRAS, 308, 119

Shimasaku, K., Ouchi, M., Furusawa, H., Yoshida, M., Kashikawa, N., & Okamura, S. 2005, PASJ, 57, 447

Shimasaku, K., et al. 2006, PASJ, 58, 313

Shull, M., & Venkatesan, A. 2007, ApJ, submitted, astro-ph/0702323

Sirianni, M., et al. 2005, PASP, 117, 1049

Sokasian, A., Abel, T., Hernquist, L., & Springel, V. 2003, MNRAS, 344, 607

Somerville, R. S., Lee, K., Ferguson, H. C., Gardner, J. P., Moustakas, L. A., & Giavalisco, M. 2004, ApJ, 600, L171

Songaila, A. 2004, AJ, 127, 2598

Spergel, D.N., et al. 2006, ApJ, in press, astro-ph/0603449

Springel, V., & Hernquist, L. 2003, MNRAS, 339, 289

Stanway, E. R., Bunker, A. J., & McMahon, R. G. 2003, MNRAS, 342, 439

Stanway, E. R., et al. 2004, ApJ, 604, L13

Stanway, E. R., McMahon, R. G., & Bunker, A. J. 2005, MNRAS, 359, 1184

Stark, D. P., Bunker, A. J., Ellis, R. S., Eyles, L. P., & Lacy, M. 2007a, ApJ, 659, 84

Stark, D. P., Ellis, R. S., Richard, J., Kneib, J.-P., Smith, G. P., & Santos, M. R. 2007b, ApJ, 663, 10

Stark, D. P., Loeb, A., & Ellis, R. S. 2007c, ApJ, submitted, astro-ph/0701882

Steidel, C. C., Adelberger, K. L., Giavalisco, M., Dickinson, M. and Pettini, M. 1999, ApJ, 519, 1

Steidel, C. C., Pettini, M., & Adelberger, K. L. 2001, ApJ, 546, 665

Stiavelli, M., Fall, S. M., & Panagia, N. 2004, ApJ, 610, L1

Sullivan, M., Treyer, M. A., Ellis, R. S., Bridges, T. J., Milliard, B., & Donas, J. 2000, MNRAS, 312, 442

Szalay, A. S., Connolly, A. J., & Szokoly, G. P. 1999, AJ, 117, 68

Thompson, R. I., et al. 2005, AJ, 130, 1

Tresse, L., et al. 2006, A&A, submitted, astro-ph/0609005

Treu, T., Ellis, R. S., Liao, T. X., & van Dokkum, P. G. 2005, ApJ, 622, L5

Ueda, Y., Akiyama, M., Ohta, K., & Miyaji, T. 2003, ApJ, 598, 886

Vale, A., & Ostriker, J. P. 2004, MNRAS, 353, 189

van der Wel, A., Franx, M., van Dokkum, P. G., Rix, H.-W., Illingworth, G. D., & Rosati, P. 2005, ApJ, 631, 145

van Dokkum, P. G., et al. 2006, ApJ, 638, L59

Vanzella, E., et al. 2006, A&A, 454, 423

Verma, A., Lehnert, M. D., Förster Schreiber, N. M., Bremer, M. N., & Douglas, L. 2007, MNRAS, 377, 1024

Wang, B., & Heckman, T. M. 1996, ApJ, 457, 645

White, R. L., Becker, R. H., Fan, X., & Strauss, M. A. 2003, AJ, 126, 1

Wyder, T. K., et al. 2005, ApJ, 619, L15

Wyithe, J. S. B., & Loeb, A. 2006, Nature, 441, 322

Yan, H. & Windhorst, R. A. 2004a, ApJ, 600, L1

Yan, H. & Windhorst, R. A. 2004b, ApJ, 612, L93

Yan, H., et al. 2005, ApJ, 634, 109

Yoshida, M., et al. 2006, ApJ, 653, 988

APPENDIX

A. LF DETERMINATIONS

A.1 Modelling Incompleteness and Photometric Scatter

To compare the expectations of the model LFs with the surface densities of dropouts observed, we need to be able to include the effect of incompleteness and photometric scatter in our calculations. We will accomplish this by computing corrections which transform the surface density of dropouts from that recoverable in noise-free (infinite S/N) data to that recoverable in each of the fields considered in our study. We employ a two part strategy: first deriving corrections necessary to transform the dropout surface densities from what we would recover for noise-free data to that recoverable in our HUDF selections and second deriving corrections to transform these surface densities from HUDF depth data to that recoverable in even shallower data. Our use of a two part strategy enables us to ensure that the corrections we derive for the shallower selections are extremely model independent (the most notable corrections being derived from degradation experiments).

Both corrections are implemented using a set of transfer functions, which correct the surface density of dropouts recoverable in deeper data to that recoverable in shallower data. We express these transfer functions as two-dimensional matrices, with the rows and the columns of these matrices indicating specific magnitude bins in the deeper and shallower data, respectively. Elements in these matrices indicate the fraction of galaxies with specific magnitudes in the deeper data recovered to have some other magnitude in the shallower data (see below). These transfer functions can then be applied to the surface density of dropouts in a given field, expressed as one dimensional vectors, through simple matrix multiplication. For our B and V-dropout selections, the axes of these matrices are given in terms of the i_{775} and z_{850} band magnitudes, respectively. These bands most closely correspond to flux at an approximately constant rest-frame wavelength (1600 $\mathring{A}$) at the mean redshift of our samples ($z \sim 3.8$ and $z \sim 5$, respectively) and are not affected by attenuation from the Lyα forest. For our i-dropout selections, we express these transfer functions in terms of the total
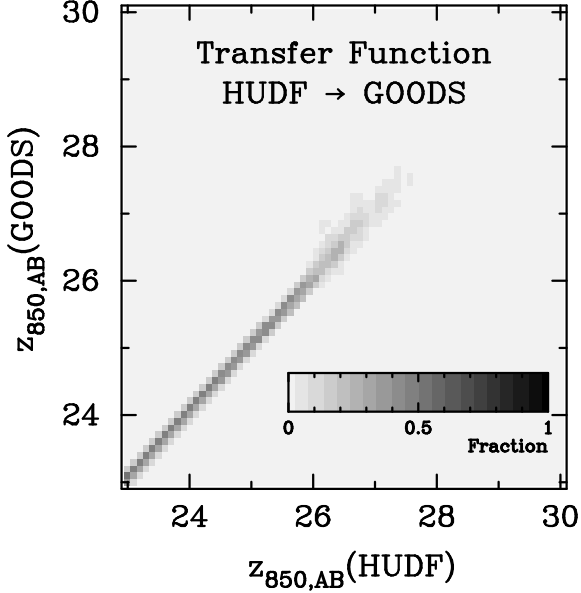
FIG. A1.— One of the transfer functions that we use in our analysis (see Appendix A.1). This transfer functions allow us to calculate the surface density of galaxies that would be identified at a given magnitude in shallower data (here the ACS GOODS data) given a specific surface density of dropouts in a deeper data set (here the ACS HUDF data). The transfer function plotted here is for a B-dropout selection and is binned on 0.1-mag intervals.

magnitude in the z_{850}-band, which corresponds to rest-frame 1350 $\mathring{A}$.

As noted, our first set of corrections is designed to correct the surface density of dropouts from what we would recover with noiseless (infinite depth) data to what we would recover in our HUDF selections. We will restrict these corrections to a modelling of the flux biases and photometric scatter – since completeness will be handled separately using a separate factor $P(m, z)$ (see Eq. 2 in §3.1). Modelling this scatter is important because of the tendency for fainter, lower significance sources to scatter into our selection through a Malmquist-like effect. To quantify this effect, we ran a series of simulations where we took B-dropout galaxies from the HUDF, artificially redshifted them across the redshift selection windows of our samples using our well-tested cloning software (Bouwens et al. 1998a,b; Bouwens et al. 2003a), measured their photometry off of the simulated frames, and finally reselected these sources using our dropout criteria. By comparing the input magnitudes with those recovered, we were able to construct the transfer functions, which successfully incorporated the photometric scatter present in the real data. The assumptions we use in these simulations (e.g., size-redshift scalings, colours) are the same as those given in Appendix A.3.

Now we derive corrections to take selections made with the HUDF data to similar selections made with shallower data. We accomplish this through a straightforward procedure, degrading the HUDF data to the depths of our shallower data and then repeating our selection and photometry at both depths. We perform these experiments for all three dropout samples and between the HUDF and all of our shallower fields (GOODS, HUDF-Ps, HUDF05). Again, we express the results of these experiments as transfer functions, which correct the surface density of dropouts from what we would recover in the deeper data to that recoverable in shallower data. To improve the statistics at bright magnitudes, we performed similar degradation experiments on our other deep fields (e.g., HUDF-Ps and HUDF05) and used those results at magnitudes where those fields appear to be essentially complete (i.e., AB mag < 26). The transfer functions were binned on 0.1-mag intervals, and then smoothed along the diagonal. The smoothing length was set so that at least 20 sources from the input images contributed to each element in the matrix. An illustration of one of the transfer functions we derived using this procedure is shown in Figure A1. Typical fluxes recovered from our GOODS data set were ~ 0.1 mag fainter than in the HUDF, with a completeness of $\gtrsim 90\%$ at $z_{850,AB} \sim 25.5$ and $\sim 50 - 70\%$ at $z_{850,AB} \sim 26.5$. Flux biases in our deeper HUDF-Ps and HUDF05 data were somewhat smaller in general at brighter magnitudes, and significant incompleteness did not set in until $i_{775,AB} \sim 27.5$ in our B-dropout selections and $z_{850,AB} \sim 27.5$ in our V-dropout and i-dropout selections.

A.2. Evaluating the Likelihood of Model LFs

In this paper (§3), we evaluate candidate LFs by comparing the predicted dropout counts from these LFs with that found in our different fields. We compute the dropout counts from the LFs using a two step procedure: first calculating the number of galaxies we would expect in our deepest selection the HUDF using Eq. 2 and then correcting this for photometric scatter and incompleteness using the transfer functions we derived in Appendix A.1.

To perform the integral in Eq. 2, we recast it in discrete form

$$\Sigma_k \phi_k V_{m,k} = N_m \qquad (A1)$$

N_m is the number counts binned in 0.1 mag intervals $\int_{m-0.05}^{m+0.05} N(m')dm'$, $\Sigma \phi_k W(M - M_k)$ is the LF binned on 0.1 mag intervals, and $V_{m,k}$ is an effective volume-type kernel which can be used to calculate the number counts N_m given

some LF. It is calculated as

$$V_{m,k} = \int_z \int_{m-0.05}^{m+0.05} W(M(m',z) - M_k)P(m',z)\frac{dV}{dz}dm'dz \tag{A2}$$

where

$$W(x) = \begin{array}{ll} 0, & x < -0.05 \\ 1, & -0.05 < x < 0.05 \\ 0, & x > 0.05 \end{array} \tag{A3}$$

Because of the minimal k-correction required in using the i_{775}-band fluxes of $z \sim 4$ B-dropouts to derive luminosities at rest-frame $\sim 1600\,\mathring{A}$ and in using the z_{850}-band fluxes of $z \sim 5$ V-dropouts to derive luminosities at $\sim 1600\,\mathring{A}$ (no Lyman forest absorption to consider), there is a fairly tight relationship between apparent and absolute magnitudes in our $z \sim 4$ and $z \sim 5$ determinations (the only sizeable differences are due to small changes in the distance modulus: see Figure A2). The only elements which are non-zero in the kernel $V_{m,k}$ span a small range in magnitude ($\Delta m \sim 0.3$ mag). At $z \sim 6$, there is no deep wide-area imaging which probes rest-frame $\sim 1600\,\mathring{A}$ for i-dropouts, and therefore we must resort to examining galaxy luminosities at a slightly bluer wavelength (i.e., $\sim 1350\,\mathring{A}$) using the z_{850}-band fluxes of i-dropouts. Since the z_{850}-band flux is affected by attenuation from the Lyman forest, the relationship between the apparent and absolute magnitudes is considerably less tight (see Figure A2), so the non-zero elements in the kernel $V_{m,k}$ span a much wider range in magnitude (i.e., $\Delta m \gtrsim 1.5$ mag: see Figure 7 of B06).

To incorporate the effects of incompleteness and photometric scatter on our results, we need to modify Eq. A1 to include the transfer functions we computed in Appendix A.1. The resultant formula is

$$\Sigma_{l,k}\phi_k T_{m,l}V_{l,k} = N_m \tag{A4}$$

where $T_{m,l}$ are the transfer functions we derived in Appendix A.1 to take galaxies from a true total magnitude of l to an observed total magnitude of m. This is the equation we use throughout our analysis in computing the surface density of dropouts in a given field from a model LF.

With the ability to calculate the number counts $N(m)$ given a LF, we need some means to decide which model LF fits our data the best. Our two primary approaches, STY79 and SWML, accomplish this by maximizing the likelihood of reproducing the distribution of galaxies as a function of magnitude. Since we consider the surface density of galaxies over multiple fields in our analysis, we express this likelihood L as a simple product

$$\mathcal{L} = \Pi_{field}(\Pi_i p(m_i)) \tag{A5}$$

where

$$p(m_i) = \left(\frac{n_{expected,i}}{\Sigma_j n_{expected,j}}\right)^{n_{observed,i}}. \tag{A6}$$

and $n_{observed,i}$ is the number of sources observed in the magnitude interval i and $n_{expected,j}$ is the number of sources expected in the magnitude interval j. In Eq. A5, note that we only include magnitude intervals i where $n_{observed,i}$ is positive. The value of $n_{expected,i}$ has no bearing on whether a magnitude interval i is included or not.

A.3. Selection Efficiencies

In the determinations of the LF we performed in this paper, it was essential for us to account for the efficiency with which we can select dropouts in our data. We computed this efficiency as a function of redshift z and the apparent magnitude m of the star-forming galaxy in question. We establish these selection efficiencies for galaxies in the HUDF since we reference our shallower selections to the HUDF through transfer functions (Appendix A.1). The apparent magnitudes here are in the same passband as we use to bin our dropout samples, i.e., the i_{775} band for our B-dropout sample, the z_{850} band for our V-dropout sample, and the z_{850} band for i-dropout sample.

We estimate the selection efficiencies $P(m,z)$ using our well-tested cloning software (Bouwens et al. 1998a,b; Bouwens et al. 2003a; R.J. Bouwens et al. 2007, in preparation) to project individual sources from our $z \sim 4$ HUDF B-dropout sample across the redshift range of our high-redshift samples. In calculating the selection efficiencies $P(m,z)$ for our $z \sim 4$ B-dropout selection, our projected B-dropout sample was taken to have mean UV continuum slopes β of -1.5 at $L^*_{z=3}$ UV luminosities, but steeper mean UV continuum slopes β of -2.1 at lower UV luminosities ($< 0.1L^*_{z=3}$) while at intermediate luminosities the mean β is varied smoothly between these two extremes. This is to account for the fact that UV luminous galaxies at high-redshift ($z \sim 2 - 4$) are found to have redder UV continuum slopes (Adelberger & Steidel 2000; Ouchi et al. 2004) than lower luminosity galaxies at these redshifts (Meurer et al. 1999; Beckwith et al. 2006; Iwata et al. 2007; R.J. Bouwens et al. 2007, in preparation). For our $z \sim 5$ V-dropout and $z \sim 6$ i-dropout selections, the mean UV-continuum slope of galaxies was taken to be -2.0 to match the bluer observed colours for these sources (Lehnert & Bremer 2003; Stanway et al. 2005; B06; Yan et al. 2005). The 1σ scatter in the β distribution was taken to be 0.6, which gives a good fit to the observed colours. Instead of using simple power laws to represent model SEDs of given UV continuum slope β, we elected to use 10^8-yr continuous star-formation models (Bruzual & Charlot 2003) where the dust extinction (Calzetti et al. 1994) is varied to reproduce the model slopes. This should provide for a slightly more realistic representation of the SEDs of star-forming galaxies at $z \sim 4 - 5$ than can be obtained from simple power law spectra. The sizes of B-dropouts in our simulations are scaled as $(1 + z)^{-1.1}$
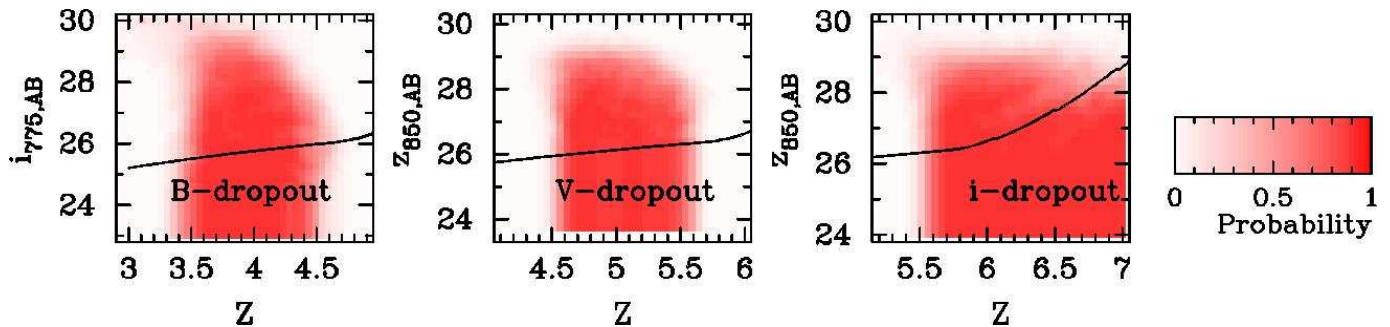
FIG. A2.— Selection functions $P(m, z)$ for our HUDF B, V, and i-dropout samples (*top, middle, and bottom panels, respectively*). These functions were estimated by artificially redshifting HUDF B-dropouts over the redshift intervals of our samples $z \sim 3 - 7$, adding them to the HUDF data, and then attempting to recover them as dropouts using the procedure described in §2. The sizes of sources were scaled as $(1+z)^{-1.1}$ to match the size-redshift relationship observed at $z \gtrsim 3$ for sources of fixed UV luminosity (e.g., B06; Bouwens et al. 2004b; Ferguson et al. 2004). Other details relevant to our simulations are provided in Appendix A.3. As a result of the covering area of foreground sources in the HUDF, the selection function $P(m, z)$ never exceeds ~ 0.9. The solid black lines show the apparent magnitudes of $0.5L^*_{z=3}$ galaxies as a function of redshift. Galaxies at $z \gtrsim 6.5$ only contribute a small fraction of the sources in our i-dropout selection at all z_{850}-band magnitudes considered due to the significant impact of Lyman forest absorption on their apparent magnitudes. As such, galaxies at $z \gtrsim 6.5$ do not provide an important contribution to the "effective" selection volumes for our i-dropout samples.

(for fixed luminosity) to match the observed size-redshift relationship (B06; see also Bouwens et al. 2004b; Ferguson et al. 2004).

We include the opacity from the Lyman series line and continuum absorption from neutral hydrogen using the Monte-Carlo approach of Bershady et al. (1999). With this approach, absorbers are randomly laid down along the line of sight to each model galaxy according to a distribution of HI column densities and then the colours computed based upon the net opacity in a given passband. For the distribution of column densities, we adopt that given in Eq. (10) of Madau (1995), but modified so that the volume densities of absorbers varied much more rapidly with redshift, i.e., as $\sim (1+z)^3$ instead of $\sim (1+z)^2$. The latter change was necessary to match the substantial Lyman decrements measured by Songaila (2004) for very high-redshift ($z \gtrsim 5$) quasars.

The resultant selection functions $P(m, z)$ for our B, V, and i-dropout samples are presented in Figure A2.

B. ALTERNATE DETERMINATIONS OF THE UV LF AT $Z \sim 4 - 6$

To test the robustness of our LF determinations against the many significant uncertainties (e.g., large-scale structure and the model k-corrections) which can affect our results, it is useful to consider a variety of different approaches in the determination of these LFs.

In this appendix, we consider seven such approaches. Our first two approaches employ alternative techniques to cope with large-scale structure uncertainties and to explore the resulting uncertainties. Our third approach explores possible uncertainties related to measuring the rest-frame UV LF at a bluer rest-frame wavelength where Lyman forest absorption is a concern. Our fourth and fifth approaches examine the dependence of our LF results on the assumptions we make about the form of SED templates and Lyα emission. Our sixth approach explores the dependence of these LF results on different selection criteria. Finally, with our final approach, we investigate the effect that an inherent evolution in M^* across the selection windows of each of our samples would have on our results. A summary of the LF determinations is provided in Table 6.

B.1. χ^2 Method (LSS correction)

One of the most significant uncertainties in the determination of the luminosity function is the effect of large-scale structure ("cosmic variance"). Large-scale structure can result in significant variations in the effective normalization of the LF as a function of position or line of sight. In this paper, we cope with these variations by fitting for the shape of the LF (i.e., α and M^*) in each of our fields using the STY79 maximum likelihood procedure. Since the normalization of the LF ϕ^* does not factor into the fits, our determinations of M^* and α should be robust to the presence of large-scale structure.

An alternate approach is to establish the relative normalization of the LF in each of our fields and then correct for field-to-field variations directly. The relative normalization is established through a two stage process, where we first establish the relative normalization of the UDF to our intermediate depth fields (HUDF-Ps, HUDF05) and second establish the relative normalization of the intermediate depth fields to the GOODS fields. In each step, we establish the relative normalization by degrading our deeper fields down to the depth of our shallower fields, reapplying our selection procedure, and then comparing the surface densities to those found in the shallower field. To maximize the significance of these measurements of the relative normalization, we repeated these degradation experiments 10 times and then took the average. Appendix B of B06 provides a detailed description of our degradation procedure. The numbers and surface densities found for each of our degraded and observed fields are presented in Table B1 and B2. Then, using these results and the same procedure presented in §3.6 of B06, we estimated the relative normalization of dropouts in each of our fields. We scaled the surface density of dropouts in these fields by the reciprocal of the tabulated factors to make them consistent with the GOODS fields, which sampling the largest comoving volume should provide us with the best estimate of the cosmic average.

TABLE B1
Surface Densities of B, V, and i-dropouts by field, to a fixed magnitude limit.[a]

| | Surface Density[b] | | |
Field	B-dropouts	V-dropouts	i-dropouts
HDFN GOODS	8.05±0.22	2.23±0.12	0.49±0.06
CDFS GOODS	8.67±0.23	2.06±0.11	0.67±0.06
HUDFP1	7.97±1.09	1.56±0.46	0.56±0.25
HUDFP2	6.66±1.11	3.00±0.80	0.15±0.15
HUDF05-1	—	2.92±0.53	0.49±0.22
HUDF05-2	—	2.55±0.52	0.55±0.24
HUDF	8.09±0.79	1.45±0.32	0.83±0.26

[a]As observed in these fields after degrading the imaging data to the depth of the GOODS fields and reselecting dropouts in the same way as performed on the GOODS data.

[b]Units are arcmin^{-2}. Only B-dropouts with $i_{775,AB} < 27$, V-dropouts with $z_{850,AB} < 27$, and i-dropouts with $z_{850,AB} < 27$ are included in the quoted surface densities. We chose 27.0 AB mag as a limit here because our GOODS dropout selections are still $\gtrsim 50\%$ complete to this limit.

TABLE B2
Comparison of the number of B, V, and i-dropouts in our intermediate depth fields with the HUDF degraded to the same depths.[a]

| | B-dropouts | | V-dropouts | | i-dropouts | |
Field	Observed	HUDF[b]	Observed	HUDF[b]	Observed	HUDF[b]
HUDFP1	127	137	46	34	34	31
HUDFP2	78	88	35	19	10	19
HUDF05-1	—	—	130	96	53	63
HUDF05-2	—	—	113	74	28	49

[a]Only B-dropouts, V-dropouts, and i-dropouts to a depth $i_{775,AB} < 28$, $z_{850,AB} < 28$, $z_{850,AB} < 28$, respectively, are considered in these comparisons for the HUDF-Ps. For the HUDF05 fields, this comparison is made to a depth of $z_{850,AB} < 28.5$ for our V and i-dropout selections.

[b]Number of dropouts found in the HUDF after degrading the HUDF to the depths of the shallower intermediate depth fields and repeating the selection. Note that the HUDF is underabundant in V-dropouts relative to all four intermediate depth fields (see also Oesch et al. 2007).

TABLE B3
Surface density of dropouts in our deep ACS fields relative to that present in GOODS.[a]

Field	B-dropouts	V-dropouts	i-dropouts
HUDFP	0.88±0.08	1.18±0.18	0.93±0.23
HUDF05	—	1.11±0.17	0.76±0.19
HUDF	0.96±0.10	0.77±0.11	1.06±0.25

[a]Computed from Table B1 and B2 using the procedures outlined in §3.6 of B06. Factors greater than 1.0 indicate that the dropouts in those fields are overdense relative to the cosmic average defined by the GOODS fields and factors less than 1.0 indicate an underdensity.

After normalizing the surface density of dropouts in each of our fields to the GOODS areas, we computed the luminosity function by comparing the expected counts with the surface densities (binned in 0.5 mag intervals) observed in each of our fields, computing χ^2, and then calculating the corresponding likelihood. To account for the uncertainties in the LF that result from the uncertain normalizations of our various fields (Table B1), we ran a series of simulations to compute the effect on the Schechter parameters M^*, α, ϕ^* (see, e.g., Appendix E from B06). In these simulations, we varied the normalizations of our different fields according to the approximate errors given in Table B3 and calculated the resulting covariance matrix. We then smoothed our likelihood contours according to this covariance matrix and also included an additional $\sim 14\%$ uncertainty in the value of ϕ^* due to field-to-field variations on the scale of the two GOODS fields (Somerville et al. 2004; see also §3.1). The latter two effects make up a significant fraction of our overall error budget in deriving the LFs. The best-fit Schechter parameters are provided in Table 6 and are in excellent agreement with our fiducial STY79 determinations. Previously we used this approach in our determination of the LF at $z \sim 6$ (§5.1 of B06), where it was called the "Direct Method."

B.2. χ^2 Method (no LSS correction)

In our STY79 determinations (§3.1) and the above determination (Appendix B.1), we considered two different methods for computing the LF at $z \sim 4 - 5$ in the presence of large-scale structure. In the first approach (§3.1), we

attempted to treat large-scale structure by using the STY79 fitting procedure, and in the second (Appendix B.1), we accomplished this by renormalizing the surface density of dropouts found in the HUDF, HUDF05, and HUDF-Ps fields to match the GOODS fields. Though both approaches should provide us with an effective means of dealing with large-scale structure, it is also interesting to determine the LF at $z \sim 4 - 5$ ignoring these considerations altogether (and thus implicitly assuming that each survey field is representative of the cosmic average). This will allow us to better assess the impact that large-scale structure could have on the current LF determinations. Using the same χ^2 methodology as we described in Appendix B.1, we repeat our determination of the LFs without making any large-scale structure corrections to the observed surface densities. The results are presented in Table 6 and are quite consistent with our fiducial STY79 determinations. This suggests that large-scale structure variations only have a modest effect on the Schechter parameters we derive.

B.3. STY79 Method (at $\sim 1350 \, \AA$)

Thus far we have presented two alternate determinations of the rest-frame UV LFs at $z \sim 4 - 6$. Each determination offered a different approach for dealing with the uncertainties that arise from large-scale structure. However, in both the $z \sim 4$ and $z \sim 5$ determinations, we have derived the LFs using the surface density of dropouts binned as a function of their magnitude at the same approximate rest-frame wavelength ($\sim 1600 \, \AA$). For our $z \sim 4$ B-dropout sample, dropouts were binned according to their i_{775} band magnitudes, and for our $z \sim 5$ V-dropout sample, dropouts were binned according to their z_{850}-band magnitudes. These two bands are sufficiently redward of Lyα (1216$\AA$) that they are not contaminated by absorption from the Lyα forest. This makes the determination of the UV LF relatively straightforward using approaches like the effective-volume technique of Steidel et al. (1999).

Unfortunately, when moving to our highest redshift $z \sim 6$ i-dropout sample, it simply has not been possible to determine the LF in the same manner as at $z \sim 4 - 5$ due to the lack of deep near-infrared ('J'-band) data to obtain coverage at $\sim 1600 \, \AA$. Consequently, in our determinations of the $z \sim 6$ LF (here and in B06), we had to resort to use of the flux in the z_{850} band (rest-frame $\sim 1350 \, \AA$) as a measure of the UV-continuum luminosity. The difficulty with this is that since the z_{850} band extends below 1216$\AA$ for galaxies at $z \gtrsim 5.7$, flux in this band is significantly attenuated by the Lyα forest, and so it was necessary for us to carefully model the redshift distribution of i-dropouts in our sample to remove this effect.

Though this latter procedure should be effective in treating the effects of the Lyα forest, it is not obvious that it will not result in any significant systematics in our determination of the LF. After all, the results will clearly depend somewhat upon the rest-frame wavelength at which LF is determined as well as the model redshift distributions and assumed forest absorption model (see Appendix A.3 and B.7). To verify that no large systematics are introduced, it is useful to repeat the determinations of the rest-frame UV LF at $z \sim 4$ and $z \sim 5$ but instead compiling the dropout surface densities in terms of their magnitudes in the optical passband just redward of the dropout band (i.e., the V_{606} band for our B-dropout samples and the i_{775} band for our V-dropout samples) to parallel use of the z_{850} band for our i-dropout samples. In this way, we will obtain a determination of the rest-frame UV LF at $z \sim 4$ and $z \sim 5$ at $\sim 1350 \, \AA$ to match our determination at $z \sim 6$. The best-fit parameters obtained using this approach are as follows: $\phi^* = 1.4 \pm 0.3 \times 10^{-3}$ Mpc^{-3}, $M_{1350}^* = -20.84 \pm 0.10$, and $\alpha = -1.81 \pm 0.05$ for our $z \sim 4$ B-dropout samples and $\phi^* = 0.8 \pm 0.4 \times 10^{-3}$ Mpc^{-3}, $M_{1350}^* = -20.73 \pm 0.26$, and $\alpha = -1.68 \pm 0.19$ for our V-dropout samples. Here the value of M^* at $z \sim 4$ is somewhat fainter than in our fiducial STY79 determination. However, to make a fair comparison, it is necessary to account for the k-correction from 1350 $\AA$ to 1600 $\AA$. The typical L^* galaxy at $z \sim 4$ has an approximate UV-continuum slope β of -1.5 (e.g., Ouchi et al. 2004), but at $z \sim 5 - 6$, the UV-continuum slope is much bluer, i.e., $\lesssim -2.0$ (Lehnert & Bremer 2003; Stanway et al. 2005; B06; Yan et al. 2005). This results in a typical k-correction of ~ -0.14 mag for $z \sim 4$ galaxies and ~ 0 mag for $z \sim 5 - 6$ galaxies, resulting in an approximate value of M^* at 1600 $\AA$ of -20.9 at $z \sim 4$ and -20.7 at $z \sim 5$. These values are in good agreement with our other determinations (Table 6), particularly when one considers the fact that the results of this approach are sensitive to the forest absorption model, large-scale structure along the line of sight, and an accurate model of the redshift distributions for each of our dropout samples.

B.4. STY79 Method (Alternate SED templates)

Throughout this paper, we have modelled the spectra of LBGs with 10^8-yr constant star formation systems with varying amounts of dust extinction. We have used these model spectra to estimate the selection volumes of star-forming galaxies in our B, V, and i-dropout selections. For our $z \sim 4$ B-dropout selections, the model SEDs were taken to have mean UV continuum slopes of -1.5 at higher UV luminosities while at lower UV luminosities (see Appendix A.3), the model SEDs were taken to have much bluer mean UV slopes in accordance with the observations (Meurer et al. 1999; R.J. Bouwens et al. 2007, in preparation). At $z \sim 5$ and $z \sim 6$, the model SEDs were assumed to have UV continuum slopes of -2 to match that present in the observations (Lehnert & Bremer 2003; Stanway et al. 2005; B06).

However, it is legitimate to ask how much our estimated selection volumes may depend upon the form of the SED templates. For example, we could have just as easily have modelled high-redshift galaxies using different star formation histories, dust content, or metallicities, even electing to model these systems as power laws $f_\lambda \propto \lambda^\beta$. Fortunately, these choices can largely be constrained by the observed colours of our sample galaxies, and in fact in our simulations of the HUDF B, V, and i-dropout data (§3) we find excellent agreement between our model results and the observed colors. Even so, different SED templates only have a modest effect ($\lesssim 20\%$) on the selection volumes of our dropout

samples (e.g., see Tables 9-10 of Beckwith et al. 2006), particularly if we ignore concerns about the limited S/N of the data and photometric scatter. Within $\sim 1-2$ mag of the selection limit, however, the limited S/N of the data becomes a real concern and the selection volume can often be quite different. This makes it necessary to run detailed Monte-Carlo simulations like those described in Appendix A.3 (Figure A2) to compute these selection volumes.

To test the sensitivity of our LF determinations to the precise assumptions we make about the colour and UV-continuum slopes of high-redshift galaxies, we repeated our determination of the LF at $z \sim 4$, $z \sim 5$, and $z \sim 6$ assuming a mean UV-continuum slope of -1.4 and -2.1, with 1σ scatter of 0.6. As in our fiducial STY79 determinations, we use 10^8-yr constant star-formation models (Bruzual & Charlot 2003) with the extinction (Calzetti et al. 1994) varied to match these UV-continuum slopes. In general, we found Schechter parameters (Table 6) consistent with our fiducial determinations. One important exception was in our determinations of the $z \sim 4$ LF assuming the redder $\beta = -1.4$ UV-continuum slopes. In that case, we found a significantly steeper faint-end slope α (i.e., ~ -2.1) than we obtained in our fiducial determinations. A quick investigation indicated that this resulted from the fact that red galaxies have a significantly more difficult time satisfying our $(B_{435} - V_{606})_{AB} > (V_{606} - z_{850})_{AB} + 1.1$ dropout criterion than blue galaxies, and therefore it is much more difficult to select red galaxies to fainter magnitudes than blue galaxies. To see whether our $z \sim 4$ $\beta = -1.4$ LF fit results were driven by the selection efficiency of faint ($\gtrsim 28$ AB mag) galaxies, we repeated our LF determination but restricted ourselves to galaxies brighter than 28.0 mag. In this case, we recovered Schechter parameters which were in good agreement with our fiducial STY79 determinations (Table 6).

B.5. STY79 Method (Significant Contribution of Lyα emission to Broadband Fluxes)

Another significant uncertainty in modelling the SEDs of high-redshift star-forming galaxies – and therefore estimating their selection volumes – is the distribution of Lyα equivalent widths. At $z \sim 3$, it is known that only a small fraction ($\sim 25\%$) of star-forming galaxies show significant Lyα emission, i.e., EW(Lyα) $> 20\mathring{A}$ (Shapley et al. 2003). At $z > 3$, the incidence of Lyα emission is thought to increase, both in strength and overall prevalence, though the numbers remain somewhat controversial. Some groups, using a narrowband selection, claim that $\gtrsim 80\%$ of star-forming galaxies at the high-redshift end of our range ($z \sim 5.7$) have Lyα equivalent widths of $\gtrsim 100\mathring{A}$ (Shimasaku et al. 2006), while spectroscopic follow-up of pure dropout selections indicate that the fraction is closer to $\sim 32\%$, with typical Lyα equivalent widths of $30\mathring{A}$ to $50\mathring{A}$ (Dow-Hygelund et al. 2007; Stanway et al. 2004; Vanzella et al. 2006). These results suggest a modest to substantial increase in the fraction of Lyα emitting galaxies from $z \sim 3$ to $z \sim 6$.

It is interesting to model the effect such emission would have on our computed selection volumes and thus overall determinations of the LF at $z \sim 4$ and $z \sim 5$. We do this using the same procedure as we used in §3, but assume that 33% of the star-forming galaxies at $z \sim 4 - 5$ have Lyα equivalent widths of $50\mathring{A}$. This fraction exceeds slightly the findings of the Dow-Hygelund et al. (2007) study above and was chosen partially as a compromise with the Shimasaku et al. (2006) work. The Schechter parameters we find following this procedure are presented in Table 6 for our B, V, and i-dropout samples. At $z \sim 4$, these LFs have slightly lower ϕ^*'s than similar LF determinations assuming no such emission. At $z \sim 5$ and $z \sim 6$, however, the derived ϕ^*'s are higher. This owes to the fact that Lyα lies outside of the dropout band at the lower redshift end of our B-dropout selections, but inside this band at the lower redshift end of our V and i-dropout selections. Note that we did not include such emission in the SEDs for our fiducial STY79 determinations since (1) Lyα can also be seen in absorption, not just emission (which would counteract this effect somewhat) and (2) the overall distribution of Lyα equivalent widths in star-forming galaxies at $z \sim 4 - 6$ still has not been firmly established.

B.6. STY79 Method (With Alternate Selection Criteria)

The present dropout selections rely upon the presence of a two-colour selection to isolate a sample of high-redshift star-forming galaxies at $z \sim 4$ and $z \sim 5$ and a one-colour criterion at $z \sim 6$. These colour criteria were chosen to maximize our sampling of the high-reshift galaxies, while minimizing contamination by low-redshift galaxies. However, we could have just as easily chosen a different set of colour criteria for our B, V, and i-dropout selections and computed our LFs on the basis of those criteria. To test the robustness of the present LFs, we elected to modify the present selection criteria slightly and repeat our determination of the $z \sim 4$, $z \sim 5$, and $z \sim 6$ LFs using the methodology laid out in §2 and §3. The criteria we chose were $((B_{435} - V_{606}) > 1.2) \wedge (B_{435} - V_{606} > 1.4(V_{606} - z_{850}) + 1.2) \wedge (V_{606} - z_{850} < 1.2)$ for our alternate B-dropout selection, $(V_{606} - i_{775} > 0.9(i_{775} - z_{850})) \vee (V_{606} - i_{775} > 1.8)) \wedge (V_{606} - i_{775} > 1.2) \wedge (i_{775} - z_{850} < 1.3)$ for our alternate V-dropout selection, and $(i_{775} - z_{850} > 1.4) \wedge ((V_{606} - i_{775} > 2.8) \vee (S/N(V_{606}) < 2))$ for our alternate i-dropout selection. The B-dropout criterion above is the same as used in the Giavalisco et al. (2004b) work and results in a sample about half the size of the present one, with a narrower selection window in redshift and similar mean redshift. The V-dropout criterion is similar to that used in our primary selection, except that the $(V_{606} - i_{775})$ colour cut was lowered to make our selection more complete at the higher redshift end of the V-dropout selection window. The best-fit Schechter parameters for these selections are presented in Table 6 and are in reasonable agreement with our fiducial STY79 determinations.

B.7. STY79 Method (Madau Opacities)

In this work, we use the Monte-Carlo procedure of Bershady et al. (1999) to model the effects that HI line and continuum absorption have on the colours of high-redshift galaxies (Appendix A.3). We adopted this approach rather than the more conventional approach of using the Madau (1995) opacities to better account for the stochastic effects that line of sight variations have on the colours of high-redshift galaxies and to take advantage of advances in our

knowledge of HI column densities at $z \gtrsim 5$ (e.g., from Songaila 2004). This should make the present determinations of the LF slightly more accurate overall than we would have obtained had we not made these refinements. This being said, it is useful nevertheless to compare our LF results with what we would have obtained using the wavelength and redshift dependent opacities compiled by Madau (1995). This will allow us to ascertain what the effect of these changes are on the present results. Repeating our determination of the selection efficiencies of B, V, and i dropouts with the Madau (1995) opacities (Appendix A.3), we find that our V and i-dropout selection windows are shifted to slightly higher redshifts in general, by $\Delta z \sim 0.05$, but overall look very similar. The LFs we derive using these assumptions are presented in Table 6 and are quite similar to our fiducial STY79 determinations, except at $z \sim 5 - 6$ M^* is ~ 0.05 mag brighter and at $z \sim 6$ the value of ϕ^* is $\sim 10\%$ higher.

B.8. STY79 Method (With An Evolving M*)

In our fiducial STY79 determinations of the LF for each dropout sample, we assume that the LF does not evolve in redshift across the selection window of each sample. Since we observe significant evolution in the LF over the redshift range probed by our LFs ($z \sim 6$ to $z \sim 4$), this assumption clearly cannot be correct in detail. To investigate whether our determinations may have been affected by this assumption, we repeated our determination of the LF for each of our samples, but assumed that M^* evolves by 0.35 mag per unit redshift. This evolution in M^* is a good match to the evolution we observe in the UV LF from $z \sim 6$ to $z \sim 4$. The values of M^*, ϕ^*, and α we derive at $z \sim 3.8$, $z \sim 5$, and $z \sim 5.9$ assuming an evolving M^* are presented in Table 6. Encouragingly enough, the values we obtain including evolution are very similar to those recovered without evolution. This suggests that the overall Schechter parameters we have derived here are quite robust. Nonetheless, there do appear to be small systematic changes in the best-fit Schechter parameters if evolution is included. Accounting for evolution, the M^*'s recovered are ~ 0.06 mag fainter, the ϕ^*'s recovered are $\sim 10\%$ higher, and the faint-end slopes α are marginally shallower (by ~ 0.02). Since the inclusion of evolution in the determination of the LF is presumably a better assumption than not including this evolution, the LF parameters we adopt in this paper (Table 7) will be from this section.

C. EFFECT OF LARGE-SCALE STRUCTURE VARIATIONS ALONG THE LINE OF SIGHT ON OUR RESULTS

The standard SWML and STY79 maximum likelihood approaches allow us to determine the shape of the LF in a way that is insensitive to the presence of large-scale structure. Unfortunately, since we do not have exact redshift information for the galaxies in our samples, we cannot determine the absolute magnitudes for individual galaxies in our sample and therefore we must modify the SWML and STY79 maximum likelihood approaches slightly so that the likelihoods are expressed in terms of the apparent magnitude for individual sources (instead of the absolute magnitude). Since the apparent magnitudes are related to the absolute magnitudes via the redshift and the distribution of redshifts is uncertain due to the presence of large-scale structure along the line of sight, our LF fit results will show some sensitivity to this structure.

To determine the effect of this structure on the derived values of M^*, ϕ^*, and α, we ran a number of Monte-Carlo simulations where we introduced large-scale structure variations upon a canonical mock catalog of dropouts for each dropout sample which we generated using the Schechter parameters given in Table 7. Our use of one standard mock catalog for each sample was necessary to ensure that variations in the best-fit parameters only resulted from large-scale structure fluctuations and not poissonian-type fluctuations (which would arise if we regenerated these catalogs for each trial in our Monte-Carlo simulations). We then proceeded to introduce large-scale structure fluctuations into this catalog. Within redshift slices of size $\Delta z = 0.05$, we calculated the expected density variations expected for each of our dropout samples assuming the values of the bias given in §3.1, made random realizations of these density variations, applied these variations to our mock catalogs, and then recomputed the Schechter parameters using our implementation of the STY79 method. Repeating this process several hundred times for each dropout sample, we computed the 1σ RMS variations in ϕ^*, M^*, and α expected to result from large-scale structure along the line of sight. For our $z \sim 4$ B-dropout sample, we found 1σ RMS variations of 0.07 mag, 13%, and 0.01 in M^*, ϕ^*, and α, respectively. For our $z \sim 5$ V-dropout sample, we found 1σ RMS variations of 0.05 mag, 12%, and 0.01, respectively, and for our $z \sim 5.9$ i-dropout sample, we found 1σ RMS variations of 0.05 mag, 16%, and 0.04, respectively. Since the nominal errors from the STY79 method on M^* and α are typically at least two to three times as large as this, this structure only increases the uncertainties on M^* and α by a minimal $\sim 10\%$.